Solid Earth, 11, 437–467, 2020
https://doi.org/10.5194/se-11-437-2020

Solid Earth Open Access EGU

Cenozoic deformation in the Tauern Window (Eastern Alps) constrained by in situ Th-Pb dating of fissure monazite

Emmanuelle Ricchi[1], **Christian A. Bergemann**[2], **Edwin Gnos**[3], **Alfons Berger**[4], **Daniela Rubatto**[4,5], **Martin J. Whitehouse**[6], **and Franz Walter**[7]

[1]Department of Earth Sciences, University of Geneva, Rue des Maraîchers 13, 1205 Geneva, Switzerland
[2]Institute of Geosciences, Heidelberg University, Im Neuenheimer Feld 236, 69120 Heidelberg, Germany
[3]Natural History Museum of Geneva, Route de Malagnou 1, 1208 Geneva, Switzerland
[4]Institute of Geological Sciences, University of Bern, Baltzerstrasse 1+3, 3012 Bern, Switzerland
[5]Institute of Earth Sciences, University of Lausanne, Geopolis, 1015 Lausanne, Switzerland
[6]Swedish Museum of Natural History, P.O. Box 50007, 104-05 Stockholm, Sweden
[7]Institut für Erdwissenschaften, Karl-Franzens-Universität, Universitätsplatz 2, 8010 Graz, Austria

Correspondence: Emmanuelle Ricchi (emmanuelle.ricchi@unige.ch)

Received: 21 October 2019 – Discussion started: 30 October 2019
Revised: 14 February 2020 – Accepted: 24 February 2020 – Published: 3 April 2020

Abstract. Thorium–lead (Th-Pb) crystallization ages of hydrothermal monazites from the western, central and eastern Tauern Window provide new insights into Cenozoic tectonic evolution of the Tauern metamorphic dome. Growth domain crystallization ages range from 21.7 ± 0.4 to 10.0 ± 0.2 Ma. Three major periods of monazite growth are recorded between ∼ 22–20 (peak at 21 Ma), 19–15 (major peak at 17 Ma) and 14–10 Ma (major peak around 12 Ma), respectively, interpreted to be related to prevailing N–S shortening, in association with E–W extension, beginning strike-slip movements and reactivation of strike-slip faulting. Fissure monazite ages largely overlap with zircon and apatite fission track data. Besides tracking the thermal evolution of the Tauern dome, monazite dates reflect episodic tectonic movement along major shear zones that took place during the formation of the dome. Geochronological and structural data from the Pfitschtal area in the western Tauern Window show the existence of two cleft generations separated in time by 4 Ma and related to strike-slip to oblique-slip faulting. Moreover, these two phases overprint earlier phases of fissure formation.

Highlights.

- In situ dating of hydrothermal monazite-(Ce).
- New constraints on the exhumation of the Tauern metamorphic dome.
- Distinct tectonic pulses recorded from east to west.

1 Introduction

In situ thorium–lead (Th-Pb) dating of hydrothermal fissure monazite-(Ce) (in the following simply monazite) has recently been demonstrated to be a reliable method for dating tectonic activity under retrograde metamorphic conditions (Bergemann et al., 2017, 2018, 2019, 2020; Berger et al., 2013; Fitz-Diaz et al., 2019; Gasquet et al., 2010; Gnos et al., 2015; Grand'Homme et al., 2016a; Janots et al., 2012; Ricchi et al., 2019). These studies conducted through the entire Alpine orogenic belt allowed constraining tectonic activity in relation with exhumation and fault activity under retrograde lower greenschist to sub-greenschist facies metamorphic conditions.

Hydrothermal fissure monazite, concentrating light rare earth elements (LREE), Th and U, generally crystallizes in Ca-poor lithologies, outside the stability field of titanite or epidote / allanite. However, once formed, hydrothermal processes may cause dissolution–reprecipitation events leading to resetting of the monazite Th-Pb decay

Published by Copernicus Publications on behalf of the European Geosciences Union.

system in parts of the crystal. Chemically and isotopically homogeneous crystals indicate a single, rapid growth episode (e.g. Grand'Homme et al., 2016a). However, crystals showing different growth domains indicative of successive growth episodes are more common. In other cases, parts of, or entire, grains display a patchy zoning due to dissolution–reprecipitation processes (e.g. Ayers et al., 1999; Grand'Homme et al., 2016b). These processes involve element fractionation resulting in crystal zones with often distinct Th/U values (Seydoux-Guillaume et al., 2012).

The advantage of using hydrothermal monazite for dating tectonic activity is related to the high closure temperature of monazite of > 800 °C, implying that diffusion in monazite is negligible (Cherniak et al., 2004; Gardés et al., 2006, 2007) under P–T conditions at or below 450–500 °C and 0.3–0.4 GPa (e.g. Mullis et al., 1994; Mullis, 1996; Sharp et al., 2005) where hydrothermal fissures form. Fissure monazites date crystallization following chemical disequilibrium within a fissure. This causes a dissolution–precipitation cycle that may include dissolution or partial dissolution of existing fissure monazite. This has the consequence that late dissolution–precipitation steps may be well recorded, whereas earlier growth domains may be completely destroyed. Thus, monazite crystallization due to chemical disequilibrium is interpreted as being related to tectonic activity (e.g. volume change, fissure propagation, exposure of fresh host rock, delamination of fissure wall, seismic activity, fluid loss or gain).

Recent studies have shown that fissure monazite typically forms between generally lower to higher 200–400 °C (Gnos et al., 2015; Janots et al., 2019). For this reason, fissure monazite ages are generally interpreted as dating crystallization or re-crystallization. Monazite geochronology can thus be utilized to constrain shear and damage zone activity under greenschist and very low-grade metamorphic conditions at least down to 200 °C (e.g. Bergemann et al., 2017, 2018; Gnos et al., 2015).

Fissures and clefts develop close to the brittle–ductile transition (< 450 °C; Mullis, 1996) and are usually oriented perpendicular to the foliation and lineation of the host rock (Gnos et al., 2015). Fissures are generally straight when they form and either became enlarged by subsequent tectonic activity to form fluid-filled decimetre- to metre-sized clefts, displaying a more open shape with rounded surfaces (e.g. Ricchi et al., 2019) when the stress field retains the same orientation, or become completely filled to form mineral veins. However, they may show a complex shape when the stress field direction changes during deformation. Fluid inclusion studies (e.g. Mullis, 1996) show that clefts generally suffered several deformation episodes.

Interaction of the fluid that fills the fissures with the surrounding rock leads to dissolution of minerals in the wall rock and mineral precipitation in the fissure. As long as deformation continues, fluid-filled clefts will react to deformation via dissolution–precipitation cycles due to disequilibrium between fluid, rock wall and mineral assemblage within the cleft (e.g. Putnis, 2009). Thus, hydrothermal minerals like monazite do not only grow following the initial fissure formation but form, continue to grow or dissolve during subsequent deformation stages. The timing of these growth or alteration stages may not always be resolvable with the precision of currently available geochronological methods, but different growth stages may be distinguishable through differences in the chemical composition (Grand'Homme et al., 2018). In contrast to the surrounding country rock, the fissures and clefts remain highly reactive at low temperature due to the presence of fluids. For this reasons, deformation steps during brittle deformation may be registered through mineral growth or recrystallization in clefts (e.g. Berger et al., 2013) down to conditions where clay minerals form in fault gauges.

The Tauern Window (TW) is a thermal and structural dome of the eastern Alps (Fig. 1) exhumed over a period of about 30 Ma starting from the Early Oligocene (e.g. Rosenberg et al., 2018; Schmid et al., 2013). Previous monazite crystallization ages obtained in the eastern subdome of the TW record tectonic activity between 19.0 ± 0.5 and 15.0 ± 0.5 Ma (Gnos et al., 2015). In the current study, monazite geochronology is extended to the entire TW in order to investigate its Cenozoic deformation history. We particularly aim to establish a chronological record for the younger exhumation history recorded by fissure monazite crystallization, to be compared with known deformation phases.

A total of 23 monazite grains together with provenance data, and in some cases host-rock information, were dated (Table 1). Seven grains come from the western limb of the TW (INNB1 ZEI1, SCHR1, MAYR4, PFIT1, BURG2 and PLAN1; samples 1–7; Fig. 1), another seven grains come from the eastern border of the western subdome (central TW; SCHEI1, HOPF2, GART1, NOWA3, GART3, STEI2 and KNOR1; samples 8–14; Fig. 1), and nine grains were collected in the eastern subdome (KAIS6, SALZ18, LOHN4, ORT1, EUKL2, HOAR1, MOKR1, SAND1 and REIS1; samples 15–25; Fig. 1, Table 1). In order to capture at best the tectonic activity during the exhumation of the TW, the investigated samples were selected in a way that gives priority to sample localities in regions affected by major fault zones and at lithological boundaries. In the following, we will discuss the ages in terms of sample ID numbers (1–25) provided in Table 1.

2 Geologic settings

In the largest tectonic window of the Austroalpine nappe stack, the TW, Penninic (Glockner nappe system and Matrei zone; Fig. 1) and Subpenninic nappes (mainly the Venediger Duplex) are exposed (e.g. Schmid et al., 2013; Fig. 1). The TW metamorphic and structural dome consists of two subdomes, with E–W-striking upright folds in the internal parts

Table 1. Summary of monazite samples investigated in this study and by Gnos et al. (2015). Samples name, number, location, host-rock lithology, metamorphic degree and fissure mineral association are provided. Samples with approximate finding location are marked with "approx.".

Locality	Sample	No.	Latitude (° N)	Longitude (° E)	Remark	Host rock	Host rock Alpine met.	Fissure mineral association	Reference	Ion probe
Western Tauern Window										
Innerböden, Zillertal, Tyrol, Austria	INNB1	1	47°05.850′	011°47.667′	approx.	gneiss	AM	Qtz, Adl, Chl	this study	SwissSIMS
Zeischalm, Valsertal, Tyrol, Austria	ZEI1	2	47°01.400′	011°35.767′	approx.	gneiss	AM	Qtz, Adl, Chl	this study	SwissSIMS
Schrammacher, Zillertal, Tyrol, Italy	SCHR1	3	47°01.47′	011°38.60′	approx.	gneiss	AM	Qtz, Chl, Adl, Rt, Snt	this study	NordSIMS
Kluppen, Pfitschtal, South Tyrol, Italy	MAYR4	4	47°00.400′	011°36.217′	approx.	gneiss	AM	Qtz, Adl, Ant, Cc, Rt, Xnt	this study	SwissSIMS
Pfitscherjoch, Tyrol, Austria	PFIT1	5	46°59.65′	011°39.60′		mica schist	AM	Qtz, Hm, Adl, Trm, Rt, Brk, Ant, Syn, Asc	this study	NordSIMS
Burgumalpe, Pfitschtal, South Tyrol, Italy[a]	BURG2	6	46°55.217′	011°33.350′	approx.	serpentinite	GAT	Ilm, Rt, Cc	this study	SwissSIMS
Schwarzenbach, Ahrntal, South Tyrol, Italy	PLAN1	7	46°58.641′	011°53.302′	approx.	gneiss	AM	Qtz, Adl	this study	SwissSIMS
Central Tauern Window										
Scheissgraben (Kotriesen), Habachtal, Salzburg, Austria	SCHEI1	8	47°14.483′	012°18.667′		mica schist	UGS	Qtz, Ab, Ant, Ank, Rt	this study	SwissSIMS
Hopffeldboden, Obersulzbachtal, Salzburg, Austria	HOPF2	9	47°12.278′	012°14.844′		gneiss	GAT	Qtz, Ilm, Rt, Ant, Brk, Asc, Syn, Ap, Chl, Lm	this study	NordSIMS
Hopffeldgraben, Obersulzbachtal, Salzburg, Austria	GART1	10	47°12.100′	012°14.167′		gneiss	GAT	Qtz, Adl, Ant, Rtl, Asc + Bt and Chl from EDS analyses	this study	SwissSIMS
Wildenkarer Wald, Habachtal, Salzburg, Austria	NOWA3	11	47°12.633′	012°20.000′	approx.	gneiss	GAT	Qtz, Ab, Adl	this study	SwissSIMS
Beryller, Untersulzbachtal, Salzburg, Austria	GART3	12	47°11.250′	012°18.517′	approx.	gneiss	AM	Qtz, Adl	this study	SwissSIMS
Sattelkar, Obersulzbachtal, Salzburg, Austria	STEI2	13	47°09.783′	012°17.250′	approx.	gneiss	AM	Qtz, Adl, Rt, Chl	this study	SwissSIMS
Innerer Knorrkogel, East Tyrol, Austria	KNOR1	14	47°06.117′	012°25.183′		gneiss	AM	Adl, Qtz, Chl	this study	NordSIMS
Eastern Tauern Window										
Kaiserer Steinbruch, Hüttwinkeltal, Rauris, Salzburg, Austria[b]	KAIS6	15	47°07.787′	012°58.708′		meta-arenite	GAT	Qtz, Adl, Trm, Cc, Hm, Rt, Chl	this study	NordSIMS
Lohninger Quarry, Hüttwinkeltal, Rauris, Salzburg, Austria[b]	SALZ18	16a	47°07.20′	012°59.33′		meta-arenite	GAT	Qtz, Adl, Trm, Cc, Hm, Rt, Chl	this study	NordSIMS
Lohninger Quarry, Hüttwinkeltal, Rauris, Salzburg, Austria[b]	T3	16b	47°07.20′	012°59.33′		meta-arenite	GAT	Alb, Qtz, Trm, Hm, Rt	Gnos et al. (2015)	NordSIMS
Lohninger Quarry, Hüttwinkeltal, Rauris, Salzburg, Austria[b]	LOHN4	17	47°07.20′	012°59.33′		meta-arenite	GAT	Qtz, Adl, Trm, Cc, Hm, Rt, Chl	this study	NordSIMS
Ortberg bei Böckstein, Salzburg, Austria	ORT1	18	47°05.150′	013°04.217′		granitic gneiss	GAT	Qtz, Adl, Rt, Chl, Ap	this study	SwissSIMS
Euklaskluft, Griesswies, Salzburg, Austria	EUKL2	19a	47°04.683′	012°57.250′		Bt-Mu schist	GAT	Alb, Pyr, Qtz, Rt, Chl, euclase, Xnt, goethite–todorokite–nordstrandite	this study	NordSIMS
Euklaskluft, Griesswies, Salzburg, Austria	T2	19b	47°04.683′	012°57.250′		Bt-Mu schist	GAT	Alb, Pyr, Qtz, Rt, Chl, euclase, Xnt, goethite-todorokite-nordstrandite	Gnos et al. (2015)	NordSIMS
Hocharn, Kärnten, Austria	HOAR1	20	47°04.500′	012°56.083′		granitic gneiss	GAT	Qtz, Ab, Rt	this study	SwissSIMS
Erfurter Steig, Rauris, Salzburg, Austria	T1	21	47°04.133′	012°57.917′		Bt-Mu schist	GAT	Qtz, Ab, Adl, phenakite, Rt, Cc	Gnos et al. (2015)	NordSIMS
Gjaidtroghöhe, Grosses Fleisstal, Kärnten, Austria	T4	22	47°03.783′	012°54.650′		gneiss	GAT	Qtz, Ab, Ant/Rt, Chl, Cc	Gnos et al. (2015)	NordSIMS
Mokritzen, Kleines Fleisstal, Kärnten, Austria	MOKR1	23	47°03.033′	012°53.983′		graphite-bearing schist	GAT	Qtz, Sid	this study	SwissSIMS
Sandkopf, Grosses Zirknitztal, Kärnten, Austria	SAND1	24	47°01.983′	012°56.05′		banded gneiss	GAT	Qtz, Adl, Chl, Sid, Ant	this study	SwissSIMS
Kleiner Reisseck, Reisseckgruppe, Kärnten, Austria	REIS1	25	46°56.950′	013°22.433′		banded gneiss	AM	Qtz, Ant, Ab, Chl	this study	SwissSIMS

Ab – albite; Adl – adularia; Ank – ankerite; Ant – anatase; Ap – fluorapatite; Asc – aeschynite; Brk – brookite; Cc – calcite; Chl – chlorite; Clc – clinochlore; Hm – hematite; Ilm – ilmenite; Lm – limonite; Pyr – pyrite; Qtz – quartz; Rt – rutile; Sd – siderite; Snt – senaite; Str – strontianite; Syn – synchisite; Trm – tourmaline; Xnt – xenotime; Alpine metamorphism: AM (amphibolite facies), GAT (greenschist–amphibolite transition), UGS (upper greenschist facies). [a] Bloc in glacial moraine. [b] Bloc in rock slide.

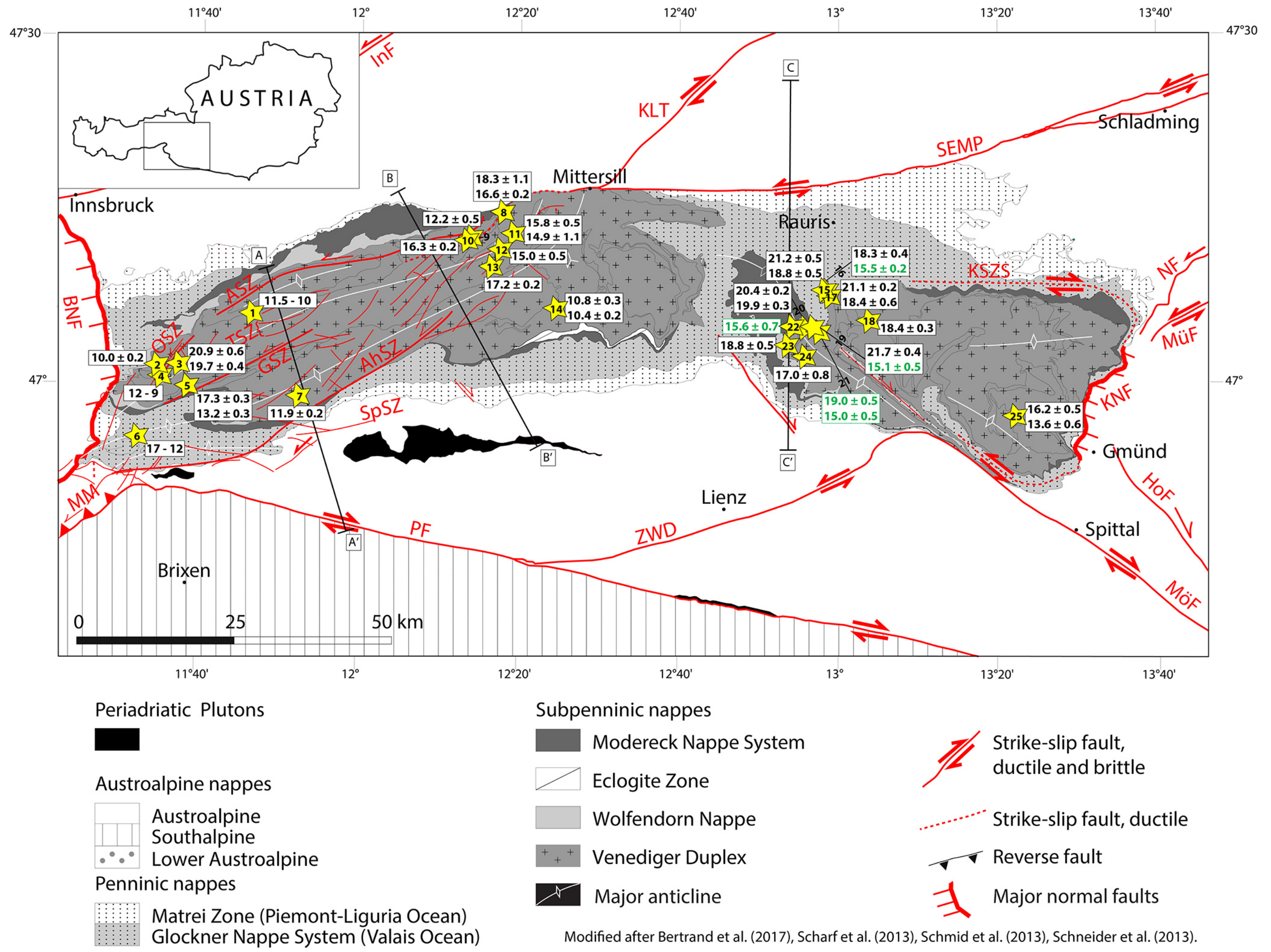

Figure 1. Tectonic map of the TW dome modified after Bertrand et al. (2017), Scharf et al. (2013), Schmid et al. (2013) and Schneider et al. (2013). Yellow stars on the map represent sample locations, and numbers inside the stars refer to samples listed in Table 1. Range of weighted mean growth domain ages are indicated for each grain from this study and Gnos et al. (2015), labelled in black and green, respectively, on the map (see Table 4 for an exhaustive summary of all the ages). Only the spot date range is indicated for grains 1, 4 and 6. Locations of AA', BB' and CC' cross sections are indicated by black lines, and individual cross sections are presented in Fig. 6 together with monazite crystallization ages. Two normal faults delimit the western and eastern borders of the TW, the Brenner normal fault (BNF) and the Katschberg normal fault (KNF), respectively. Note that the KNF prolongation results in dextral and sinistral strike slips in the north and south, respectively (KSZS: Katschberg shear zone system). Several sinistral strike-slip faults (AhSZ: Ahrntal shear zone; ASZ: Ahorn shear zone; DAV: Defereggen–Antholz–Vals fault; GSZ: Greiner shear zone; InF: Inntal fault; MüF: Mur–Mürz fault; NF: Niedere Tauern southern fault; OSZ: Olperer shear zone; SEMP: Salzach–Ennstal–Mariazell–Puchberg fault; SpSZ: Speikboden shear zone; TSZ: Tuxer shear zones; ZWD: Zwischenbergen–Wöllatratten and Drautal faults), dextral shear zones (HoF: Hochstuhl fault; IsF: Iseltal fault; KLT: Königsee–Lammertal–Traunsee fault; Mölltal fault (MöF); PF: Pustertal fault) and a reverse fault (MM: Meran–Mauls fault) are also visible in red on the map.

and bordered by two major normal faults, the Katschberg normal fault (KNF) in the east and the Brenner normal fault (BNF) in the west (Fig. 1). The western subdome is dissected by numerous sinistral shear zones (Ahorn shear zone (ASZ), Olperer shear zone (OSZ), Tuxer shear zones (TSZ), Greiner shear zone (GSZ) and Ahrntal shear zone (AhSZ)) and is bordered by the Salzach–Ennstal–Mariazell–Puchberg fault (SEMP) in the north (Fig. 1). The eastern subdome is bordered to the east by the Katschberg normal fault (KNF), continuing to the north into the dextral Katschberg shear zone system (KSZS) and to the south into an unnamed sinistral shear zone and oriented parallel to the Mölltal fault (MöF). The deformation history of these fault complexes will be discussed later.

The Alpine evolution of the TW started in the Early Paleocene with the accretion and subduction of the Piemonte–

Table 2. Summary of deformation phases in the Tauern metamorphic dome.

Age (Ma)	Phase	Fault	Domain	Characteristics	Ref.	Remarks
Estimated peaks of deformation						
∼ 65	D1		Penninic nappes	Accretion and subduction of Piemonte–Liguria Ocean	E	
∼ 41	D2		Penninic and Subpenninic nappes	Subduction of Valais Ocean and parts of the distal European margin	E	
∼ 35	D3		Central TW	Exhumation of high-pressure units	E	Folding of D2 thrust, decompression
∼ 29	D4		Subpenninic nappes	European slab break-off, Venediger Duplex formation and “Tauernkristallisation”	E	Contemporaneous intrusion of Periadriatic plutons and incipient NE-wards subduction of the Adriatic slab
∼ 23–21			East of the Giudicarie belt	Incipient indentation of the southern alpine units in the Eastern Alps	D, E	
∼ 17	D5		TW	Indentation, doming and lateral extrusion	E	
Faults’ motion						
33–15		ASZ	Western TW	Sinistral ductile shear	F, G	Ductile continuation of the SEMP fault
24–12		TSZ	Western TW	Sinistral ductile shear	B, F	
20–7		GSZ	Western TW	Sinistral ductile shear	F	
21–10		BNF	Western TW	Normal fault	C	
22–13		KNF	Eastern TW	Normal fault	C	

A: Bertrand et al. (2017, 2015); B: Blanckenburg et al. (1989); C: Favaro et al. (2017); D: Scharf et al. (2013); E: Schmid et al. (2013); F: Schneider et al. (2013); G: Rosenberg and Schneider (2008). ASZ: Ahorn shear zone, BNF: Brenner normal fault, GSZ: Greiner shear zone, KNF: Katschberg normal fault, SEMP: Salzach–Ennstal–Mariazell–Puchberg fault, TSZ: Tuxer shear zones.

Liguria Ocean (Matrei zone; Fig. 1) under the Apulian margin (Austroalpine nappe stack; e.g. Schmid et al., 2004, 2013; D1 deformation of Schmid et al., 2013; Fig. 1, Table 2). In the Middle Eocene, the Valais Ocean and parts of the distal European margin (Glockner nappe system, Eclogite zone and parts of the Modereck nappe system; Fig. 1) were equally subducted below the Austroalpine nappe stack and the Matrei zone accreted during D1 deformation (D2 deformation of Schmid et al., 2013; Table 2). In the Late Eocene, exhumation was achieved by extrusion of the high-pressure units that went together with major folding of the D2 thrust formed between the subducted Glockner nappe system and Modereck nappe system (D3 deformation of Schmid et al., 2013; Table 2). In the Early Oligocene, nearly contemporaneous break-off of the subducting European slab and formation of the Venediger Duplex (crustal-scale duplex structure) occurred, followed by the “Tauernkristallisation” (reheating of the whole nappe stack to amphibolite facies conditions) (D4 deformation of Schmid et al., 2013; Table 2). This was followed by an inversion of subduction polarity at ∼ 23 to 21 Ma (e.g. Rosenberg et al., 2018; Scharf et al., 2013; Schmid et al., 2013; Table 2). The following exhumation of the TW started in the Early to Middle Miocene by Alpine N–S collisional shortening and E–W orogen-parallel extension leading to folding, erosion and lateral extrusion through shear zone development (e.g. Luth and Willingshofer, 2008; Rosenberg and Berger, 2009; Rosenberg and Garcia, 2011; Schmid et al., 2004, 2013; Selverstone, 1988; D5 deformation of Schmid et al., 2013). Previous shear zone age dating in the TW was achieved using different geochronometers: Rb-Sr whole-rock–phengite dating (20 Ma; Blanckenburg et al., 1989), Rb-Sr whole-rock–white mica dating (39–16 Ma; Glodny et al., 2008), Sm-Nd dating on garnet (27.5–20 Ma; Pollington and Baxter, 2010, 2011) and $^{40}Ar/^{39}Ar$ dating on mica (35–28 Ma; Urbanek et al., 2002). A recent detailed study by Schneider et al. (2013) using texturally controlled in situ $^{40}Ar/^{39}Ar$ dating of syn-kinematic phengite and K-feldspar returned ages of 33–15, 24–12 and 20–7 Ma. They were interpreted as recording deformation along three major shear zones (ASZ, TSZ and GSZ, respectively) of the western subdome.

Sample location

Fissure monazite is rare and difficult to find, meaning that this study could not have been conducted without the help of crystal searchers who provided samples. Fissure monazites were selected to cover all parts of the TW areas with known shear zones within it. It was, however, unfortunately not possible to obtain exact coordinates for all of the samples (Table 1). This is due to the rarity of fissure monazite, so that some samples were obtained from old finds or collections. In other cases, the crystal searcher could not anymore precisely identify the fissure in which the monazite was found. These samples are marked with "approx." in Table 1. We could therefore only revisit some of the sample locations in order to add structural information. Experience from other parts of the Alps (e.g. Bergemann et al., 2017, 2019; Ricchi et al., 2019) shows that fissure monazite sampled within the damage or central zones of a shear zone generally records shear zone activity well. Information on the source localities, host rocks, degree of alpine metamorphism and mineral associations is in Table 1.

3 Methods

The crystals were polished individually on a lapidary disc and embedded in epoxy together with the monazite standard "44069" (425 Ma, Aleinikoff et al., 2006), following the same procedure as that in Bergemann et al. (2017). Backscatter electron (BSE) images were acquired in order to investigate the internal textural features of each grain (e.g. zoning, evidence of alteration) using an energy dispersive spectrometer (EDS)-equipped JEOL JSM7001F and a Zeiss DSM940A electron microscope at the University of Geneva with a beam current of 3.5 nA and acceleration voltage of 15 kV. BSE images helped in the selection of secondary-ion mass spectrometry (SIMS) spot analysis points, carefully placed in chemically distinct domains.

Ion probe U-Th-Pb analyses of 15 monazite crystals were conducted at the SwissSIMS ion microprobe facility, University of Lausanne, Switzerland, and analyses of another eight crystals were performed at the NordSIMS facility, Swedish Museum of Natural History, Stockholm (Tables 1 and 3). Both laboratories are equipped with a Cameca IMS 1280-HR instrument. The instruments were run following the procedure of Janots et al. (2012), applying a -13 kV O^{2-} primary beam, an intensity of ~ 3 and 6 nA focused on the sample (SwissSIMS and NordSIMS, respectively) to produce a spot of 15–20 µm in diameter. A mass resolution of 4300–5000 ($M/\Delta M$, $^{208}Pb/^{232}Th$ at 10 % peak height) and an energy window at 40 eV were applied, with data collection in peak hopping mode using an ion-counting electron multiplier. All the unknowns were standardized to 44069 (425 Ma; Aleinikoff et al., 2006) monazite, and the uncertainty on the standard $^{208}Pb/^{232}Th$-ThO / Th calibration in each session was 1.7 % on average.

A ^{207}Pb and ^{204}Pb common lead (Pbc) correction calculated at time zero was applied to the data acquired at the SwissSIMS and NordSIMS (Table 3) using the terrestrial Pb evolution model of Stacey and Kramers (1975). Cameca customizable ion probe software (CIPS) was used for data reduction. ^{204}Pb- and ^{207}Pb-corrected ages agree within uncertainty (Table 3), but we preferred to discuss ^{207}Pb-corrected ages because they are more robust and consistent (better statistics and less scatter in the data). Calculation of weighted mean ages, based on ^{207}Pb correction, and plotting was carried out using the IsoPlot Ex 4.1 programme (Ludwig, 2003). Single and weighted mean ages (or average ages) are quoted at the 1σ and at the 95 % confidence level in the text, respectively.

Weighted mean $^{208}Pb/^{232}Th$ ages were calculated for each growth domain following the approach of Bergemann et al. (2017, 2018, 2019, 2020) and Ricchi et al. (2019). Distinct chemical and textural domains were carefully defined in each grain based on Th concentrations as function of U concentrations and BSE image information. Since fissure monazite is dissolved and re-precipitated under changing chemical conditions (e.g. Grand'Homme et al., 2018), spot analyses affected by Pbc (resulting in older dates directly related to higher Pbc, i.e. positive age-f208 correlation), inclusions or those with high uncertainty ($1\sigma > 1$ abs.) were removed from the dataset and marked in italic in Table 3. However, spot dates located on dissolution trails, generally providing younger dates, were considered in the age ranges because they likely record a later phase of monazite crystallization.

4 Results

4.1 Field observations

An example of deformed fissures and different stages of fissure formation is well exposed in outcrops along the road leading to Pfitscherjoch (in proximity to the PFIT1 sample locality 5, western TW; Table 1), where two fissure generations are present (Fig. 2a and b). In this outcrop, an earlier fissure generation (C_2, green ellipses) is partly deformed during subsequent deformation, and a younger generation of fissures (C_3, blue ellipses) is also present. Subhorizontal fissures (C_3) seem linked to a strongly inclined lineation (L_3, blue arrows), whereas older subvertical fissures (C_2) seem related to a weakly inclined strike-slip lineation (L_2, green arrows). The older fissures are wider and sigmoidal in shape and contain muscovite which is not found in the younger fissures. In some cases, younger fissures crosscut older ones (Fig. 2b). Moreover, the orientation of the foliation ($S_{2,3}$; Fig. 2c) of these two fissure generations (C_2 and C_3) is different from the foliation (S_1; Fig. 2c) of early fissure formation mainly observed in the eastern part of the TW (C_1, Fig. 2c, discussed below). This suggests that, in the Pfitscherjoch area, early fissures C_1 were overprinted by younger tectonic movements.

The large majority of the fissures present in all the investigated localities are oriented subvertically (C_1 and C_2 type in Fig. 2c), roughly striking NE–SW. For C_2, this would indicate a similar direction of extension for the development of this fissure type, which is in line with palaeostress orientations provided by Bertrand et al. (2015). However, even if all subvertical fissures are subparallel, at least two generations exist. (i) Early subvertical fissures (C_1, Fig. 2c) are re-

Table 3. Th-U-Pb analyses of monazite by ion microprobe (SwissSIMS and NordSIMS). Analyses resulting in unreliable dates (e.g. presence of cracks, affected by Pbc causing high uncertainty) were not considered and are written in italic.

												204-corr		204-corr spot ages		207-corr		207-corr spot ages	
Groups	Analysis ID	U (ppm)	Th (ppm)	Th / U	^{208}Pb / ^{204}Pb	1σ (%)	^{207}Pb / ^{206}Pb	1σ (%)	^{208}Pb / ^{232}Th	1σ (%)	f208 from 207 (%)	^{208}Pb / ^{232}Th	1σ (%)	^{208}Pb / ^{232}Th Age (Ma)	1σ (abs.)	^{208}Pb / ^{232}Th	1σ (%)	^{208}Pb / ^{232}Th Age (Ma)	1σ (abs.)
Western Tauern Window																			
	INNB1@01	258	8810	34	180	11	0.359	3.0	0.000621	1.4	13	0.000514	2.7	10.39	0.29	0.000543	1.5	10.97	0.16
	INNB1@02	397	26461	67	497	10	0.253	2.8	0.000592	1.6	4	0.000560	1.7	11.32	0.19	0.000570	1.6	11.52	0.18
	INNB1@03	341	19205	56	421	11	0.280	3.0	0.000589	1.4	5	0.000547	1.6	11.05	0.18	0.000561	1.4	11.34	0.16
	INNB1@04	1098	8717	8	202	12	0.158	2.7	0.000607	1.6	12	0.000536	2.8	10.83	0.31	0.000534	1.6	10.80	0.18
	INNB1@05	924	23297	25	421	10	0.216	2.3	0.000552	1.8	7	0.000518	1.9	10.47	0.20	0.000516	1.8	10.43	0.18
	INNB1@06	883	24902	28	364	9	0.215	2.3	0.000557	1.4	6	0.000514	1.7	10.39	0.17	0.000521	1.4	10.54	0.15
	INNB1@07	923	10635	12	200	11	0.194	2.6	0.000594	1.6	12	0.000508	2.6	10.26	0.27	0.000521	1.6	10.53	0.17
	INNB1@08	*1217*	*15622*	*13*	*283*	*13*	*0.228*	*2.7*	*0.000466*	*5.1*	*13*	*0.000433*	*5.1*	*8.74*	*0.45*	*0.000406*	*5.1*	*8.21*	*0.42*
A	ZEI1@01	84	2630	31	393	21	0.202	5.2	0.000515	2.6	6	0.000465	3.1	9.39	0.29	0.000485	2.7	9.80	0.26
	ZEI1@04	75	2041	27	408	25	0.196	5.8	0.000509	3.0	6	0.000475	3.8	9.60	0.36	0.000477	3.0	9.65	0.29
	ZEI1@06	147	2086	14	251	18	0.185	4.2	0.000558	2.6	9	0.000485	3.6	9.79	0.36	0.000505	2.7	10.20	0.28
	ZEI1@07	185	2785	15	547	24	0.159	4.4	0.000524	2.6	7	0.000503	3.2	10.16	0.32	0.000487	2.7	9.84	0.26
	ZEI1@08	189	2292	12	316	21	0.185	4.2	0.000519	2.7	10	0.000456	3.5	9.21	0.32	0.000465	2.7	9.39	0.26
	ZEI1@10	198	3078	16	421	20	0.143	4.0	0.000542	2.7	7	0.000493	3.0	9.96	0.30	0.000505	2.7	10.21	0.27
	ZEI1@11	107	1820	17	298	20	0.180	4.6	0.000546	2.6	9	0.000475	3.5	9.60	0.34	0.000496	2.7	10.03	0.27
	ZEI1@13	230	5870	26	559	15	0.163	3.2	0.000558	2.6	5	0.000519	2.6	10.49	0.28	0.000532	2.6	10.75	0.28
	ZEI1@14	226	4846	21	532	18	0.153	3.8	0.000542	2.6	5	0.000509	2.8	10.29	0.29	0.000514	2.6	10.38	0.27
	ZEI1@15	284	4694	16	412	16	0.204	3.4	0.000523	2.7	8	0.000474	2.8	9.58	0.27	0.000482	2.7	9.75	0.26
	ZEI1@16	192	3057	16	422	18	0.158	3.7	0.000553	2.6	7	0.000506	2.9	10.23	0.30	0.000513	2.7	10.37	0.28
	ZEI1@17	200	3756	19	282	14	0.234	3.1	0.000561	2.7	11	0.000484	3.0	9.79	0.30	0.000500	2.7	10.11	0.28
	ZEI1@19	325	1152	4	188	22	0.114	3.8	0.000622	3.3	18	0.000495	5.2	10.00	0.52	0.000513	3.6	10.37	0.38
	ZEI1@20	391	2715	7	485	27	0.094	4.6	0.000533	2.8	6	0.000491	3.3	9.91	0.33	0.000499	2.8	10.09	0.28
	ZEI1@21	115	7335	64	555	15	0.219	4.3	0.000509	2.6	3	0.000476	2.7	9.62	0.26	0.000492	2.6	9.95	0.26
	ZEI1@22	74	9153	124	780	15	0.281	4.0	0.000509	2.8	3	0.000484	2.7	9.78	0.27	0.000495	2.8	10.01	0.28
	ZEI1@24	58	4809	82	617	19	0.235	4.7	0.000523	2.2	3	0.000491	2.4	9.91	0.24	0.000507	2.2	10.24	0.23
	ZEI1@25	60	5152	86	670	21	0.230	4.8	0.000485	2.3	3	0.000459	2.5	9.28	0.23	0.000470	2.3	9.49	0.22
	ZEI1@26	70	8182	117	609	18	0.255	4.8	0.000499	2.3	3	0.000468	2.4	9.45	0.23	0.000486	2.3	9.81	0.22
	ZEI1@27	207	6179	30	565	21	0.109	4.4	0.000485	2.3	3	0.000455	2.6	9.19	0.24	0.000471	2.3	9.52	0.22
B	ZEI1@02	99	2499	25	352	23	0.194	6.0	0.000451	2.8	6	0.000402	3.6	8.12	0.29	0.000423	2.8	8.56	0.24
	ZEI1@03	130	2246	17	663	41	0.177	7.7	0.000378	2.7	6	0.000356	3.5	7.19	0.25	0.000355	2.8	7.18	0.20
	ZEI1@05	45	2301	51	447	26	0.286	5.9	0.000468	3.1	7	0.000434	3.7	8.78	0.33	0.000436	3.2	8.82	0.28
	ZEI1@09	325	2860	9	615	35	0.127	6.4	0.000429	2.7	6	0.000402	3.4	8.12	0.27	0.000403	2.8	8.15	0.22
	ZEI1@12	117	1943	17	312	24	0.139	5.4	0.000394	2.7	8	0.000352	3.9	7.12	0.28	0.000361	2.7	7.30	0.20
	ZEI1@18	258	3058	12	393	25	0.127	5.0	0.000398	2.6	8	0.000365	3.5	7.37	0.26	0.000365	2.7	7.38	0.20
	ZEI1@23	78	6403	82	744	20	0.307	4.7	0.000464	2.6	4	0.000440	2.7	8.89	0.24	0.000447	2.6	9.03	0.24
A	SCHR1@01	423	37708	89	1766	6	0.126	2.4	0.001025	2.19	1	0.001011	2.2	20.42	0.44	0.001016	2.2	20.53	0.45
	SCHR1@02	499	36495	73	2194	8	0.124	2.7	0.001012	2.51	1	0.001004	2.5	20.29	0.51	0.001004	2.5	20.28	0.51
	SCHR1@03	417	45163	108	1969	5	0.132	2.2	0.001090	2.18	1	0.001079	2.2	21.80	0.47	0.001082	2.2	21.85	0.48
	SCHR1@04	438	43245	99	1960	6	0.142	2.3	0.001048	2.18	1	0.001038	2.2	20.97	0.45	0.001039	2.2	20.98	0.46
	SCHR1@05	465	37059	80	2172	7	0.126	2.5	0.001016	2.18	1	0.001006	2.2	20.32	0.44	0.001007	2.2	20.35	0.44
	SCHR1@06	443	46170	104	1859	5	0.137	2.3	0.001064	2.20	1	0.001051	2.2	21.24	0.46	0.001056	2.2	21.33	0.47
B	SCHR1@07	509	24001	47	1168	6	0.160	2.0	0.001037	2.18	2	0.001009	2.1	20.38	0.43	0.001013	2.2	20.47	0.45
	SCHR1@08	482	25025	52	1167	6	0.158	2.0	0.001060	2.20	2	0.001033	2.2	20.88	0.45	0.001037	2.2	20.95	0.46
	SCHR1@09	478	26320	55	1119	6	0.167	1.9	0.001040	2.19	2	0.001012	2.1	20.44	0.44	0.001016	2.2	20.54	0.45
	SCHR1@10	510	28255	55	1211	6	0.168	2.0	0.001051	2.17	2	0.001026	2.1	20.72	0.44	0.001030	2.2	20.81	0.45
	SCHR1@11	465	26453	57	1145	6	0.169	1.8	0.001076	2.18	2	0.001053	2.1	21.28	0.46	0.001052	2.2	21.25	0.46
	SCHR1@12	331	27180	82	1099	6	0.212	2.0	0.001043	2.18	2	0.001018	2.1	20.57	0.44	0.001020	2.2	20.60	0.45
	SCHR1@13	312	28957	93	1243	6	0.233	2.0	0.001052	2.19	2	0.001028	2.1	20.76	0.44	0.001027	2.2	20.75	0.45
	SCHR1@14	316	29632	94	1200	6	0.239	2.1	0.001031	2.22	2	0.001004	2.2	20.29	0.44	0.001008	2.2	20.37	0.45
	SCHR1@15	331	31105	94	1151	5	0.247	2.1	0.001016	2.21	2	0.000993	2.2	20.05	0.43	0.000993	2.2	20.07	0.44
	SCHR1@16	471	25641	54	1676	7	0.132	2.3	0.001020	2.19	1	0.001004	2.2	20.27	0.44	0.001005	2.2	20.31	0.44
	SCHR1@17	477	28482	60	1358	6	0.151	2.3	0.001020	2.20	2	0.001001	2.2	20.23	0.44	0.001005	2.2	20.30	0.45
	SCHR1@18	480	18234	38	1599	9	0.119	2.5	0.000998	2.21	2	0.000976	2.2	19.72	0.43	0.000981	2.2	19.83	0.44
	SCHR1@19	492	18252	37	1339	8	0.116	2.5	0.001004	2.21	2	0.000981	2.2	19.81	0.43	0.000988	2.2	19.95	0.44
	SCHR1@20	506	18432	36	1461	8	0.117	2.5	0.000992	2.25	2	0.000973	2.2	19.66	0.44	0.000976	2.3	19.72	0.44
	SCHR1@21	443	21802	49	1500	8	0.134	2.4	0.000997	2.19	2	0.000979	2.2	19.78	0.43	0.000980	2.2	19.81	0.43
	SCHR1@22	453	24816	55	1475	7	0.149	2.4	0.001007	2.18	2	0.000991	2.2	20.03	0.43	0.000991	2.2	20.01	0.44

Table 3. Continued.

												204-corr		204-corr spot ages		207-corr		207-corr spot ages	
Groups	Analysis ID	U (ppm)	Th (ppm)	Th / U	^{208}Pb / ^{204}Pb	1σ (%)	^{207}Pb / ^{206}Pb	1σ (%)	^{208}Pb / ^{232}Th	1σ (%)	f208 from 207 (%)	^{208}Pb / ^{232}Th	1σ (%)	^{208}Pb / ^{232}Th Age (Ma)	1σ (abs.)	^{208}Pb / ^{232}Th	1σ (%)	^{208}Pb / ^{232}Th Age (Ma)	1σ (abs.)
Western Tauern Window																			
C	SCHR1@23	211	16187	77	921	7	0.323	2.4	0.000994	2.42	4	0.000957	2.3	19.34	0.45	0.000954	2.4	19.27	0.47
	SCHR1@24	306	17861	58	513	5	0.371	2.0	0.001025	2.39	6	0.000960	2.3	19.39	0.44	0.000963	2.4	19.45	0.47
	SCHR1@25	363	17322	48	546	6	0.370	2.3	0.001036	2.65	6	0.000968	2.5	19.55	0.49	0.000975	2.7	19.70	0.52
	SCHR1@26	447	17105	38	1579	11	0.168	3.8	0.001047	3.28	2	0.001027	3.2	20.74	0.67	0.001029	3.3	20.78	0.68
	SCHR1@27	351	18354	52	1635	10	0.177	3.3	0.000973	2.75	2	0.000954	2.7	19.28	0.52	0.000955	2.8	19.30	0.53
	SCHR1@28	499	18145	36	1394	11	0.215	3.5	0.001031	3.21	3	0.001006	3.1	20.33	0.64	0.001004	3.2	20.28	0.65
	MAYR4@01	259	5113	20	514	18	0.127	3.3	0.000567	1.3	4	0.000527	1.8	10.65	0.19	0.000542	1.3	10.95	0.14
	MAYR4@02	340	3449	10	341	19	0.120	3.5	0.000527	1.5	6	0.000468	2.5	9.45	0.23	0.000493	1.5	9.96	0.15
	MAYR4@03	336	3763	11	305	17	0.109	3.6	0.000541	1.5	5	0.000476	2.5	9.62	0.24	0.000512	1.5	10.35	0.15
	MAYR4@04	368	3691	10	424	21	0.114	3.8	0.000496	1.6	6	0.000451	2.4	9.12	0.22	0.000467	1.7	9.44	0.16
	MAYR4@05	311	2301	7	246	17	0.135	3.0	0.000636	1.9	11	0.000536	3.1	10.84	0.34	0.000565	2.0	11.41	0.23
	MAYR4@06	385	1190	3	189	21	0.097	3.2	0.000618	2.3	15	0.000504	4.8	10.19	0.49	0.000524	2.6	10.58	0.28
	MAYR4@07	136	6949	51	411	13	0.294	2.8	0.000601	1.2	7	0.000544	1.6	10.99	0.18	0.000561	1.2	11.33	0.13
	MAYR4@08	192	5038	26	370	15	0.224	2.9	0.000599	1.2	8	0.000536	1.9	10.84	0.21	0.000553	1.3	11.17	0.14
	MAYR4@09	201	4829	24	293	13	0.233	2.7	0.000602	1.4	9	0.000522	2.1	10.55	0.22	0.000547	1.4	11.06	0.16
	MAYR4@10	251	4665	19	427	16	0.139	3.2	0.000600	1.2	5	0.000553	1.9	11.17	0.21	0.000568	1.3	11.48	0.15
	MAYR4@11	334	1748	5	300	24	0.103	3.4	0.000511	2.2	14	0.000446	3.7	9.00	0.33	0.000442	2.4	8.93	0.21
	MAYR4@12	295	2169	7	229	18	0.112	3.5	0.000582	2.0	9	0.000491	3.5	9.92	0.35	0.000531	2.1	10.72	0.22
	MAYR4@13	81	5010	62	404	16	0.335	3.4	0.000627	1.3	7	0.000574	1.9	11.60	0.23	0.000584	1.3	11.80	0.15
	MAYR4@14	103	5475	53	381	14	0.289	3.3	0.000602	1.2	6	0.000541	1.8	10.92	0.20	0.000564	1.2	11.39	0.13
	MAYR4@15	94	6085	65	457	15	0.274	3.6	0.000545	1.4	5	0.000499	1.8	10.09	0.18	0.000519	1.4	10.48	0.15
	MAYR4@16	122	6082	50	486	15	0.236	3.5	0.000546	1.0	4	0.000503	1.5	10.16	0.15	0.000522	1.0	10.56	0.11
	MAYR4@17	134	5776	43	381	14	0.270	3.1	0.000553	0.9	6	0.000497	1.6	10.04	0.16	0.000519	1.0	10.50	0.10
	MAYR4@18	180	4227	23	351	14	0.200	3.0	0.000603	1.1	7	0.000543	1.9	10.96	0.21	0.000561	1.1	11.34	0.12
A	PFIT1@12	103	11683	114	554	6	0.387	2.6	0.000852	2.19	5	0.000809	2.1	16.34	0.35	0.000813	2.2	16.42	0.36
	PFIT1@13	112	18466	165	580	5	0.450	2.4	0.000891	2.29	4	0.000845	2.2	17.06	0.38	0.000852	2.3	17.21	0.39
	PFIT1@14	117	13986	120	569	5	0.413	2.4	0.000918	2.31	5	0.000868	2.2	17.54	0.39	0.000874	2.3	17.66	0.41
	PFIT1@15	104	13449	130	473	5	0.430	2.3	0.000895	2.41	5	0.000835	2.3	16.87	0.39	0.000849	2.4	17.15	0.41
	PFIT1@16	65	15956	244	629	5	0.497	2.8	0.000913	2.26	4	0.000877	2.2	17.72	0.39	0.000881	2.3	17.80	0.40
	PFIT1@17	78	13368	171	586	7	0.506	3.3	0.000877	2.25	4	0.000833	2.2	16.82	0.37	0.000843	2.3	17.03	0.38
	PFIT1@18	79	12054	153	662	7	0.365	3.6	0.000892	2.40	3	0.000859	2.4	17.35	0.41	0.000866	2.4	17.49	0.42
	PFIT1@19	121	9937	82	697	10	0.328	4.6	0.000896	2.19	3	0.000856	2.2	17.29	0.38	0.000869	2.2	17.57	0.39
	PFIT1@20	119	8358	70	871	11	0.287	4.9	0.000885	2.19	3	0.000853	2.2	17.23	0.37	0.000862	2.2	17.42	0.38
	PFIT1@01	*30*	*5962*	*199*	*808*	*12*	*0.360*	*5.4*	*0.000658*	*2.29*	*3*	*0.000631*	*2.3*	*12.74*	*0.29*	*0.000640*	*2.3*	*12.94*	*0.30*
	PFIT1@02	*32*	*6627*	*209*	*723*	*10*	*0.350*	*5.0*	*0.000754*	*2.25*	*2*	*0.000721*	*2.2*	*14.57*	*0.32*	*0.000736*	*2.3*	*14.86*	*0.34*
	PFIT1@03	*13*	*5940*	*466*	*1033*	*11*	*0.414*	*6.9*	*0.000824*	*2.24*	*1*	*0.000808*	*2.2*	*16.33*	*0.37*	*0.000814*	*2.2*	*16.45*	*0.37*
	PFIT1@04	*36*	*6027*	*166*	*859*	*13*	*0.317*	*5.7*	*0.000705*	*2.28*	*3*	*0.000681*	*2.3*	*13.77*	*0.31*	*0.000687*	*2.3*	*13.88*	*0.32*
	PFIT1@05	*84*	*8610*	*102*	*1011*	*19*	*0.389*	*7.1*	*0.000710*	*3.39*	*4*	*0.000690*	*3.4*	*13.94*	*0.47*	*0.000685*	*3.4*	*13.84*	*0.47*
	PFIT1@11	*110*	*13146*	*119*	*548*	*6*	*0.428*	*2.7*	*0.000800*	*2.18*	*4*	*0.000756*	*2.1*	*15.28*	*0.32*	*0.000764*	*2.2*	*15.43*	*0.34*
B	PFIT1@06	245	5464	22	525	10	0.155	3.0	0.000697	2.20	6	0.000664	2.2	13.42	0.30	0.000658	2.2	13.30	0.29
	PFIT1@07	336	4523	13	381	11	0.161	3.6	0.000706	2.33	6	0.000642	2.4	12.98	0.31	0.000661	2.3	13.35	0.31
	PFIT1@08	347	3300	10	314	12	0.201	3.5	0.000728	2.21	11	0.000647	2.4	13.07	0.32	0.000648	2.3	13.09	0.30
	PFIT1@09	383	3220	8	343	13	0.170	3.9	0.000704	2.21	9	0.000636	2.5	12.86	0.32	0.000638	2.3	12.89	0.29
	PFIT1@10	388	2889	7	238	11	0.190	3.7	0.000740	2.33	12	0.000641	2.8	12.95	0.36	0.000650	2.4	13.13	0.32
	BURG2@07	30	769	26	193	20	0.165	4.7	0.000732	2.3	10	0.000585	4.4	11.83	0.53	0.000659	2.4	13.32	0.31
	BURG2@08	18	1014	57	219	16	0.306	3.6	0.000959	2.2	12	0.000790	3.4	15.97	0.54	0.000844	2.3	17.06	0.39
	BURG2@09	53	626	12	275	24	0.087	5.1	0.000797	2.3	6	0.000685	3.9	13.85	0.54	0.000751	2.4	15.17	0.36
	BURG2@10	30	1067	36	324	19	0.179	4.1	0.000878	2.3	7	0.000774	3.0	15.63	0.47	0.000818	2.3	16.53	0.38
	BURG2@13	164	529	3	403	55	0.112	7.5	0.000683	2.3	12	0.000660	6.5	13.35	0.86	0.000600	2.8	12.12	0.33
	BURG2@12	*52*	*2273*	*44*	*69*	*18*	*0.415*	*3.7*	*0.001048*	*8.6*	*46*	*0.000462*	*10.7*	*9.34*	*1.00*	*0.000571*	*9.5*	*11.53*	*1.10*

Table 3. Continued.

Groups	Analysis ID	U (ppm)	Th (ppm)	Th / U	$^{208}Pb / ^{204}Pb$	1σ (%)	$^{207}Pb / ^{206}Pb$	1σ (%)	$^{208}Pb / ^{232}Th$	1σ (%)	f208 from 207 (%)	204-corr $^{208}Pb / ^{232}Th$	204-corr 1σ (%)	204-corr spot ages $^{208}Pb / ^{232}Th$ Age (Ma)	204-corr spot ages 1σ (abs.)	207-corr $^{208}Pb / ^{232}Th$	207-corr 1σ (%)	207-corr spot ages $^{208}Pb / ^{232}Th$ Age (Ma)	207-corr spot ages 1σ (abs.)
Western Tauern Window																			
A	PLAN1@01	190	1647	9	56	9	0.577	2.2	0.001582	3.1	63	0.000706	6.9	14.27	0.98	0.000580	5.1	11.73	0.60
	PLAN1@02	177	12498	71	284	11	0.361	2.9	0.000643	1.4	9	0.000585	2.1	11.81	0.25	0.000587	1.5	11.86	0.17
	PLAN1@03	209	2322	11	56	8	0.620	1.9	0.001634	3.3	63	0.000578	5.5	11.67	0.64	0.000605	4.7	12.23	0.57
	PLAN1@04	410	3160	8	101	12	0.269	2.8	0.000788	2.2	28	0.000583	5.4	11.78	0.63	0.000565	2.6	11.41	0.29
	PLAN1@05	438	1542	4	59	11	0.261	2.7	0.001043	3.3	45	0.000489	7.9	9.88	0.78	0.000574	4.5	11.61	0.52
	PLAN1@06	458	1687	4	58	10	0.377	2.4	0.001231	6.5	55	0.000575	8.0	11.62	0.93	0.000550	7.5	11.11	0.84
	PLAN1@07	462	2662	6	90	12	0.284	2.5	0.000864	4.0	40	0.000635	6.3	12.83	0.81	0.000520	4.5	10.50	0.47
	PLAN1@08	509	3332	7	104	14	0.242	3.3	0.000751	2.3	24	0.000607	6.0	12.26	0.74	0.000569	2.7	11.50	0.31
	PLAN1@09	594	4167	7	101	12	0.238	2.9	0.000690	2.4	24	0.000501	5.1	10.12	0.51	0.000522	2.6	10.55	0.28
	PLAN1@10	774	5878	8	148	12	0.190	2.8	0.000661	2.1	17	0.000557	3.9	11.26	0.44	0.000550	2.2	11.11	0.25
	PLAN1@13	1215	1759	1	68	12	0.136	2.5	0.000967	5.4	41	0.000576	8.2	11.65	0.96	0.000567	6.6	11.45	0.75
	PLAN1@14	589	4750	8	176	14	0.167	3.2	0.000680	1.5	15	0.000581	3.7	11.73	0.43	0.000579	1.6	11.71	0.19
	PLAN1@15	424	3653	9	98	11	0.233	2.9	0.000783	1.8	22	0.000624	5.1	12.61	0.65	0.000610	2.0	12.32	0.25
	PLAN1@16	448	3567	8	86	10	0.288	2.4	0.000869	2.9	30	0.000596	5.2	12.04	0.63	0.000611	3.2	12.35	0.39
	PLAN1@17	454	3815	8	108	11	0.198	3.0	0.000744	1.9	18	0.000566	4.7	11.44	0.54	0.000608	2.1	12.28	0.26
	PLAN1@18	443	4422	10	161	13	0.250	2.7	0.000763	3.9	21	0.000670	4.9	13.53	0.67	0.000600	4.0	12.13	0.48
	PLAN1@19	365	10351	28	214	10	0.305	2.7	0.000685	1.8	11	0.000596	2.5	12.04	0.31	0.000609	1.8	12.30	0.22
	PLAN1@20	467	8041	17	153	9	0.359	2.1	0.000751	1.5	22	0.000606	2.8	12.25	0.34	0.000588	1.6	11.88	0.20
	PLAN1@21	627	6050	10	103	9	0.322	2.0	0.000836	2.0	28	0.000577	3.7	11.66	0.43	0.000600	2.2	12.12	0.27
	PLAN1@23	373	4646	12	715	17	0.102	2.9	0.000645	2.6	4	0.000611	2.7	12.34	0.33	0.000617	2.7	12.46	0.33
	PLAN1@24	390	4664	12	677	18	0.090	3.5	0.000610	2.6	4	0.000576	2.7	11.63	0.31	0.000588	2.7	11.89	0.32
	PLAN1@25	359	5180	14	519	17	0.121	3.0	0.000639	2.7	6	0.000591	2.8	11.94	0.33	0.000598	2.7	12.09	0.32
	PLAN1@26	365	4817	13	401	15	0.116	3.0	0.000627	2.6	6	0.000570	2.8	11.52	0.32	0.000588	2.7	11.88	0.32
	PLAN1@27	476	3538	7	541	19	0.101	2.9	0.000650	2.7	8	0.000603	2.8	12.19	0.35	0.000601	2.7	12.14	0.33
	PLAN1@28	564	8192	15	460	11	0.125	2.3	0.000660	2.6	6	0.000604	2.6	12.21	0.32	0.000622	2.6	12.56	0.33
	PLAN1@29	620	14199	23	619	10	0.130	2.1	0.000637	2.6	4	0.000598	2.6	12.09	0.31	0.000609	2.6	12.32	0.33
	PLAN1@30	528	8241	16	420	13	0.127	2.7	0.000632	2.7	6	0.000574	2.7	11.60	0.31	0.000595	2.7	12.02	0.32
	PLAN1@31	1028	1527	1	124	12	0.090	2.0	0.000802	3.1	26	0.000552	4.4	11.16	0.49	0.000595	3.8	12.02	0.45
	PLAN1@32	1152	1721	1	227	19	0.066	2.7	0.000661	2.7	12	0.000548	4.0	11.08	0.44	0.000579	3.1	11.70	0.36
	PLAN1@33	926	4303	5	361	14	0.085	2.2	0.000642	2.7	8	0.000573	2.8	11.57	0.33	0.000588	2.8	11.87	0.33
	PLAN1@34	623	7966	13	483	12	0.125	2.3	0.000669	2.6	7	0.000615	2.6	12.43	0.32	0.000624	2.6	12.61	0.33
	PLAN1@35	408	6529	16	185	8	0.307	1.7	0.000746	3.1	19	0.000592	3.0	11.97	0.36	0.000605	3.2	12.22	0.39
	PLAN1@36	304	7521	25	427	13	0.182	2.7	0.000646	2.6	7	0.000587	2.7	11.87	0.31	0.000603	2.6	12.19	0.32
	PLAN1@38	580	9607	17	525	14	0.112	2.4	0.000626	2.2	5	0.000580	2.3	11.73	0.27	0.000596	2.2	12.05	0.27
	PLAN1@39	331	10707	32	497	13	0.164	2.7	0.000628	2.2	4	0.000581	2.3	11.74	0.27	0.000600	2.2	12.12	0.27
	PLAN1@40	344	2342	7	311	21	0.143	2.9	0.000698	2.3	15	0.000612	3.3	12.36	0.41	0.000593	2.5	11.98	0.30
	PLAN1@41	487	10698	22	360	11	0.172	2.1	0.000654	2.2	7	0.000584	2.3	11.80	0.27	0.000608	2.3	12.28	0.28
B	PLAN1@11	1410	6659	5	175	20	0.204	4.3	0.000568	2.5	18	0.000578	6.4	11.69	0.74	0.000464	2.8	9.38	0.26
	PLAN1@12	1310	7371	6	160	23	0.206	5.3	0.000467	2.1	18	0.000509	7.9	10.28	0.81	0.000384	2.5	7.75	0.19
	PLAN1@37	619	3146	5	312	20	0.085	2.7	0.000555	2.6	11	0.000493	3.5	9.96	0.34	0.000492	2.7	9.94	0.27
	PLAN1@22	*733*	*1514*	*2*	*52*	*9*	*0.291*	*2.1*	*0.001227*	*7.7*	*60*	*0.000544*	*8.3*	*10.99*	*0.92*	*0.000491*	*9.1*	*9.91*	*0.90*
Central Tauern Window																			
A	SCHEI1@16	408	58860	144	1205	6	0.181	1.8	0.000876	2.6	1	0.000849	2.6	17.14	0.44	0.000864	2.6	17.46	0.46
	SCHEI1@17	304	61361	202	1483	7	0.210	1.9	0.000939	2.6	1	0.000915	2.6	18.49	0.48	0.000928	2.6	18.75	0.50
	SCHEI1@18	265	60179	227	1432	6	0.235	1.9	0.000949	2.6	1	0.000924	2.6	18.66	0.48	0.000937	2.6	18.93	0.50
	SCHEI1@20	311	62554	201	1416	7	0.222	2.0	0.000906	2.7	1	0.000881	2.6	17.81	0.46	0.000893	2.7	18.05	0.48
B	SCHEI1@11	394	53473	136	780	7	0.309	2.0	0.000868	1.4	3	0.000829	1.4	16.75	0.23	0.000842	1.4	17.02	0.23
	SCHEI1@12	434	47204	109	857	9	0.268	2.2	0.000886	1.4	3	0.000855	1.4	17.28	0.24	0.000862	1.4	17.41	0.24
	SCHEI1@13	360	50556	140	639	8	0.349	2.1	0.000907	1.4	3	0.000861	1.4	17.39	0.24	0.000876	1.4	17.71	0.24
	SCHEI1@14	321	53530	167	655	7	0.402	1.9	0.000911	1.4	4	0.000863	1.4	17.45	0.24	0.000876	1.4	17.69	0.25
	SCHEI1@32	291	55126	189	1026	6	0.303	1.5	0.000868	2.8	2	0.000836	2.7	16.88	0.46	0.000848	2.8	17.14	0.48

Table 3. Continued.

Groups	Analysis ID	U (ppm)	Th (ppm)	Th / U	^{208}Pb / ^{204}Pb	1σ (%)	^{207}Pb / ^{206}Pb	1σ (%)	^{208}Pb / ^{232}Th	1σ (%)	f208 from 207 (%)	204-corr ^{208}Pb / ^{232}Th	204-corr 1σ (%)	204-corr spot ages ^{208}Pb / ^{232}Th Age (Ma)	204-corr spot ages 1σ (abs.)	207-corr ^{208}Pb / ^{232}Th	207-corr 1σ (%)	207-corr spot ages ^{208}Pb / ^{232}Th Age (Ma)	207-corr spot ages 1σ (abs.)
Central Tauern Window																			
C	SCHEI1@01	776	17285	22	303	8	0.196	2.1	0.000888	1.4	7	0.000802	1.7	16.20	0.27	0.000825	1.4	16.67	0.23
	SCHEI1@02	485	32602	67	655	11	0.283	2.6	0.000843	1.4	4	0.000808	1.5	16.33	0.25	0.000808	1.4	16.33	0.24
	SCHEI1@03	496	23525	47	411	9	0.285	2.2	0.000899	1.4	6	0.000826	1.6	16.70	0.26	0.000844	1.4	17.05	0.25
	SCHEI1@04	619	20187	33	312	10	0.254	2.5	0.000862	1.5	7	0.000797	1.9	16.10	0.31	0.000802	1.5	16.21	0.25
	SCHEI1@05	702	14215	20	252	9	0.255	2.1	0.000929	1.5	11	0.000806	1.9	16.29	0.32	0.000825	1.5	16.66	0.25
	SCHEI1@06	831	11524	14	190	8	0.274	1.7	0.000974	1.8	18	0.000810	2.3	16.36	0.37	0.000800	1.8	16.16	0.30
	SCHEI1@07	545	19842	36	279	8	0.383	1.9	0.000949	1.6	12	0.000839	1.8	16.95	0.31	0.000840	1.6	16.97	0.27
	SCHEI1@08	902	10829	12	216	9	0.220	2.0	0.000979	1.4	14	0.000843	2.1	17.04	0.36	0.000843	1.5	17.03	0.25
	SCHEI1@09	888	10863	12	239	11	0.212	2.3	0.000942	1.8	13	0.000809	2.4	16.35	0.39	0.000819	1.8	16.55	0.31
	SCHEI1@10	1103	20671	19	314	11	0.206	2.6	0.000864	1.5	7	0.000791	2.0	15.98	0.31	0.000801	1.5	16.18	0.24
	SCHEI1@15	427	31409	74	280	6	0.426	1.7	0.000933	1.6	9	0.000818	1.7	16.53	0.28	0.000851	1.6	17.19	0.28
	SCHEI1@19	650	22198	34	1132	11	0.093	2.6	0.000890	2.6	1	0.000860	2.6	17.37	0.45	0.000878	2.6	17.73	0.47
	SCHEI1@21	704	20090	29	1036	10	0.086	2.2	0.000849	2.6	2	0.000818	2.6	16.52	0.42	0.000836	2.6	16.89	0.44
	SCHEI1@22	815	10348	13	1078	15	0.078	2.3	0.000846	2.6	3	0.000818	2.6	16.52	0.43	0.000825	2.6	16.66	0.44
	SCHEI1@23	417	36731	88	1703	12	0.133	2.8	0.000865	2.6	1	0.000847	2.6	17.11	0.44	0.000855	2.6	17.28	0.45
	SCHEI1@24	656	16727	25	1183	11	0.083	2.3	0.000848	2.6	2	0.000821	2.6	16.59	0.43	0.000834	2.6	16.86	0.44
	SCHEI1@27	720	19708	27	976	10	0.108	2.0	0.000831	2.6	3	0.000798	2.6	16.13	0.41	0.000809	2.6	16.35	0.43
	SCHEI1@28	420	36082	86	1062	9	0.169	2.4	0.000860	2.6	2	0.000829	2.6	16.76	0.43	0.000846	2.6	17.08	0.45
	SCHEI1@29	513	37241	73	665	9	0.231	2.2	0.000854	2.6	4	0.000804	2.5	16.25	0.41	0.000823	2.6	16.64	0.44
	SCHEI1@30	588	23098	39	738	10	0.122	2.3	0.000808	2.7	3	0.000765	2.6	15.46	0.40	0.000787	2.7	15.89	0.43
	SCHEI1@31	435	37275	86	945	8	0.176	2.0	0.000817	2.6	2	0.000784	2.5	15.84	0.40	0.000800	2.6	16.16	0.43
	SCHEI1@33	678	12021	18	1406	18	0.060	2.6	0.000800	2.2	1	0.000778	2.2	15.73	0.35	0.000792	2.2	16.00	0.36
	SCHEI1@34	996	8782	9	2159	31	0.056	3.1	0.000807	2.3	1	0.000793	2.3	16.02	0.37	0.000796	2.3	16.08	0.37
A	HOPF2@15	82	61530	749	720	4	0.611	2.2	0.000560	2.37	2	0.000542	2.3	10.94	0.25	0.000546	2.4	11.03	0.26
	HOPF2@16	69	33784	490	619	4	0.641	2.6	0.000647	2.36	3	0.000620	2.3	12.54	0.29	0.000625	2.4	12.63	0.30
	HOPF2@17	97	33439	343	972	7	0.571	3.6	0.000663	2.91	2	0.000643	2.8	13.00	0.37	0.000647	2.9	13.08	0.38
	HOPF2@18	77	40713	530	274	3	0.761	1.5	0.000762	2.67	11	0.000667	2.4	13.48	0.32	0.000677	2.7	13.67	0.37
	HOPF2@19	120	62586	520	840	5	0.572	2.8	0.000623	3.49	2	0.000605	3.4	12.23	0.42	0.000609	3.5	12.30	0.43
	HOPF2@20	120	49522	413	853	7	0.590	3.7	0.000594	2.39	3	0.000571	2.3	11.54	0.27	0.000577	2.4	11.67	0.28
	HOPF2@21	173	37157	215	1309	13	0.585	6.1	0.000683	2.78	2	0.000667	2.7	13.47	0.37	0.000667	2.8	13.47	0.38
B	HOPF2@07	49	28763	591	480	5	0.735	2.5	0.000600	2.26	6	0.000559	2.1	11.29	0.24	0.000561	2.3	11.35	0.26
	HOPF2@08	46	28779	627	495	5	0.740	2.3	0.000630	2.20	6	0.000593	2.1	11.98	0.25	0.000592	2.2	11.97	0.26
	HOPF2@09	55	32338	593	429	4	0.721	1.9	0.000649	2.17	7	0.000603	2.1	12.18	0.25	0.000604	2.2	12.20	0.27
	HOPF2@10	76	22645	296	595	9	0.714	4.1	0.000637	3.67	6	0.000597	3.5	12.06	0.42	0.000596	3.7	12.05	0.44
	HOPF2@11	40	28273	701	140	3	0.810	1.2	0.000782	3.59	24	0.000580	2.8	11.72	0.32	0.000597	3.6	12.07	0.43
	HOPF2@12	38	26357	689	346	4	0.780	2.1	0.000694	2.20	9	0.000628	2.1	12.68	0.26	0.000628	2.2	12.69	0.28
	HOPF2@13	52	40578	775	305	3	0.777	1.7	0.000688	2.54	10	0.000615	2.3	12.43	0.29	0.000616	2.5	12.45	0.32
	HOPF2@14	55	27790	505	261	3	0.773	1.6	0.000708	2.22	12	0.000614	2.0	12.41	0.25	0.000626	2.2	12.65	0.28
C	HOPF2@01	40	23096	582	683	6	0.646	3.0	0.000591	2.20	4	0.000565	2.1	11.43	0.24	0.000567	2.2	11.45	0.25
	HOPF2@02	42	25870	612	584	6	0.682	3.3	0.000619	2.23	4	0.000590	2.2	11.92	0.26	0.000594	2.2	11.99	0.27
	HOPF2@03	45	29023	642	538	5	0.659	2.6	0.000647	2.27	4	0.000617	2.2	12.46	0.27	0.000619	2.3	12.50	0.28
	HOPF2@04	50	30246	610	510	4	0.677	2.3	0.000656	2.35	5	0.000621	2.2	12.54	0.28	0.000622	2.3	12.58	0.30
	HOPF2@05	57	32908	577	451	4	0.690	2.1	0.000670	2.48	6	0.000627	2.4	12.67	0.30	0.000629	2.5	12.70	0.32
	HOPF2@06	58	28865	500	481	4	0.680	2.1	0.000642	2.18	6	0.000602	2.1	12.16	0.25	0.000602	2.2	12.17	0.27
A	GART1@07	232	13668	59	1022	10	0.175	2.0	0.000830	2.3	2	0.000799	2.3	16.14	0.36	0.000811	2.3	16.38	0.38
	GART1@08	302	9312	31	523	8	0.208	1.6	0.000831	2.3	6	0.000769	2.3	15.54	0.35	0.000785	2.3	15.85	0.37
	GART1@09	206	14195	69	1054	9	0.173	2.0	0.000815	2.0	2	0.000785	2.0	15.86	0.31	0.000799	2.0	16.14	0.32
	GART1@10	199	17962	90	716	7	0.192	2.1	0.000838	2.1	2	0.000793	2.1	16.01	0.33	0.000823	2.1	16.63	0.36
	GART1@11	221	9789	44	881	12	0.162	2.5	0.000813	2.3	3	0.000778	2.3	15.71	0.36	0.000792	2.3	16.00	0.38
	GART1@22	86	8047	93	412	8	0.321	1.8	0.000889	2.0	6	0.000806	2.0	16.29	0.32	0.000835	2.0	16.86	0.34
	GART1@23	142	9137	65	454	8	0.317	1.8	0.000858	1.9	6	0.000786	1.9	15.88	0.29	0.000810	1.9	16.36	0.31
	GART1@24	133	7292	55	371	8	0.322	1.8	0.000864	2.3	7	0.000774	2.2	15.64	0.35	0.000808	2.3	16.32	0.38
	GART1@25	132	8048	61	435	9	0.318	2.0	0.000855	2.4	6	0.000779	2.3	15.74	0.37	0.000804	2.5	16.24	0.40
	GART1@26	139	9550	69	512	8	0.328	1.8	0.000866	2.1	6	0.000800	2.1	16.17	0.33	0.000816	2.1	16.49	0.35

Table 3. Continued.

												204-corr		204-corr spot ages		207-corr		207-corr spot ages	
Groups	Analysis ID	U (ppm)	Th (ppm)	Th / U	^{208}Pb / ^{204}Pb	1σ (%)	^{207}Pb / ^{206}Pb	1σ (%)	^{208}Pb / ^{232}Th	1σ (%)	f208 from 207 (%)	^{208}Pb / ^{232}Th	1σ (%)	^{208}Pb / ^{232}Th Age (Ma)	1σ (abs.)	^{208}Pb / ^{232}Th	1σ (%)	^{208}Pb / ^{232}Th Age (Ma)	1σ (abs.)
Central Tauern Window																			
B	GART1@01	14	7467	551	446	9	0.626	2.3	0.000807	2.3	6	0.000737	2.3	14.89	0.34	0.000758	2.4	15.32	0.37
	GART1@02	16	11180	718	285	14	0.707	3.8	0.000774	2.3	7	0.000669	2.7	13.51	0.37	0.000716	2.4	14.47	0.35
	GART1@04	28	11198	401	967	11	0.299	3.0	0.000783	2.2	1	0.000752	2.2	15.19	0.33	0.000771	2.2	15.59	0.35
	GART1@05	31	13066	424	1149	11	0.232	3.4	0.000731	3.0	1	0.000707	2.9	14.28	0.42	0.000724	3.0	14.64	0.44
	GART1@17	86	22525	263	679	7	0.397	1.5	0.000854	1.8	4	0.000806	1.8	16.28	0.29	0.000820	1.8	16.56	0.30
	GART1@18	110	23948	218	894	7	0.307	1.7	0.000820	1.8	2	0.000784	1.8	15.84	0.28	0.000799	1.8	16.15	0.30
	GART1@19	14	7182	501	832	14	0.437	3.9	0.000778	2.2	2	0.000742	2.2	14.98	0.32	0.000763	2.2	15.42	0.34
	GART1@20	108	19460	180	740	7	0.321	1.8	0.000828	2.0	3	0.000785	2.0	15.86	0.31	0.000805	2.0	16.26	0.33
	GART1@21	106	23334	220	775	7	0.330	1.6	0.000839	2.0	3	0.000797	2.0	16.10	0.32	0.000816	2.0	16.48	0.34
	GART1@03	*16*	*15175*	*927*	53	*3*	*0.802*	*0.8*	*0.001916*	*11.9*	*62*	*0.000516*	*4.1*	*10.43*	*0.43*	*0.000729*	*17.7*	*14.72*	*2.61*
	GART1@04	*19*	*13099*	*696*	69	*4*	*0.810*	*1.0*	*0.001303*	*7.8*	*48*	*0.000571*	*4.2*	*11.53*	*0.48*	*0.000679*	*12.9*	*13.72*	*1.76*
	GART1@06	*93*	*12315*	*133*	2322	*26*	*0.182*	*6.4*	*0.000453*	*4.0*	*1*	*0.000446*	*3.9*	*9.01*	*0.35*	*0.000450*	*4.0*	*9.09*	*0.36*
A	NOWA3@01	99	7183	73	397	10	0.433	2.1	0.000894	4.3	9	0.000807	4.0	16.31	0.65	0.000809	4.3	16.35	0.71
	NOWA3@02	111	7973	72	205	7	0.569	1.8	0.000864	3.8	15	0.000704	3.4	14.23	0.48	0.000733	3.8	14.80	0.57
	NOWA3@03	95	10612	112	506	9	0.474	2.1	0.000852	3.8	7	0.000787	3.6	15.90	0.57	0.000793	3.8	16.03	0.61
	NOWA3@04	93	10175	109	103	5	0.724	1.2	0.001132	5.8	37	0.000707	4.1	14.29	0.58	0.000713	5.9	14.40	0.84
	NOWA3@05	107	6658	62	94	5	0.695	1.4	0.001145	5.8	38	0.000674	4.1	13.62	0.56	0.000711	5.9	14.37	0.84
	NOWA3@06	146	7715	53	176	9	0.606	2.0	0.000875	5.6	22	0.000683	4.8	13.80	0.66	0.000681	5.6	13.75	0.77
	NOWA3@07	162	4216	26	137	7	0.461	1.6	0.001023	4.8	27	0.000734	4.0	14.84	0.59	0.000743	4.8	15.01	0.72
	NOWA3@09	187	2571	14	81	7	0.445	1.7	0.001077	5.9	36	0.000565	4.4	11.42	0.50	0.000686	5.9	13.86	0.82
	NOWA3@10	178	3925	22	124	7	0.478	1.5	0.001053	6.0	30	0.000726	4.6	14.68	0.68	0.000738	6.0	14.91	0.89
	NOWA3@11	106	5924	56	188	7	0.477	1.8	0.000922	4.7	17	0.000732	4.0	14.80	0.59	0.000761	4.7	15.38	0.72
	NOWA3@22	106	6470	61	1230	19	0.133	3.9	0.000837	1.2	2	0.000811	1.3	16.38	0.22	0.000824	1.2	16.65	0.20
	NOWA3@23	94	9038	96	1036	14	0.300	2.7	0.000864	0.9	4	0.000832	1.0	16.81	0.18	0.000834	0.9	16.85	0.16
	NOWA3@24	100	9053	90	896	14	0.265	3.1	0.000786	1.0	3	0.000752	1.2	15.19	0.18	0.000765	1.1	15.45	0.16
	NOWA3@25	91	7689	84	1010	15	0.176	3.6	0.000857	0.9	2	0.000824	1.0	16.65	0.17	0.000842	0.9	17.01	0.15
B	NOWA3@17	192	9482	50	555	10	0.290	1.7	0.000859	3.7	7	0.000799	3.5	16.15	0.57	0.000799	3.7	16.15	0.61
	NOWA3@18	193	8656	45	388	8	0.288	1.7	0.000838	3.8	8	0.000755	3.5	15.24	0.53	0.000774	3.8	15.64	0.59
	NOWA3@19	179	11023	62	531	9	0.286	1.7	0.000832	3.9	6	0.000771	3.7	15.58	0.57	0.000786	3.9	15.87	0.62
	NOWA3@20	189	10600	56	451	8	0.278	1.7	0.000836	3.9	6	0.000765	3.6	15.45	0.56	0.000786	3.9	15.87	0.62
	NOWA3@21	212	10750	51	225	13	0.368	2.5	0.000907	4.0	17	0.000752	4.0	15.18	0.60	0.000757	4.0	15.30	0.61
C	NOWA3@12	50	12537	253	347	7	0.547	1.8	0.000868	3.9	8	0.000771	3.6	15.58	0.56	0.000796	3.9	16.08	0.63
	NOWA3@13	34	9676	287	371	8	0.556	1.9	0.000839	3.8	8	0.000751	3.5	15.18	0.54	0.000773	3.8	15.62	0.60
	NOWA3@14	39	10246	260	323	8	0.534	2.0	0.000783	3.9	8	0.000689	3.6	13.93	0.50	0.000723	3.9	14.61	0.58
	NOWA3@15	48	11123	231	498	10	0.504	2.1	0.000777	3.8	7	0.000717	3.6	14.48	0.52	0.000726	3.8	14.66	0.56
	NOWA3@16	48	10718	225	349	9	0.590	2.0	0.000745	4.4	9	0.000663	4.0	13.39	0.53	0.000677	4.4	13.68	0.60
	NOWA3@08	*212*	*3097*	*15*	*123*	*8*	*0.375*	*1.7*	*0.001111*	*6.8*	*29*	*0.000763*	*5.3*	*15.41*	*0.81*	*0.000788*	*6.9*	*15.93*	*1.09*
A	GART3@13	85	8547	101	226	9	0.537	2.1	0.000901	2.6	14	0.000747	2.7	15.09	0.41	0.000775	2.6	15.65	0.41
	GART3@14	112	9936	89	207	10	0.541	2.4	0.000879	2.8	14	0.000715	3.0	14.46	0.43	0.000760	2.9	15.36	0.44
	GART3@15	95	9197	97	184	10	0.595	2.1	0.000969	3.9	19	0.000769	3.7	15.54	0.58	0.000781	3.9	15.78	0.62
	GART3@16	94	9295	99	183	9	0.585	1.9	0.000917	3.2	20	0.000723	3.2	14.61	0.47	0.000733	3.3	14.82	0.48
	GART3@17	159	9327	59	179	13	0.621	2.6	0.000881	2.9	25	0.000691	3.7	13.95	0.51	0.000662	3.0	13.38	0.40
	GART3@18	161	8380	52	128	11	0.623	2.6	0.000904	2.9	25	0.000638	4.0	12.90	0.51	0.000676	3.0	13.65	0.41
B	GART3@07	251	11739	47	318	10	0.312	2.1	0.000865	2.8	8	0.000760	2.7	15.36	0.41	0.000794	2.8	16.04	0.44
	GART3@08	318	9593	30	219	11	0.374	2.3	0.000836	2.7	15	0.000689	3.0	13.92	0.41	0.000711	2.7	14.37	0.39
	GART3@09	335	8995	27	220	11	0.379	2.2	0.000858	2.7	17	0.000711	3.0	14.37	0.44	0.000714	2.8	14.43	0.40
	GART3@10	318	9819	31	221	11	0.377	2.2	0.000875	2.8	15	0.000722	3.0	14.58	0.44	0.000745	2.9	15.05	0.43
	GART3@11	387	10683	28	244	13	0.326	2.8	0.000829	2.7	11	0.000703	3.1	14.20	0.44	0.000738	2.7	14.92	0.41
	GART3@12	484	11366	24	210	13	0.388	3.1	0.000864	2.6	12	0.000712	3.3	14.38	0.47	0.000760	2.6	15.35	0.40
	GART3@19	129	5307	41	100	7	0.543	1.7	0.001103	4.2	31	0.000681	3.9	13.75	0.53	0.000756	4.3	15.27	0.65
	GART3@20	251	4358	17	122	10	0.408	2.1	0.000990	3.6	29	0.000676	4.1	13.65	0.56	0.000707	3.7	14.29	0.53
	GART3@21	247	13787	56	218	8	0.411	1.9	0.000901	2.7	12	0.000742	2.7	14.99	0.40	0.000797	2.7	16.09	0.44
	GART3@22	431	10631	25	215	13	0.466	2.5	0.000880	2.6	19	0.000734	3.3	14.83	0.49	0.000712	2.7	14.38	0.39
	GART3@23	240	12846	54	247	10	0.414	2.2	0.000879	2.9	12	0.000745	2.9	15.05	0.44	0.000773	2.9	15.61	0.45
C	GART3@01	114	7936	69	285	12	0.352	2.7	0.000762	2.6	10	0.000659	2.8	13.31	0.37	0.000689	2.6	13.92	0.36
	GART3@03	183	3983	22	100	13	0.392	3.3	0.000778	2.9	23	0.000477	5.4	9.65	0.52	0.000602	3.1	12.17	0.37
	GART3@04	176	3297	19	138	17	0.392	3.3	0.000802	2.9	26	0.000578	5.1	11.67	0.60	0.000595	3.1	12.02	0.37
	GART3@05	123	4784	39	191	14	0.393	2.9	0.000770	2.8	17	0.000614	3.6	12.41	0.44	0.000639	2.8	12.92	0.36
	GART3@06	166	4521	27	197	17	0.374	3.5	0.000763	2.6	17	0.000623	4.0	12.58	0.51	0.000630	2.7	12.72	0.34
	GART3@02	*161*	*3479*	*22*	109	12	*0.449*	*2.6*	0.000824	8.0	*32*	*0.000531*	*6.8*	*10.73*	*0.73*	*0.000558*	*8.1*	*11.28*	*0.91*

Table 3. Continued.

												204-corr		204-corr spot ages		207-corr		207-corr spot ages	
Groups	Analysis ID	U (ppm)	Th (ppm)	Th / U	$^{208}Pb / ^{204}Pb$	1σ (%)	$^{207}Pb / ^{206}Pb$	1σ (%)	$^{208}Pb / ^{232}Th$	1σ (%)	f208 from 207 (%)	$^{208}Pb / ^{232}Th$	1σ (%)	$^{208}Pb / ^{232}Th$ Age (Ma)	1σ (abs.)	$^{208}Pb / ^{232}Th$	1σ (%)	$^{208}Pb / ^{232}Th$ Age (Ma)	1σ (abs.)
Central Tauern Window																			
	STEI2@01	395	15567	39	1346	11	0.106	2.0	0.000873	2.12	2	0.000848	2.1	17.14	0.36	0.000859	2.1	17.36	0.37
	STEI2@02	403	16229	40	1096	10	0.113	2.0	0.000862	2.11	2	0.000833	2.1	16.82	0.35	0.000847	2.1	17.11	0.36
	STEI2@03	417	16643	40	1022	9	0.115	1.9	0.000869	2.04	2	0.000836	2.0	16.89	0.34	0.000854	2.0	17.25	0.35
	STEI2@04	376	17989	48	1436	11	0.097	2.2	0.000854	2.15	1	0.000831	2.1	16.79	0.35	0.000844	2.1	17.05	0.37
	STEI2@05	348	7706	22	844	13	0.101	2.2	0.000860	2.50	3	0.000820	2.5	16.57	0.41	0.000837	2.5	16.92	0.42
	STEI2@06	288	6287	22	700	13	0.125	2.3	0.000892	1.90	4	0.000843	1.9	17.02	0.33	0.000857	1.9	17.32	0.33
	STEI2@07	257	5814	23	556	12	0.176	2.0	0.000915	2.06	6	0.000851	2.1	17.20	0.36	0.000858	2.1	17.34	0.36
	STEI2@08	387	5851	15	730	13	0.090	2.3	0.000874	2.49	3	0.000830	2.5	16.76	0.41	0.000848	2.5	17.13	0.43
	STEI2@09	443	5143	12	649	14	0.080	2.3	0.000859	2.51	3	0.000810	2.5	16.37	0.41	0.000832	2.5	16.82	0.43
	STEI2@10	295	6041	20	689	14	0.118	2.4	0.000875	2.18	3	0.000828	2.2	16.73	0.37	0.000844	2.2	17.06	0.37
	STEI2@11	370	7478	20	1151	15	0.088	2.4	0.000858	2.11	2	0.000829	2.1	16.76	0.35	0.000841	2.1	16.99	0.36
	STEI2@12	548	11690	21	755	10	0.103	1.8	0.000884	1.96	3	0.000838	1.9	16.94	0.33	0.000859	2.0	17.36	0.34
	STEI2@13	579	10095	17	798	11	0.101	1.8	0.000871	2.26	3	0.000829	2.2	16.75	0.37	0.000844	2.3	17.06	0.39
	STEI2@14	601	10283	17	745	10	0.099	1.8	0.000869	2.15	3	0.000824	2.1	16.65	0.35	0.000843	2.2	17.03	0.37
	STEI2@15	352	19439	55	962	9	0.138	2.0	0.000864	1.83	2	0.000829	1.8	16.75	0.30	0.000848	1.8	17.14	0.31
	STEI2@16	455	10595	23	676	10	0.127	1.8	0.000891	2.06	3	0.000840	2.0	16.96	0.34	0.000861	2.1	17.39	0.36
	STEI2@17	387	8068	21	902	13	0.091	2.2	0.000864	2.03	2	0.000827	2.0	16.71	0.34	0.000846	2.0	17.10	0.35
	STEI2@18	348	11391	33	1180	13	0.101	2.5	0.000846	2.09	1	0.000819	2.1	16.55	0.34	0.000835	2.1	16.87	0.35
	STEI2@19	339	12077	36	1048	11	0.095	2.3	0.000876	2.20	1	0.000844	2.2	17.05	0.37	0.000864	2.2	17.45	0.39
	STEI2@20	323	7488	23	943	13	0.084	2.6	0.000871	2.04	1	0.000835	2.0	16.87	0.34	0.000858	2.0	17.33	0.35
A	KNOR1@19	149	12269	82	466	7	0.392	3.5	0.000558	2.34	4	0.000527	2.3	10.64	0.24	0.000535	2.3	10.81	0.25
	KNOR1@20	181	9307	52	285	7	0.488	3.2	0.000587	3.28	11	0.000515	3.1	10.41	0.32	0.000522	3.3	10.55	0.35
	KNOR1@21	239	9337	39	642	13	0.400	5.1	0.000604	3.67	5	0.000574	3.6	11.60	0.42	0.000572	3.7	11.56	0.42
	KNOR1@22	172	8289	48	512	9	0.321	4.1	0.000570	2.76	4	0.000537	2.7	10.86	0.29	0.000545	2.8	11.01	0.30
	KNOR1@24	194	7199	37	605	13	0.268	5.3	0.000549	3.18	4	0.000517	3.1	10.44	0.32	0.000529	3.2	10.68	0.34
B	KNOR1@01	32	7767	246	189	5	0.737	2.5	0.000615	2.18	18	0.000498	2.1	10.06	0.21	0.000505	2.2	10.21	0.23
	KNOR1@02	35	6107	175	197	6	0.731	2.9	0.000637	2.60	18	0.000521	2.5	10.53	0.26	0.000524	2.6	10.59	0.28
	KNOR1@03	36	9885	273	115	4	0.784	1.8	0.000767	2.66	32	0.000518	2.3	10.48	0.24	0.000518	2.7	10.47	0.29
	KNOR1@05	27	9535	356	102	3	0.786	1.4	0.000869	2.35	36	0.000560	1.9	11.32	0.22	0.000558	2.4	11.28	0.27
	KNOR1@06	33	9203	277	167	4	0.734	2.1	0.000661	2.18	19	0.000522	2.0	10.54	0.21	0.000533	2.2	10.77	0.24
	KNOR1@07	33	4983	152	112	5	0.726	2.1	0.000768	2.20	31	0.000522	2.2	10.56	0.23	0.000527	2.3	10.64	0.25
	KNOR1@08	36	3783	105	136	6	0.652	2.8	0.000701	2.17	24	0.000516	2.4	10.42	0.25	0.000533	2.3	10.76	0.24
	KNOR1@09	39	5846	149	281	7	0.573	3.4	0.000577	2.30	11	0.000513	2.3	10.37	0.24	0.000514	2.3	10.38	0.24
	KNOR1@04	30	6902	234	95	3	0.759	1.6	0.000920	2.21	37	0.000555	1.9	11.21	0.22	0.000576	2.3	11.63	0.27
C	KNOR1@10	48	5633	118	428	11	0.495	5.2	0.000542	2.37	6	0.000499	2.4	10.07	0.24	0.000508	2.4	10.27	0.24
	KNOR1@11	48	4611	96	444	12	0.478	5.6	0.000560	2.48	6	0.000525	2.6	10.61	0.27	0.000528	2.5	10.67	0.27
	KNOR1@12	57	4583	81	399	11	0.355	5.3	0.000540	2.18	5	0.000498	2.3	10.06	0.23	0.000513	2.2	10.36	0.23
	KNOR1@13	54	4104	77	445	11	0.331	5.0	0.000541	2.29	5	0.000500	2.4	10.10	0.24	0.000513	2.3	10.37	0.24
	KNOR1@14	56	6093	108	729	13	0.285	5.6	0.000516	2.19	3	0.000495	2.2	10.00	0.22	0.000501	2.2	10.12	0.22
	KNOR1@15	76	6847	91	639	11	0.237	5.4	0.000529	2.19	2	0.000508	2.2	10.27	0.23	0.000515	2.2	10.41	0.23
	KNOR1@16	65	5872	91	524	11	0.224	5.8	0.000529	2.17	2	0.000503	2.2	10.17	0.23	0.000517	2.2	10.45	0.23
	KNOR1@18	77	8867	114	628	10	0.141	5.7	0.000559	2.52	1	0.000544	2.6	11.00	0.28	0.000552	2.5	11.15	0.28
	KNOR1@17	73	6281	86	585	10	0.191	5.4	0.000590	2.24	2	0.000564	2.3	11.41	0.26	0.000578	2.2	11.68	0.26
Eastern Tauern Window																			
A	KAIS6@29	12	32285	2726	324	2	0.816	1.1	0.001135	2.68	11	0.001014	2.4	20.48	0.49	0.001015	2.7	20.51	0.55
	KAIS6@37	10	35152	3587	322	2	0.817	1.1	0.001192	2.71	10	0.001065	2.4	21.51	0.52	0.001072	2.7	21.66	0.59
	KAIS6@38	10	35481	3480	428	3	0.797	1.4	0.001137	2.74	8	0.001046	2.5	21.13	0.54	0.001045	2.8	21.12	0.58
	KAIS6@39	10	31600	3326	316	3	0.820	1.3	0.001154	2.73	11	0.001022	2.4	20.65	0.50	0.001030	2.7	20.81	0.57
	KAIS6@41	8	32642	4280	351	2	0.824	1.2	0.001173	2.74	9	0.001057	2.5	21.36	0.53	0.001063	2.8	21.48	0.59
	KAIS6@42	6	29873	4677	292	2	0.836	1.2	0.001200	2.69	11	0.001054	2.4	21.28	0.51	0.001066	2.7	21.54	0.58

Table 3. Continued.

Groups	Analysis ID	U (ppm)	Th (ppm)	Th / U	$^{208}Pb / ^{204}Pb$	1σ (%)	$^{207}Pb / ^{206}Pb$	1σ (%)	$^{208}Pb / ^{232}Th$	1σ (%)	f208 from 207 (%)	204-corr $^{208}Pb / ^{232}Th$	204-corr 1σ (%)	204-corr spot ages $^{208}Pb / ^{232}Th$ Age (Ma)	204-corr spot ages 1σ (abs.)	207-corr $^{208}Pb / ^{232}Th$	207-corr 1σ (%)	207-corr spot ages $^{208}Pb / ^{232}Th$ Age (Ma)	207-corr spot ages 1σ (abs.)
Eastern Tauern Window																			
B	KAIS6@15	5	21644	4568	142	2	0.833	0.9	0.001399	2.69	25	0.001031	2.0	20.83	0.43	0.001045	2.8	21.12	0.59
	KAIS6@16	5	22052	4771	161	2	0.831	0.9	0.001329	2.69	23	0.001020	2.1	20.61	0.44	0.001022	2.7	20.65	0.57
	KAIS6@17	5	25100	4752	189	2	0.825	1.0	0.001299	2.73	19	0.001046	2.2	21.12	0.47	0.001049	2.8	21.20	0.59
	KAIS6@18	5	25260	4905	148	2	0.827	0.9	0.001392	2.81	26	0.001040	2.2	21.01	0.45	0.001025	2.9	20.71	0.61
	KAIS6@19	5	23495	5173	148	2	0.825	0.9	0.001390	2.75	24	0.001038	2.1	20.96	0.44	0.001053	2.8	21.28	0.60
	KAIS6@20	5	24260	5377	157	2	0.829	0.9	0.001351	2.83	24	0.001032	2.2	20.85	0.46	0.001033	2.9	20.86	0.61
	KAIS6@21	5	25950	5040	155	2	0.837	0.9	0.001320	2.73	24	0.001003	2.1	20.27	0.43	0.001007	2.8	20.35	0.57
	KAIS6@22	4	20175	4625	134	2	0.813	0.9	0.001424	2.76	27	0.001034	2.1	20.88	0.43	0.001043	2.8	21.07	0.60
	KAIS6@23	3	18427	5349	153	2	0.828	1.0	0.001353	2.82	24	0.001028	2.2	20.76	0.46	0.001027	2.9	20.74	0.60
	KAIS6@24	4	17328	4822	178	2	0.830	1.1	0.001313	2.69	21	0.001045	2.2	21.11	0.46	0.001041	2.7	21.02	0.58
	KAIS6@25	5	17901	3588	154	2	0.833	0.9	0.001366	2.77	24	0.001042	2.2	21.05	0.46	0.001039	2.8	20.98	0.59
	KAIS6@26	4	19477	5281	167	2	0.820	1.0	0.001304	2.75	22	0.001020	2.2	20.60	0.46	0.001017	2.8	20.56	0.58
	KAIS6@27	4	19595	5290	165	2	0.821	1.1	0.001325	2.72	22	0.001030	2.2	20.80	0.45	0.001036	2.8	20.93	0.58
	KAIS6@28	3	17683	5368	162	2	0.817	1.0	0.001354	2.76	23	0.001043	2.2	21.06	0.46	0.001041	2.8	21.02	0.59
	KAIS6@31	3	19464	6314	207	2	0.826	1.2	0.001275	2.67	17	0.001049	2.2	21.19	0.48	0.001059	2.7	21.39	0.58
	KAIS6@32	3	17623	5729	145	2	0.823	1.0	0.001352	2.75	26	0.001007	2.1	20.35	0.43	0.001003	2.8	20.26	0.57
	KAIS6@33	4	23433	5395	191	2	0.819	1.0	0.001257	2.79	18	0.001018	2.3	20.56	0.47	0.001026	2.8	20.73	0.59
	KAIS6@34	3	22517	6923	175	2	0.836	0.9	0.001289	2.73	21	0.001016	2.2	20.52	0.45	0.001015	2.8	20.51	0.57
	KAIS6@35	4	23426	6129	175	2	0.827	0.9	0.001299	2.72	21	0.001025	2.2	20.70	0.45	0.001031	2.8	20.82	0.58
	KAIS6@36	4	24762	6924	169	2	0.821	0.9	0.001316	2.76	21	0.001031	2.2	20.83	0.46	0.001034	2.8	20.89	0.59
	KAIS6@43	4	19511	4948	229	2	0.828	1.2	0.001210	2.76	15	0.001024	2.4	20.68	0.49	0.001023	2.8	20.66	0.58
	KAIS6@44	5	20543	3995	252	3	0.828	1.5	0.001177	2.72	14	0.001007	2.4	20.35	0.48	0.001009	2.8	20.39	0.56
	KAIS6@45	4	17366	4418	225	3	0.834	1.4	0.001269	2.67	15	0.001067	2.3	21.55	0.49	0.001076	2.7	21.73	0.59
	KAIS6@46	4	14595	3614	231	3	0.813	1.5	0.001284	2.70	15	0.001083	2.3	21.88	0.51	0.001094	2.7	22.11	0.61
C	KAIS6@01	2	13078	6002	83	2	0.844	0.8	0.001865	2.70	46	0.001011	1.7	20.43	0.34	0.001001	3.1	20.21	0.63
	KAIS6@02	3	14140	4835	97	2	0.823	0.9	0.001682	2.76	40	0.001031	1.9	20.83	0.39	0.001012	3.0	20.44	0.62
	KAIS6@05	3	10157	2957	96	2	0.837	1.0	0.001672	2.69	38	0.001010	1.9	20.41	0.38	0.001035	3.0	20.91	0.63
	KAIS6@06	4	15227	3566	104	2	0.828	1.0	0.001564	2.84	36	0.000995	2.0	20.11	0.40	0.000994	3.1	20.09	0.63
	KAIS6@09	3	10348	3946	74	1	0.828	0.7	0.002146	2.71	52	0.001030	1.5	20.81	0.32	0.001037	3.7	20.94	0.77
	KAIS6@10	3	12624	4224	90	2	0.828	0.9	0.001795	2.74	42	0.001037	1.8	20.96	0.37	0.001033	3.1	20.87	0.64
	KAIS6@12	3	10457	3171	91	2	0.822	1.0	0.001752	2.68	41	0.001020	1.8	20.61	0.37	0.001039	3.0	20.98	0.63
D	KAIS6@03	4	15947	3922	100	2	0.844	1.0	0.001524	2.91	39	0.000944	2.0	19.07	0.38	0.000924	3.2	18.67	0.59
	KAIS6@04	4	16156	3905	91	2	0.829	1.0	0.001531	3.25	40	0.000890	2.1	17.98	0.38	0.000923	3.5	18.65	0.66
	KAIS6@07	6	11981	2002	89	4	0.843	1.6	0.001562	2.89	44	0.000887	2.3	17.93	0.40	0.000877	3.7	17.71	0.65
	KAIS6@08	3	10466	3145	87	2	0.824	0.8	0.001711	2.68	44	0.000959	1.7	19.37	0.33	0.000956	3.1	19.31	0.59
	KAIS6@11	4	13094	3210	89	2	0.830	1.1	0.001493	2.92	42	0.000846	2.0	17.09	0.33	0.000870	3.3	17.58	0.58
	KAIS6@13	4	13271	3273	88	2	0.842	1.0	0.001621	2.84	41	0.000917	1.9	18.52	0.35	0.000950	3.3	19.19	0.63
	KAIS6@14	9	13459	1568	105	4	0.827	1.7	0.001323	3.57	33	0.000836	2.6	16.89	0.44	0.000881	3.8	17.79	0.68
	KAIS6@30	14	25376	1840	225	2	0.837	1.1	0.001130	2.68	16	0.000950	2.3	19.20	0.44	0.000951	2.7	19.22	0.52
	KAIS6@40	10	32326	3141	301	3	0.800	1.4	0.001094	2.93	12	0.000962	2.6	19.44	0.51	0.000967	3.0	19.53	0.58
	KAIS6@47	9	31411	3692	311	3	0.818	1.3	0.001069	2.68	11	0.000949	2.4	19.16	0.46	0.000955	2.7	19.28	0.52
	KAIS6@48	*13*	*18728*	*1403*	*217*	*3*	*0.836*	*1.5*	*0.001218*	*2.67*	*17*	*0.001014*	*2.3*	*20.49*	*0.47*	*0.001014*	*2.7*	*20.48*	*0.56*
	KAIS6@49	*13*	*18241*	*1449*	*248*	*3*	*0.813*	*1.3*	*0.001252*	*2.69*	*14*	*0.001072*	*2.3*	*21.66*	*0.51*	*0.001083*	*2.7*	*21.87*	*0.59*
	SALZ18@01	11	443	40	428	6	0.642	2.9	0.001001	2.30	8	0.000928	2.2	18.75	0.41	0.000921	2.31	18.61	0.43
	SALZ18@02	19	11907	639	515	6	0.546	3.0	0.000970	2.16	4	0.000914	2.1	18.46	0.39	0.000928	2.17	18.75	0.41
	SALZ18@03	23	12452	552	1291	11	0.191	7.3	0.000859	2.25	1	0.000853	2.3	17.23	0.39	0.000854	2.25	17.25	0.39
	SALZ18@04	20	8334	407	800	10	0.246	6.5	0.000943	2.52	1	0.000909	2.5	18.36	0.46	0.000933	2.52	18.84	0.47
	SALZ18@05	28	6912	245	1239	12	0.235	6.6	0.000911	2.20	1	0.000903	2.2	18.24	0.41	0.000902	2.20	18.22	0.40
	SALZ18@06	11	2256	200	1200	13	0.314	7.5	0.000947	2.26	1	0.000941	2.3	19.00	0.44	0.000935	2.26	18.90	0.43
	SALZ18@07	23	9797	429	1862	19	0.208	9.6	0.000863	2.34	1	0.000858	2.4	17.33	0.41	0.000857	2.34	17.31	0.40
	SALZ18@08	20	4607	232	980	14	0.186	10.0	0.000880	2.39	1	0.000856	2.4	17.29	0.42	0.000874	2.39	17.66	0.42
	SALZ18@09	18	3952	224	1353	18	0.180	9.3	0.000942	2.42	1	0.000934	2.5	18.87	0.47	0.000934	2.42	18.88	0.46
	SALZ18@10	19	3681	189	894	18	0.178	10.2	0.000917	2.57	1	0.000889	2.6	17.96	0.47	0.000907	2.57	18.33	0.47
	SALZ18@11	13	1751	134	1123	15	0.312	7.3	0.000979	2.38	2	0.000962	2.4	19.44	0.47	0.000963	2.38	19.46	0.46
	SALZ18@12	17	4555	267	731	19	0.169	10.8	0.000922	2.74	1	0.000881	2.8	17.80	0.50	0.000910	2.74	18.39	0.50
	SALZ18@13	17	1752	106	617	27	0.207	11.1	0.000887	3.43	3	0.000850	3.8	17.18	0.65	0.000860	3.43	17.37	0.60
	SALZ18@14	22	1037	48	975	11	0.270	6.1	0.000953	2.24	1	0.000938	2.3	18.95	0.43	0.000941	2.24	19.01	0.43
	SALZ18@15	37	9684	262	1073	14	0.224	7.5	0.000792	2.37	1	0.000781	2.4	15.79	0.38	0.000783	2.37	15.81	0.37

Table 3. Continued.

Groups	Analysis ID	U (ppm)	Th (ppm)	Th / U	$^{208}Pb/^{204}Pb$	1σ (%)	$^{207}Pb/^{206}Pb$	1σ (%)	$^{208}Pb/^{232}Th$	1σ (%)	f208 from 207 (%)	204-corr		204-corr spot ages		207-corr		207-corr spot ages	
												$^{208}Pb/^{232}Th$	1σ (%)	$^{208}Pb/^{232}Th$ Age (Ma)	1σ (abs.)	$^{208}Pb/^{232}Th$	1σ (%)	$^{208}Pb/^{232}Th$ Age (Ma)	1σ (abs.)
Eastern Tauern Window																			
A	LOHN4@01	14	14552	1076	79	1	0.826	0.7	0.001981	2.96	47	0.001031	1.7	20.84	0.35	0.001059	3.57	21.39	0.76
	LOHN4@02	39	25804	662	272	3	0.779	1.4	0.001112	3.21	13	0.000964	2.8	19.47	0.55	0.000969	3.24	19.58	0.63
	LOHN4@03	11	12883	1175	151	2	0.805	1.2	0.001356	2.67	24	0.001026	2.1	20.73	0.44	0.001033	2.76	20.86	0.58
	LOHN4@04	16	16561	1017	173	2	0.820	1.2	0.001332	2.87	22	0.001051	2.3	21.23	0.49	0.001045	2.96	21.12	0.63
	LOHN4@07	34	35456	1048	338	2	0.779	1.1	0.001218	2.68	10	0.001094	2.4	22.11	0.53	0.001097	2.69	22.16	0.60
	LOHN4@08	31	32345	1044	312	2	0.782	1.0	0.001208	2.75	11	0.001074	2.5	21.70	0.53	0.001070	2.77	21.62	0.60
	LOHN4@09	33	34180	1040	323	2	0.790	1.1	0.001224	2.70	11	0.001094	2.4	22.09	0.54	0.001092	2.71	22.07	0.60
	LOHN4@10	33	35690	1072	349	2	0.788	1.1	0.001171	2.68	10	0.001058	2.4	21.38	0.52	0.001060	2.69	21.41	0.57
	LOHN4@11	34	29955	888	355	3	0.796	1.3	0.001085	2.67	10	0.000977	2.4	19.75	0.48	0.000977	2.68	19.74	0.53
	LOHN4@12	27	29155	1065	366	3	0.776	1.3	0.001185	2.68	9	0.001078	2.5	21.77	0.53	0.001082	2.69	21.86	0.59
	LOHN4@13	26	23964	935	97	2	0.823	0.7	0.001750	2.99	39	0.001071	1.9	21.64	0.42	0.001066	3.32	21.54	0.72
	LOHN4@14	28	22365	792	156	2	0.806	1.0	0.001418	2.83	23	0.001087	2.2	21.97	0.49	0.001089	2.96	22.01	0.65
	LOHN4@15	24	20864	866	523	4	0.742	1.9	0.001109	2.69	6	0.001040	2.5	21.00	0.53	0.001044	2.70	21.09	0.57
	LOHN4@16	30	23937	797	575	4	0.728	2.2	0.001062	2.75	5	0.001003	2.6	20.25	0.53	0.001006	2.76	20.33	0.56
	LOHN4@19	27	21599	807	299	3	0.788	1.3	0.001221	2.71	12	0.001075	2.4	21.71	0.52	0.001080	2.72	21.82	0.59
	LOHN4@20	29	23422	801	350	3	0.785	1.4	0.001156	2.67	10	0.001042	2.4	21.06	0.51	0.001041	2.68	21.02	0.56
	LOHN4@21	16	17205	1046	171	2	0.798	1.0	0.001354	2.70	22	0.001064	2.2	21.49	0.47	0.001060	2.76	21.41	0.59
	LOHN4@22	17	16983	991	165	2	0.810	1.1	0.001359	2.76	22	0.001055	2.2	21.31	0.47	0.001057	2.82	21.35	0.60
	LOHN4@23	16	17269	1091	162	2	0.819	1.0	0.001388	2.79	23	0.001074	2.2	21.70	0.48	0.001065	2.85	21.52	0.61
	LOHN4@24	20	21768	1108	176	2	0.810	1.1	0.001258	2.87	22	0.000990	2.3	20.00	0.46	0.000985	2.93	19.90	0.58
	LOHN4@25	18	15361	875	174	3	0.823	1.2	0.001232	2.68	21	0.000969	2.2	19.58	0.43	0.000979	2.74	19.77	0.54
	LOHN4@26	15	17857	1172	172	2	0.806	1.1	0.001276	2.68	21	0.001001	2.2	20.21	0.44	0.001012	2.73	20.44	0.56
	LOHN4@27	27	26405	974	184	2	0.819	0.9	0.001317	2.72	19	0.001056	2.2	21.34	0.47	0.001064	2.76	21.50	0.59
	LOHN4@28	28	27181	955	190	2	0.816	0.9	0.001324	2.80	20	0.001068	2.3	21.58	0.49	0.001066	2.84	21.53	0.61
	LOHN4@29	27	25484	955	191	2	0.809	1.0	0.001304	2.85	20	0.001051	2.3	21.22	0.50	0.001048	2.90	21.18	0.61
	LOHN4@30	27	25099	915	190	2	0.798	0.9	0.001322	2.71	19	0.001067	2.2	21.55	0.48	0.001068	2.75	21.58	0.59
	LOHN4@31	30	25226	855	433	3	0.777	1.6	0.001235	2.67	8	0.001139	2.5	23.00	0.57	0.001134	2.68	22.92	0.61
	LOHN4@32	36	21812	606	287	4	0.797	1.7	0.001212	2.70	13	0.001061	2.4	21.43	0.52	0.001053	2.73	21.27	0.58
	LOHN4@33	27	23182	856	199	2	0.805	1.0	0.001233	2.67	18	0.001002	2.2	20.24	0.45	0.001011	2.71	20.42	0.55
	LOHN4@34	26	24807	948	188	2	0.812	1.0	0.001293	2.71	19	0.001043	2.2	21.06	0.47	0.001044	2.75	21.09	0.58
	LOHN4@35	25	23076	925	174	2	0.812	0.9	0.001327	3.07	21	0.001045	2.5	21.11	0.52	0.001052	3.14	21.26	0.67
	LOHN4@36	26	25326	972	190	2	0.786	0.9	0.001308	2.73	19	0.001052	2.2	21.25	0.47	0.001061	2.77	21.43	0.59
	LOHN4@37	27	26268	980	210	2	0.802	1.0	0.001282	2.78	17	0.001062	2.3	21.45	0.50	0.001061	2.81	21.43	0.60
	LOHN4@38	27	27571	1016	218	2	0.812	1.0	0.001239	2.72	16	0.001033	2.3	20.87	0.48	0.001040	2.75	21.02	0.58
	LOHN4@39	26	25481	988	207	2	0.806	0.9	0.001272	2.69	18	0.001047	2.2	21.16	0.48	0.001044	2.72	21.08	0.57
	LOHN4@40	26	26144	1007	211	2	0.814	1.0	0.001245	2.78	17	0.001029	2.3	20.78	0.48	0.001032	2.81	20.85	0.59
	LOHN4@41	19	24124	1248	221	2	0.800	1.0	0.001271	2.72	17	0.001061	2.3	21.44	0.49	0.001057	2.75	21.35	0.59
	LOHN4@42	19	23602	1235	226	2	0.816	1.1	0.001279	2.74	16	0.001078	2.3	21.78	0.51	0.001076	2.77	21.73	0.60
	LOHN4@43	21	23764	1157	236	2	0.802	1.1	0.001247	2.70	15	0.001057	2.3	21.36	0.49	0.001059	2.72	21.40	0.58
	LOHN4@44	20	23194	1138	231	2	0.803	1.1	0.001254	2.72	15	0.001055	2.3	21.32	0.49	0.001067	2.74	21.56	0.59
	LOHN4@45	20	23831	1188	232	2	0.787	1.0	0.001255	2.70	15	0.001058	2.3	21.37	0.49	0.001065	2.72	21.51	0.58
	LOHN4@46	20	20913	1027	204	2	0.813	1.0	0.001277	2.67	17	0.001047	2.2	21.16	0.47	0.001058	2.70	21.38	0.58
	LOHN4@48	22	23727	1093	262	2	0.808	1.1	0.001210	2.78	14	0.001045	2.4	21.12	0.51	0.001046	2.80	21.13	0.59
	LOHN4@49	22	23546	1065	259	2	0.789	1.1	0.001179	2.73	13	0.001018	2.4	20.56	0.49	0.001022	2.75	20.65	0.57
	LOHN4@50	21	22193	1049	260	2	0.806	1.2	0.001208	2.70	13	0.001045	2.4	21.12	0.50	0.001047	2.72	21.15	0.57
	LOHN4@51	20	22103	1121	259	2	0.800	1.2	0.001179	2.67	14	0.001014	2.3	20.48	0.48	0.001011	2.69	20.43	0.55
	LOHN4@52	20	20091	1023	242	2	0.785	1.2	0.001146	2.68	14	0.000973	2.3	19.66	0.45	0.000987	2.70	19.93	0.54
	LOHN4@53	10	15092	1539	136	2	0.818	1.0	0.001422	2.69	28	0.001029	2.0	20.80	0.42	0.001030	2.79	20.80	0.58
	LOHN4@54	10	13028	1330	137	2	0.812	1.1	0.001350	2.66	26	0.000979	2.0	19.78	0.40	0.000993	2.78	20.07	0.56
	LOHN4@55	10	14821	1515	137	2	0.806	1.0	0.001355	2.67	27	0.000982	2.0	19.83	0.40	0.000983	2.78	19.85	0.55
B	LOHN4@05	19	14990	787	171	4	0.821	1.6	0.001129	3.06	22	0.000882	2.5	17.83	0.45	0.000875	3.15	17.68	0.56
	LOHN4@06	31	9191	298	146	5	0.794	2.3	0.001237	3.80	26	0.000913	3.1	18.45	0.58	0.000912	3.95	18.42	0.73
	LOHN4@17	32	23011	717	714	6	0.732	2.8	0.000980	3.29	5	0.000936	3.2	18.91	0.60	0.000933	3.29	18.85	0.62
	LOHN4@18	39	23334	591	461	5	0.760	2.3	0.001003	3.06	8	0.000927	2.9	18.73	0.54	0.000923	3.07	18.66	0.57
	LOHN4@47	23	19054	816	222	3	0.808	1.2	0.001120	2.66	15	0.000933	2.3	18.85	0.43	0.000946	2.70	19.12	0.52
	LOHN4@56	9	11815	1254	129	2	0.833	1.2	0.001272	2.78	28	0.000895	2.1	18.07	0.38	0.000913	2.90	18.45	0.53
	LOHN4@57	13	11550	862	133	3	0.826	1.5	0.001194	3.44	28	0.000847	2.6	17.12	0.45	0.000855	3.58	17.28	0.62

Table 3. Continued.

Groups	Analysis ID	U (ppm)	Th (ppm)	Th / U	$^{208}Pb / ^{204}Pb$	1σ (%)	$^{207}Pb / ^{206}Pb$	1σ (%)	$^{208}Pb / ^{232}Th$	1σ (%)	f208 from 207 (%)	204-corr $^{208}Pb / ^{232}Th$	204-corr 1σ (%)	204-corr spot ages $^{208}Pb / ^{232}Th$ Age (Ma)	204-corr spot ages 1σ (abs.)	207-corr $^{208}Pb / ^{232}Th$	207-corr 1σ (%)	207-corr spot ages $^{208}Pb / ^{232}Th$ Age (Ma)	207-corr spot ages 1σ (abs.)
Eastern Tauern Window																			
	ORT1@01	367	5825	16	1263	17	0.084	2.3	0.000945	2.48	2	0.000912	2.5	18.43	0.46	0.000922	2.5	18.63	0.47
	ORT1@02	316	4437	14	711	23	0.087	2.4	0.000956	2.43	3	0.000905	2.4	18.27	0.44	0.000930	2.5	18.80	0.46
	ORT1@03	277	4950	18	1166	16	0.097	2.5	0.000936	2.26	3	0.000896	2.3	18.10	0.41	0.000911	2.3	18.41	0.42
	ORT1@04	356	4831	14	926	16	0.088	2.4	0.000905	2.92	3	0.000861	2.9	17.40	0.50	0.000877	3.0	17.73	0.53
	ORT1@05	161	5336	33	930	18	0.139	2.6	0.000970	2.17	3	0.000924	2.2	18.67	0.41	0.000941	2.2	19.01	0.42
	ORT1@06	222	3688	17	382	16	0.166	2.1	0.001012	2.99	7	0.000897	3.0	18.12	0.54	0.000938	3.2	18.95	0.61
	ORT1@07	219	5005	23	277	13	0.272	1.6	0.001039	2.23	13	0.000893	2.3	18.05	0.41	0.000902	2.4	18.21	0.43
	ORT1@08	189	5091	27	422	18	0.220	2.0	0.000979	2.96	8	0.000896	2.9	18.09	0.52	0.000901	3.1	18.21	0.56
	ORT1@09	262	6320	24	591	17	0.139	2.3	0.000880	3.78	4	0.000824	3.6	16.65	0.60	0.000841	3.8	16.98	0.65
	ORT1@10	199	7415	37	214	11	0.411	1.2	0.001086	2.24	16	0.000892	2.1	18.01	0.38	0.000912	2.4	18.43	0.44
	ORT1@11	101	3205	32	655	17	0.172	3.0	0.000981	2.61	4	0.000926	2.7	18.71	0.50	0.000941	2.7	19.01	0.51
	ORT1@12	106	3602	34	661	28	0.191	2.9	0.000933	3.58	4	0.000863	3.5	17.44	0.60	0.000895	3.6	18.08	0.66
	ORT1@13	95	4969	52	607	18	0.195	2.9	0.000910	2.82	3	0.000855	2.8	17.28	0.48	0.000883	2.9	17.83	0.51
	ORT1@14	96	3780	40	628	13	0.183	2.9	0.000960	2.17	4	0.000884	2.3	17.86	0.40	0.000923	2.2	18.65	0.42
	ORT1@15	*105*	*4304*	*41*	*445*	*21*	*0.370*	*1.9*	*0.001022*	*4.60*	*12*	*0.000894*	*4.2*	*18.06*	*0.76*	*0.000903*	*5.7*	*18.24*	*1.04*
	EUKL2@01	9	296	32	160	3	0.803	1.2	0.001359	2.12	22	0.001043	1.7	21.07	0.37	0.001063	2.21	21.47	0.47
	EUKL2@02	14	301	22	209	3	0.803	1.2	0.001317	2.51	18	0.001089	2.1	22.00	0.47	0.001080	2.56	21.81	0.56
	EUKL2@03	13	21097	1580	205	2	0.824	1.2	0.001303	2.25	17	0.001072	1.9	21.65	0.41	0.001078	2.30	21.77	0.50
	EUKL2@04	14	18352	1313	231	3	0.812	1.5	0.001253	2.08	16	0.001059	1.8	21.39	0.39	0.001048	2.13	21.16	0.45
	EUKL2@05	33	52673	1620	345	3	0.782	1.3	0.001194	2.17	10	0.001076	2.0	21.74	0.43	0.001079	2.18	21.79	0.48
	EUKL2@06	19	25562	1351	218	2	0.795	1.2	0.001315	2.10	16	0.001097	1.8	22.17	0.40	0.001102	2.14	22.26	0.48
	EUKL2@07	19	16767	868	234	3	0.800	1.2	0.001282	2.10	15	0.001085	1.8	21.91	0.40	0.001085	2.14	21.92	0.47
A	HOAR1@27	148	1591	11	235	13	0.195	2.2	0.001164	1.5	14	0.000973	2.4	19.65	0.48	0.001003	1.6	20.26	0.32
	HOAR1@28	100	1383	14	149	11	0.248	2.2	0.001269	1.2	19	0.000940	2.9	19.00	0.55	0.001031	1.3	20.84	0.28
	HOAR1@29	95	19676	208	1211	8	0.201	2.5	0.001023	0.8	1	0.000990	0.9	20.00	0.17	0.001013	0.8	20.47	0.17
	HOAR1@30	80	650	8	214	19	0.170	3.3	0.001153	3.6	15	0.000946	4.6	19.10	0.88	0.000978	3.7	19.76	0.74
	HOAR1@31	124	2725	22	497	14	0.169	2.6	0.001070	0.9	6	0.000987	1.4	19.94	0.28	0.001007	0.9	20.35	0.19
	HOAR1@32	316	1076	3	160	12	0.132	2.0	0.001240	3.4	21	0.000950	4.0	19.20	0.76	0.000985	3.5	19.91	0.70
B	HOAR1@01	50	926	18	322	20	0.244	3.7	0.001121	4.3	9	0.000999	4.6	20.18	0.92	0.001017	4.4	20.55	0.91
	HOAR1@02	51	782	15	200	18	0.296	3.5	0.001128	3.5	15	0.000911	4.5	18.40	0.83	0.000954	4.5	19.27	0.87
	HOAR1@03	48	969	20	250	17	0.205	3.5	0.001088	4.7	8	0.000920	4.8	18.59	0.89	0.000997	5.0	20.13	1.00
	HOAR1@04	71	1075	15	259	18	0.182	3.5	0.001075	4.3	9	0.000926	4.6	18.70	0.85	0.000982	4.5	19.84	0.89
	HOAR1@05	79	643	8	233	21	0.197	3.4	0.001118	4.2	16	0.000932	4.9	18.84	0.92	0.000940	5.0	18.98	0.94
	HOAR1@06	118	1676	14	330	15	0.148	2.9	0.001046	2.8	7	0.000924	3.1	18.66	0.57	0.000977	3.0	19.73	0.59
	HOAR1@07	106	1764	17	448	17	0.162	2.9	0.001065	2.6	7	0.000973	2.8	19.66	0.55	0.000993	2.8	20.07	0.56
	HOAR1@08	67	1358	20	339	18	0.237	3.2	0.001049	2.8	11	0.000938	3.3	18.94	0.62	0.000938	3.0	18.95	0.57
	HOAR1@09	62	1579	25	364	16	0.191	3.3	0.001110	3.0	5	0.000992	3.1	20.04	0.63	0.001050	3.2	21.20	0.67
	HOAR1@10	266	1995	8	433	15	0.097	2.4	0.001076	2.4	5	0.000980	2.6	19.79	0.52	0.001019	2.6	20.59	0.54
	HOAR1@11	56	6609	117	714	11	0.242	2.7	0.001032	2.2	3	0.000976	2.2	19.71	0.43	0.001005	2.2	20.31	0.45
	HOAR1@12	104	2748	26	263	10	0.359	1.8	0.001163	2.3	15	0.000992	2.4	20.04	0.49	0.000988	2.4	19.96	0.48
	HOAR1@13	103	3259	32	679	15	0.171	2.7	0.000998	3.0	4	0.000941	3.0	19.01	0.56	0.000959	3.0	19.37	0.59
	HOAR1@14	107	1940	18	272	12	0.213	2.3	0.001115	3.9	10	0.000957	3.7	19.33	0.72	0.001005	4.4	20.30	0.88
	HOAR1@16	145	2711	19	632	16	0.139	2.6	0.001076	2.5	4	0.001010	2.5	20.41	0.51	0.001029	2.5	20.78	0.53
	HOAR1@17	72	1305	18	263	15	0.211	3.1	0.001059	3.7	8	0.000904	3.9	18.26	0.71	0.000969	3.9	19.58	0.77
	HOAR1@18	74	1381	19	292	15	0.196	3.1	0.001088	4.2	8	0.000944	4.2	19.07	0.79	0.000998	4.4	20.16	0.89
	HOAR1@19	60	1129	19	389	19	0.240	3.0	0.001129	3.7	10	0.001026	3.9	20.73	0.81	0.001019	4.0	20.58	0.82
	HOAR1@20	60	1818	30	499	17	0.206	3.2	0.001035	2.6	5	0.000955	2.7	19.29	0.53	0.000978	2.8	19.76	0.55
	HOAR1@21	45	1000	22	183	14	0.309	3.0	0.001130	3.8	15	0.000891	4.2	18.01	0.76	0.000964	4.2	19.47	0.82
	HOAR1@22	49	1540	31	194	12	0.305	2.8	0.001127	2.5	9	0.000909	3.1	18.37	0.57	0.001025	2.9	20.70	0.59
	HOAR1@23	126	1838	15	824	24	0.119	3.4	0.001015	3.2	5	0.000968	3.2	19.55	0.63	0.000966	3.3	19.52	0.64
	HOAR1@24	85	1927	23	511	18	0.147	3.3	0.001026	2.6	5	0.000954	2.8	19.27	0.53	0.000974	2.8	19.67	0.54
	HOAR1@25	53	1330	25	384	19	0.230	3.5	0.001022	2.9	8	0.000919	3.2	18.57	0.60	0.000944	3.0	19.08	0.58
	HOAR1@26	60	1206	20	343	18	0.197	3.5	0.001023	3.1	8	0.000908	3.5	18.34	0.63	0.000940	3.3	18.99	0.63
	HOAR1@15	*111*	*2877*	*26*	*112*	*6*	*0.516*	*1.2*	*0.001353*	*5.1*	*29*	*0.000885*	*3.9*	*17.88*	*0.70*	*0.000964*	*7.9*	*19.47*	*1.53*

Table 3. Continued.

												204-corr		204-corr spot ages		207-corr		207-corr spot ages	
Groups	Analysis ID	U (ppm)	Th (ppm)	Th / U	$^{208}Pb/^{204}Pb$	1σ (%)	$^{207}Pb/^{206}Pb$	1σ (%)	$^{208}Pb/^{232}Th$	1σ (%)	f208 from 207 (%)	$^{208}Pb/^{232}Th$	1σ (%)	$^{208}Pb/^{232}Th$ Age (Ma)	1σ (abs.)	$^{208}Pb/^{232}Th$	1σ (%)	$^{208}Pb/^{232}Th$ Age (Ma)	1σ (abs.)
Eastern Tauern Window																			
A	MOKR1@07	307	3840	13	172	11	0.228	2.1	0.001121	3.2	18	0.000876	3.6	17.69	0.64	0.000915	3.3	18.48	0.61
	MOKR1@08	393	5762	15	259	15	0.228	2.8	0.000997	2.7	13	0.000848	3.2	17.13	0.55	0.000869	2.8	17.55	0.48
	MOKR1@09	916	5949	6	260	14	0.128	2.3	0.000993	2.6	12	0.000845	3.1	17.08	0.52	0.000879	2.7	17.75	0.48
	MOKR1@10	814	2999	4	166	13	0.134	2.0	0.001143	3.7	22	0.000878	4.1	17.74	0.73	0.000890	3.8	17.99	0.68
	MOKR1@11	1852	2971	2	148	21	0.138	3.2	0.001168	2.9	26	0.000976	6.4	19.71	1.25	0.000859	3.3	17.36	0.57
	MOKR1@12	702	7328	10	245	16	0.224	3.1	0.001029	2.6	13	0.000867	3.4	17.51	0.59	0.000899	2.6	18.15	0.47
	MOKR1@20	442	2417	5	255	47	0.062	10.0	0.000754	1.0	5	0.000639	7.2	12.92	0.94	0.000714	1.4	14.42	0.21
	MOKR1@21	473	5279	11	1029	55	0.063	10.2	0.001134	1.0	1	0.001091	2.3	22.05	0.50	0.001124	1.1	22.70	0.24
	MOKR1@22	410	5545	14	2865	95	0.070	11.4	0.001130	1.6	1	0.001115	2.1	22.52	0.46	0.001119	1.7	22.61	0.37
	MOKR1@23	341	2318	7	483	47	0.104	6.6	0.001093	1.3	8	0.001049	4.4	21.18	0.94	0.001011	1.6	20.43	0.32
	MOKR1@24	507	7589	15	3668	67	0.057	6.1	0.001049	1.5	1	0.001038	1.7	20.97	0.35	0.001042	1.5	21.06	0.32
	MOKR1@25	336	4029	12	1546	67	0.087	7.7	0.001041	1.5	3	0.001015	2.2	20.51	0.46	0.001011	1.6	20.43	0.32
	MOKR1@26	220	4084	19	646	39	0.101	6.7	0.001072	1.3	4	0.001008	2.6	20.37	0.53	0.001034	1.3	20.89	0.28
	MOKR1@27	295	3072	10	626	55	0.108	8.3	0.001021	1.3	5	0.000958	3.6	19.35	0.69	0.000969	1.4	19.58	0.28
	MOKR1@28	395	5188	13	1611	67	0.067	9.2	0.001011	1.1	1	0.000987	1.9	19.93	0.39	0.000997	1.2	20.15	0.23
	MOKR1@29	469	3095	7	846	55	0.066	6.5	0.001059	1.0	3	0.001011	2.7	20.42	0.55	0.001025	1.2	20.72	0.25
	MOKR1@30	688	4284	6	802	55	0.062	7.1	0.000922	1.2	3	0.000878	2.9	17.74	0.51	0.000893	1.4	18.03	0.25
	MOKR1@31	683	4946	7	2982	95	0.056	7.6	0.001030	1.0	1	0.001017	1.6	20.54	0.33	0.001015	1.1	20.51	0.23
B	MOKR1@01	132	23439	178	573	9	0.324	2.3	0.000991	2.6	3	0.000924	2.5	18.68	0.46	0.000959	2.6	19.37	0.50
	MOKR1@02	167	21412	128	789	12	0.283	2.7	0.001001	2.6	3	0.000952	2.5	19.23	0.49	0.000970	2.6	19.60	0.51
	MOKR1@03	149	20039	134	694	12	0.307	2.7	0.001011	2.6	3	0.000955	2.6	19.29	0.49	0.000977	2.6	19.73	0.52
	MOKR1@04	162	15315	95	570	12	0.296	2.6	0.001007	2.7	5	0.000943	2.6	19.05	0.50	0.000960	2.7	19.40	0.51
	MOKR1@05	182	11017	61	391	12	0.299	2.6	0.000978	2.6	7	0.000882	2.6	17.81	0.47	0.000913	2.6	18.45	0.48
	MOKR1@06	239	10746	45	355	12	0.242	2.6	0.000993	2.6	6	0.000885	2.6	17.88	0.47	0.000932	2.6	18.83	0.48
	MOKR1@13	127	16222	128	541	10	0.343	2.3	0.001014	2.6	5	0.000942	2.5	19.03	0.47	0.000967	2.6	19.53	0.50
	MOKR1@14	363	17133	47	608	12	0.200	2.4	0.000949	2.6	4	0.000889	2.5	17.95	0.45	0.000908	2.6	18.35	0.47
	MOKR1@15	446	16751	38	468	11	0.191	2.5	0.000948	2.6	4	0.000869	2.5	17.57	0.45	0.000906	2.6	18.30	0.47
	MOKR1@16	517	16572	32	462	12	0.190	2.6	0.000943	2.6	5	0.000864	2.6	17.46	0.45	0.000899	2.6	18.16	0.47
	MOKR1@17	141	16023	113	717	13	0.323	2.6	0.001031	2.6	4	0.000975	2.6	19.70	0.50	0.000986	2.6	19.92	0.52
	MOKR1@18	303	8214	27	380	18	0.303	3.2	0.000949	2.7	10	0.000859	3.0	17.35	0.53	0.000851	2.7	17.19	0.46
	MOKR1@19	*263*	*4051*	*15*	/	*0*	*0.072*	*7.2*	*0.001023*	*1.1*	*2*	*0.001023*	/	*20.67*	/	*0.001002*	*1.1*	*20.24*	*0.23*
A	SAND1@01	259	3167	12	125	17	0.337	3.8	0.001114	4.0	21	0.000770	5.9	15.56	0.92	0.000877	4.1	17.72	0.73
	SAND1@02	252	3570	14	175	21	0.430	3.9	0.001104	3.1	24	0.000860	5.2	17.38	0.90	0.000843	3.3	17.03	0.56
	SAND1@04	323	5540	17	184	19	0.441	4.0	0.001150	2.6	17	0.000908	4.4	18.35	0.80	0.000958	2.7	19.34	0.51
	SAND1@05	580	5757	10	203	19	0.331	3.8	0.001106	2.8	15	0.000896	4.2	18.10	0.76	0.000938	2.9	18.96	0.54
	SAND1@06	601	5846	10	216	20	0.328	4.0	0.001123	2.7	15	0.000923	4.2	18.64	0.77	0.000959	2.8	19.38	0.54
	SAND1@07	272	5768	21	212	12	0.274	2.6	0.001006	2.6	12	0.000829	3.1	16.74	0.52	0.000883	2.6	17.85	0.47
	SAND1@08	251	6655	27	332	15	0.277	2.9	0.000972	2.6	10	0.000859	2.9	17.35	0.50	0.000879	2.6	17.76	0.46
	SAND1@21	181	7714	43	2354	55	0.087	8.6	0.001049	1.3	1	0.001032	1.6	20.85	0.33	0.001039	1.3	20.99	0.28
	SAND1@22	285	6564	23	1186	55	0.096	10.8	0.001045	1.4	1	0.001011	2.3	20.43	0.46	0.001030	1.4	20.80	0.30
	SAND1@24	289	6472	22	1758	67	0.098	10.4	0.001054	1.2	2	0.001031	1.9	20.82	0.39	0.001036	1.2	20.93	0.26
	SAND1@25	302	7743	26	2074	67	0.107	10.3	0.001107	1.1	1	0.001086	1.6	21.94	0.36	0.001090	1.1	22.03	0.25
	SAND1@26	302	7711	26	1385	55	0.140	8.6	0.001117	1.4	3	0.001086	2.1	21.94	0.45	0.001089	1.4	22.01	0.32
	SAND1@28	468	728	2	513	95	0.066	8.6	0.001116	1.4	10	0.001032	7.3	20.85	1.51	0.001004	3.4	20.28	0.68

Table 3. Continued.

Groups	Analysis ID	U (ppm)	Th (ppm)	Th / U	$^{208}Pb/^{204}Pb$	1σ (%)	$^{207}Pb/^{206}Pb$	1σ (%)	$^{208}Pb/^{232}Th$	1σ (%)	f208 from 207 (%)	204-corr $^{208}Pb/^{232}Th$	204-corr 1σ (%)	204-corr spot ages $^{208}Pb/^{232}Th$ Age (Ma)	204-corr spot ages 1σ (abs.)	207-corr $^{208}Pb/^{232}Th$	207-corr 1σ (%)	207-corr spot ages $^{208}Pb/^{232}Th$ Age (Ma)	207-corr spot ages 1σ (abs.)
Eastern Tauern Window																			
B	SAND1@09	483	2027	4	137	14	0.176	2.2	0.001145	4.2	28	0.000822	4.9	16.61	0.81	0.000820	4.4	16.56	0.72
	SAND1@10	646	2420	4	109	14	0.176	2.7	0.001136	3.3	26	0.000732	5.5	14.80	0.81	0.000842	3.5	17.01	0.60
	SAND1@12	729	3802	5	203	16	0.150	2.8	0.001027	2.6	16	0.000831	3.8	16.79	0.63	0.000858	2.7	17.34	0.47
	SAND1@13	628	2842	5	170	14	0.136	2.3	0.001072	3.0	19	0.000839	3.9	16.95	0.67	0.000873	3.0	17.63	0.54
	SAND1@14	966	3518	4	124	16	0.194	3.1	0.001118	2.6	23	0.000771	5.2	15.57	0.81	0.000862	2.8	17.41	0.48
	SAND1@18	278	1247	4	67	14	0.309	2.9	0.001372	5.0	43	0.000578	8.4	11.67	0.97	0.000783	5.5	15.81	0.88
	SAND1@19	277	811	3	70	16	0.321	3.0	0.001620	5.1	55	0.000731	9.2	14.77	1.36	0.000725	6.5	14.66	0.96
	SAND1@11	*659*	*2325*	4	*92*	*16*	*0.217*	*3.1*	*0.001572*	*8.4*	*35*	*0.000909*	*8.5*	*18.36*	*1.56*	*0.001021*	*8.6*	*20.62*	*1.78*
	SAND1@15	*189*	*964*	5	*49*	*11*	*0.307*	*2.4*	*0.001476*	*6.1*	*49*	*0.000322*	*8.3*	*6.51*	*0.54*	*0.000751*	*6.7*	*15.17*	*1.01*
	SAND1@16	*228*	*601*	3	*59*	*15*	*0.307*	*2.8*	*0.001752*	*6.7*	*62*	*0.000612*	*10.1*	*12.36*	*1.25*	*0.000664*	*8.7*	*13.41*	*1.17*
	SAND1@17	*202*	*401*	2	*46*	*15*	*0.312*	*2.9*	*0.002061*	*8.4*	*73*	*0.000324*	*12.4*	*6.56*	*0.81*	*0.000559*	*13.0*	*11.30*	*1.47*
	SAND1@20	*233*	*376*	2	*54*	*17*	*0.305*	*3.0*	*0.002238*	*7.9*	*74*	*0.000741*	*12.4*	*14.98*	*1.86*	*0.000578*	*13.8*	*11.68*	*1.61*
	SAND1@29	*493*	*448*	*1*	*112*	*67*	*0.056*	*11.1*	*0.001114*	*2.4*	*9*	*0.000729*	*23.3*	*14.72*	*3.43*	*0.001014*	*6.8*	*20.49*	*1.39*
	SAND1@30	*640*	*398*	*1*	*186*	*95*	*0.060*	*11.3*	*0.001180*	*3.8*	*14*	*0.000935*	*20.0*	*18.88*	*3.78*	*0.001019*	*9.3*	*20.59*	*1.91*
	SAND1@31	*636*	*404*	*1*	*95*	*67*	*0.061*	*10.6*	*0.001085*	*3.4*	*21*	*0.001505*	*38.9*	*30.39*	*11.80*	*0.000856*	*10.2*	*17.30*	*1.76*
	SAND1@23	*299*	*5895*	*20*	/	*0*	*0.112*	*10.5*	*0.000878*	*1.2*	*3*	*0.000878*	/	*17.73*	/	*0.000855*	*1.2*	*17.27*	*0.21*
	SAND1@27	*284*	*679*	*2*	/	*0*	*0.069*	*7.7*	*0.001130*	*1.0*	*9*	*0.001130*	/	*22.84*	/	*0.001027*	*2.8*	*20.74*	*0.58*
	SAND1@32	*573*	*501*	*1*	*33*	*96*	*0.017*	*17.8*	*0.000118*	*15.8*	*89*	/	/	*−0.43*	*−0.49*	*0.000013*	*251*	*0.26*	*0.66*
	SAND1@33	*919*	*304*	*0*	/	*0*	*0.035*	*18.9*	*0.000222*	*13.7*	*184*	*0.000222*	/	*4.49*	/	/	*−76*	*−3.76*	*2.86*
	SAND1@35	*1160*	*691*	*1*	/	*0*	*0.057*	*12.0*	*0.001323*	*2.2*	*8*	*0.001323*	/	*26.73*	/	*0.001215*	*5.7*	*24.54*	*1.39*
	SAND1@36	*935*	*512*	*1*	/	*0*	*0.067*	*11.3*	*0.001293*	*1.9*	*20*	*0.001293*	/	*26.11*	/	*0.001037*	*8.8*	*20.95*	*1.84*
A	REIS1@27	166	541	3	188	25	0.088	4.1	0.000926	2.32	13	0.000762	5.7	15.39	0.88	0.000806	2.7	16.28	0.44
	REIS1@28	288	1516	5	601	30	0.077	3.8	0.000836	2.25	6	0.000783	2.8	15.81	0.45	0.000788	2.3	15.93	0.37
	REIS1@29	185	697	4	530	42	0.093	4.6	0.000853	2.24	11	0.000791	3.7	15.99	0.59	0.000760	2.5	15.36	0.39
	REIS1@31	141	763	5	226	42	0.121	3.8	0.000977	2.60	20	0.000810	7.6	16.37	1.24	0.000779	4.2	15.74	0.66
	REIS1@32	306	2964	10	260	26	0.059	3.6	0.000893	2.48	15	0.000760	4.4	15.36	0.68	0.000759	2.8	15.33	0.42
	REIS1@33	762	737	1	874	24	0.050	2.7	0.000877	2.56	2	0.000839	2.7	16.94	0.45	0.000863	2.6	17.44	0.45
	REIS1@35	195	618	3	290	32	0.083	4.3	0.000966	2.95	10	0.000865	5.2	17.48	0.90	0.000865	3.2	17.48	0.56
	REIS1@36	153	668	4	222	27	0.125	4.0	0.000963	2.87	18	0.000796	5.3	16.08	0.86	0.000794	3.2	16.05	0.52
	REIS1@23	236	324	1	326	47	0.053	5.0	0.000821	2.56	8	0.000771	6.7	15.57	1.04	0.000756	3.8	15.27	0.58
	REIS1@17	437	738	2	515	33	0.055	2.9	0.000903	2.26	7	0.000852	3.4	17.21	0.59	0.000842	2.7	17.01	0.45
	REIS1@19	384	454	1	318	33	0.062	3.2	0.000932	2.69	15	0.000819	4.7	16.54	0.78	0.000793	3.8	16.03	0.61
	REIS1@20	353	562	2	1500	67	0.062	3.3	0.000894	2.24	11	0.000870	2.8	17.59	0.49	0.000798	2.9	16.13	0.46
	REIS1@21	288	433	2	336	36	0.060	3.4	0.000981	2.54	10	0.000868	4.7	17.54	0.82	0.000881	3.6	17.81	0.63
B	REIS1@18	328	486	1	467	42	0.061	3.3	0.000802	2.96	18	0.000736	4.4	14.87	0.66	0.000657	4.1	13.27	0.55
	REIS1@24	218	398	2	689	67	0.064	4.9	0.000791	3.13	14	0.000747	4.8	15.08	0.72	0.000679	4.1	13.71	0.56
	REIS1@25	189	225	1	321	55	0.061	5.0	0.000851	3.74	17	0.000748	7.4	15.12	1.11	0.000705	6.1	14.25	0.87
	REIS1@30	297	441	1	778	47	0.083	5.2	0.000749	3.54	10	0.000712	4.1	14.38	0.59	0.000676	4.6	13.66	0.63
	REIS1@34	560	505	1	437	47	0.044	3.3	0.000773	3.93	14	0.000738	6.0	14.90	0.89	0.000666	6.2	13.45	0.84
	REIS1@22	*881*	*386*	0	*229*	*32*	*0.051*	*2.3*	*0.000979*	*2.77*	*25*	*0.000814*	*5.8*	*16.45*	*0.95*	*0.000736*	*34.6*	*14.88*	*5.15*
	REIS1@26	*201*	*197*	1	*199*	*47*	*0.075*	*4.5*	*0.000867*	*3.41*	*41*	*0.000781*	*10.7*	*15.79*	*1.69*	*0.000508*	*11.6*	*10.26*	*1.19*

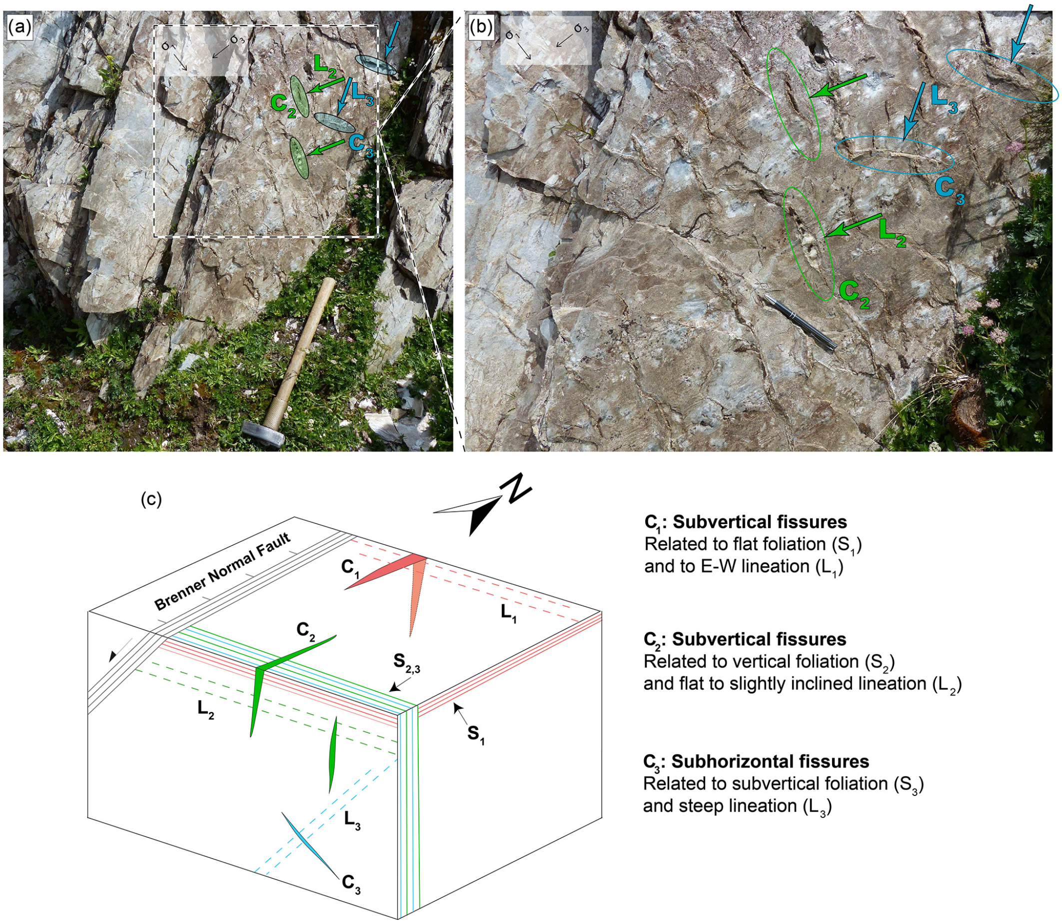

Figure 2. (a) Two generations of late fissures visible in a road outcrop located between monazite locality (46°59.436′ N, 011°39.240′ E) and Pfitscherjoch. Steeply oriented fissures (C_2: ∼ 090/65) are older and deformed (green ellipses), and seem related to a flatter lineation (L_2: ∼ 250/30, green arrows) visible on some of the foliation planes. Younger and flatter oriented fissures (C_3: ∼ 085/30) are straight (blue ellipses) and seem related to a steeper lineation (L_3: 270/70, blue arrows). These observations indicate that a fissure can be deformed during its existence. The length of the hammer handle is 60 cm. **(b)** Enlargement of panel **(a)**. **(c)** Schematic illustration of the three fissure generations observed in this study (C_1, C_2 and C_3), together with respective orientation, foliation (S_1, S_2 and S_3) and lineation (L_1, L_2 and L_3). The first fissure generation (C_1) is related to E–W extension, the second fissure generation (C_2) is linked to strike-slip movements and the third fissure generation (C_3) is related to the oblique-slip movements.

lated to flat foliation (S_1) and E–W-stretching lineation (L_1); these are oriented perpendicular to the main fold axes (and lineation) of the TW and are associated with E–W extension (e.g. Gnos et al., 2015; Rosenberg et al., 2018; Schneider et al., 2013). (ii) Younger subvertical fissures (C_2, Fig. 2c) are associated with subvertical E–W-oriented foliation (S_2) and flat to inclined lineation (L_2), and are oriented perpendicular to strike-slip faults (mainly in the western part of the TW; Fig. 2c). At Pfitscherjoch, the shape of C_2 fissures, indicating overprinting by sinistral sense of shear, is in agreement with the larger-scale sinistral shearing of the GSZ shear zone. (iii) A third generation of fissures (C_3, Fig. 2c) is locally observed, for example, in the Pfitscherjoch locality (Fig. 2a and b) and is at a high angle with C_1 and C_2 fissures. This third fissure generation observed in the Pfitscherjoch locality is associated with a subvertical E–W-striking foliation (S_3). Stretching lineation related to the BNF activity is subparallel to C_3 lineation; however, its foliation is striking N–S (Fig. 2c). We suggest that C_3 fissures are related to oblique-slip movements, in line with the observed E–W-striking foliation and not the BNF activity.

4.2 Monazite dating and composition

The monazite grains selected for in situ Th-Pb dating are millimetre sized and, when BSE zoning is visible, they show two distinct textures: regular and patchy (Figs. 3, 4 and 5; Table 4). The term “regular” refers to crystals showing growth zonation, whereas a patchy texture is interpreted as a replacement by secondary dissolution–reprecipitation processes (e.g. Ayers et al., 1999; Bergemann et al., 2018, 2019,

Table 4. Summary of weighted mean ages of monazite growth domains and spot age ranges of each grain from the TW.

Sample domain	ID no.	Figure	Table	Zoning of the grains	Weighted mean domain $^{208}Pb/^{232}Th$ ages (Ma, $\pm 1\sigma$)	MSWD	Number of analyses	Spot $^{208}Pb/^{232}Th$ age range of entire grain (Ma, $\pm 1\sigma$)	Reference
Western Tauern Window									
INNB1	1	3a	3	Regular	–	–	–	11.5 ± 0.2–10.4 ± 0.2	This study
ZEI1 – A	2	3b	3	Regular	10.0 ± 0.2	1.8	20	10.8 ± 0.3–7.2 ± 0.2	This study
SCHR1 – A	3	3c	3	Regular	20.9 ± 0.6	1.7	6	21.9 ± 0.5–19.3 ± 0.5	This study
SCHR1 – B					20.3 ± 0.2	0.98	16		
SCHR1 – C					19.7 ± 0.4	1.00	6		
MAYR4	3	3d	3	Regular	–	–	–	11.8 ± 0.2–8.9 ± 0.2	This study
PFIT1 – A	5	3e	3	Patchy core	17.3 ± 0.3	1.2	9	17.8 ± 0.4–12.9 ± 0.3	This study
PFIT1 – B					13.2 ± 0.3	0.38	5		
BURG2	6	3f	3	Regular	–	–	–	17.1 ± 0.4–12.1 ± 0.3	This study
PLAN1 – A	7	3g	3	Patchy core	11.9 ± 0.2	2.2	37	12.6 ± 0.3–7.8 ± 0.2	This study
Central Tauern Window									
SCHEI1 – A	8	4a	3	Regular	18.3 ± 1.1	2.0	4	18.9 ± 0.5–15.9 ± 0.4	This study
SCHEI1 – B					17.4 ± 0.4	1.5	5		
SCHEI1 – C					16.6 ± 0.2	1.9	23		
HOPF2 – B	9	4b	3	Regular	12.2 ± 0.4	2.6	8	13.7 ± 0.4–11.0 ± 0.3	This study
HOPF2 – C					12.2 ± 0.5	2.9	6		
GART1 – A	10	4c	3	Regular	16.3 ± 0.2	0.69	10	16.9 ± 0.3–14.5 ± 0.4	This study
NOWA3 – B	11	4d	3	Regular	15.8 ± 0.5	0.27	5	17.0 ± 0.2–13.8 ± 0.8	This study
NOWA3 – C					14.9 ± 1.1	2.4	5		
GART3 – B	12	4e	3	Regular	15.0 ± 0.5	2.3	11	16.1 ± 0.4–12.0 ± 0.4	This study
STEI2	13	4f	3	Regular/patchy tail	17.2 ± 0.2	0.24	20	17.5 ± 0.4–16.8 ± 0.4	This study
KNOR1 – A	14	4g	3	Regular	10.8 ± 0.3	1.02	5	11.6 ± 0.4–10.8 ± 0.3	This study
KNOR1 – B					10.6 ± 0.3	1.6	8		
KNOR1 – C					10.4 ± 0.2	1.4	8		
Eastern Tauern Window									
KAIS6 – A	15	5a	3	Patchy border	21.2 ± 0.5	0.64	6	22.1 ± 0.6–17.6 ± 0.6	This study
KAIS6 – B					20.9 ± 0.2	0.53	24		
KAIS6 – C					20.6 ± 0.5	0.34	7		
KAIS6 – D					18.8 ± 0.5	1.5	10		
SALZ18 – A	16a	5b	3	Regular	18.3 ± 0.4	2.6	14	19.5 ± 0.5–15.8 ± 0.4	This study
T3	16b		–	Regular	18.1 ± 0.4	0.51	4	18.5 ± 0.4–14.8 ± 0.4	Gnos et al. (2015)
					17.2 ± 0.5	3.4	10		
					16.0 ± 0.3	0.51	8		
					15.5 ± 0.2	0.74	24		
LOHN4 – A	17	5c	3	Patchy core	21.1 ± 0.2	1.4	50	22.9 ± 0.6–17.3 ± 0.6	This study
LOHN4 – B					18.4 ± 0.6	1.3	7		
ORT1	18	5d	3	Regular	18.4 ± 0.3	1.07	13	19.0 ± 0.6–17.0 ± 0.7	This study
EUKL2	19a	5e	3	Regular	21.7 ± 0.4	0.56	7	22.3 ± 0.5–21.2 ± 0.5	This study
T2	19b		–	Patchy	15.1 ± 0.5	0.26	4	15.4 ± 0.4–15.0 ± 0.7	Gnos et al. (2015)
HOAR1 – A	20	5f	3	Patchy	20.4 ± 0.2	0.80	6	21.2 ± 0.7–19.0 ± 0.9	This study
HOAR1 – B					19.9 ± 0.3	0.95	25		
T1	21		–	Regular	19.0 ± 0.5	0.51	5	19.2 ± 0.5–14.3 ± 0.5	Gnos et al. (2015)
					17.6 ± 0.6	1.6	8		
					16.3 ± 0.6	3.0	12		
					15.0 ± 0.5	1.7	8		
T4	22		–	Patchy	15.6 ± 0.7	9.1	21	18.3 ± 1.1–13.1 ± 0.8	Gnos et al. (2015)
MOKR1 – B	23	5g	3	Regular	18.8 ± 0.5	2.9	12	22.6 ± 0.4–14.4 ± 0.2	This study
SAND1 – B	24	5h	3	Regular	17.0 ± 0.8	1.8	7	22.0 ± 0.3–14.7 ± 1.0	This study
REIS1 – A	25	5i	3	Regular	16.2 ± 0.5	2.9	13	17.8 ± 0.6–13.5 ± 0.8	This study
REIS1 – B					13.6 ± 0.6	0.25	5		

2020; Gnos et al., 2015). Thorium and uranium (U) contents of the dated fissure monazites display a large variability, ranging from ∼ 200 to 63 000 ppm Th and ∼ 2 to 2000 ppm U, with variations in Th/U ratio from 1 up to ∼ 7000 (Figs. 3, 4 and 5; Table 3). ^{232}Th-^{208}Pb ages presented on the right-hand panel of Figs. 3, 4 and 5 are arranged according to the order established in Table 3. A detailed description of each monazite grain is provided in the Supplement. Average ages are reported for groups of dates on texturally and/or chemically similar domains. In order to ensure that a group of dates from a domain is internally consistent, rare outliers have been excluded to bring the mean square weighted deviation (MSWD) within acceptable values (MSWD < 3; Spencer et al., 2016). In a few cases, the dates for specific monazite domains have a scatter above analytical uncertainty (e.g. grains 6, 9 and 24), which probably reflects the complex formation process of fissure monazite.

The investigated grains from the western part of the western TW subdome come from the Venediger Duplex, with the exception of sample 6, which comes from the Glockner nappe system (Fig. 1; Table 1). Samples 2, 4 and 6 were collected near the major Brenner normal fault, which delimits the TW to the west, and samples 1, 3, 5 and 7 were collected in the vicinity of sinistral strike-slip faults (Fig. 1). Average growth domain ages range from 20.9 ± 0.6 to 10.0 ± 0.2 Ma (samples 3 and 2), with the youngest ages recorded in the western TW (Figs. 1, 3 and 6a; Tables 3 and 4).

The central part of the TW displays growth domain ages between 18.3 ± 1.1 and 10.4 ± 0.2 (samples 8 and 14; Figs. 1 and 4; Tables 3 and 4), but the majority of the dated crystals in this area record ages around 17 Ma (Fig. 6b). Samples 8, 9 and 10 were collected between the eastern and western termination of the ASZ and the SEMP fault (Fig. 1). Another three samples (11, 12 and 13; Table 1) were collected in the northern prolongation of the AhSZ, and a seventh monazite (grain 14) was sampled near the southern border of the eastern part of the western subdome (Fig. 1).

The oldest ages are principally recorded in the eastern part of the TW at around 21 Ma (Fig. 6c). Average ages of growth domains range from 21.7 ± 0.4 to 13.6 ± 0.6 Ma (samples 19a and 25; Figs. 1, 4 and 6c; Tables 3 and 4). The samples were mainly collected at the western border of the eastern subdome, in the Venediger Duplex or near the boundary with the Glockner–Modereck nappe systems (Fig. 1). Sample 25 was taken at some distance from the other samples, near the southeastern border of the eastern subdome (Fig. 1).

5 Discussion

5.1 Fissure monazite ages

The oldest monazite ages of 21.7 ± 0.4 to 19.9 ± 0.3 Ma (found in samples 19a and 20; Figs. 1, 6c and 7a and d) are common in the eastern TW but can also be found in the western area (Fig. 7a, c and d, red symbols). This in line with regional fault activity recorded at ∼ 21 Ma based on Pleuger et al. (2012) (Fig. 8a) which corresponds to the main indentation phase (Favaro et al., 2017). We interpret these as a first monazite crystallization event during E–W extension in association with the dome formation (N–S shortening) when the existing clefts reached P–T conditions at which fissure monazite starts to grow (phase 1, red symbols in Fig. 7). When comparing an assumed fissure formation temperature of 450 °C (typically obtained in quartz fluid inclusion studies on early alpine fissures (e.g. Mullis, 1996) with thermochronological data of the eastern TW (compiled in Wölfler et al., 2012), the onset of fissure formation, predating primary monazite crystallization, is estimated at around 25 Ma. Based on a comparison with thermochronological data, monazite crystallization recorded between 19 and 15 Ma was estimated to have occurred at ∼ 200–300 °C in the eastern TW (Gnos et al., 2015). New monazite ages from this study in the eastern TW are up to ∼ 22 Ma (sample 19 in Fig. 1), suggesting that early monazite crystallization in the area may have occurred at higher temperatures of 350–400 °C.

While early fissure formation is related to E–W extension (leading to flat foliation and E–W mineral lineations; Fig. 2c), we suggest that monazite formation also occurred along the sinistral strike-slip to oblique-slip movements (vertical foliation and flat to inclined lineation; Fig. 2), particularly developed in the central and western parts of the TW (e.g. Rosenberg et al., 2018; Schneider et al., 2013). These shear zones developed as a result of bending of the E–W-oriented upright folds around a vertical axis (leading edge of the Dolomite indenter) (Fig. 1). This occurred when N–S shortening could no longer be accommodated by folding and doming within the TW. Associated with these movements is the formation of a younger generation of fissures (see Pfitscherjoch example above), the peak activity of which is recorded at ∼ 17 Ma (phase 2, green symbols in Fig. 7). This fissure generation is associated with a steep foliation and a flat lineation (Fig. 2) but subparallel in orientation to the earlier fissure formation. The monazite ages at ∼ 17 Ma found in the western and central TW (Figs. 1, 6 and 7; samples 5, 8, 13; Table 4) are associated with sinistral fault zones, as in the Pfitscherjoch region or near the eastern termination of the ASZ and AhSZ faults (see above). Unfortunately, we do not have structural information on the westernmost and easternmost analysed samples (6 and 25; Figs. 1, 6 and 7), but they can be speculated to also have formed in association with a strike-slip shear zone or the BNF and KNF in the case of samples 6 and 25, respectively. At larger scale, these movements seem to have been associated with the development of the sinistral Giudicarie fault (GF, located at the southwestern corner of the TW), offsetting the Periadriatic fault (PF; Fig. 8b, e.g. Pleuger et al., 2012). Ages of ∼ 17 Ma are also recorded in the eastern part of the TW,

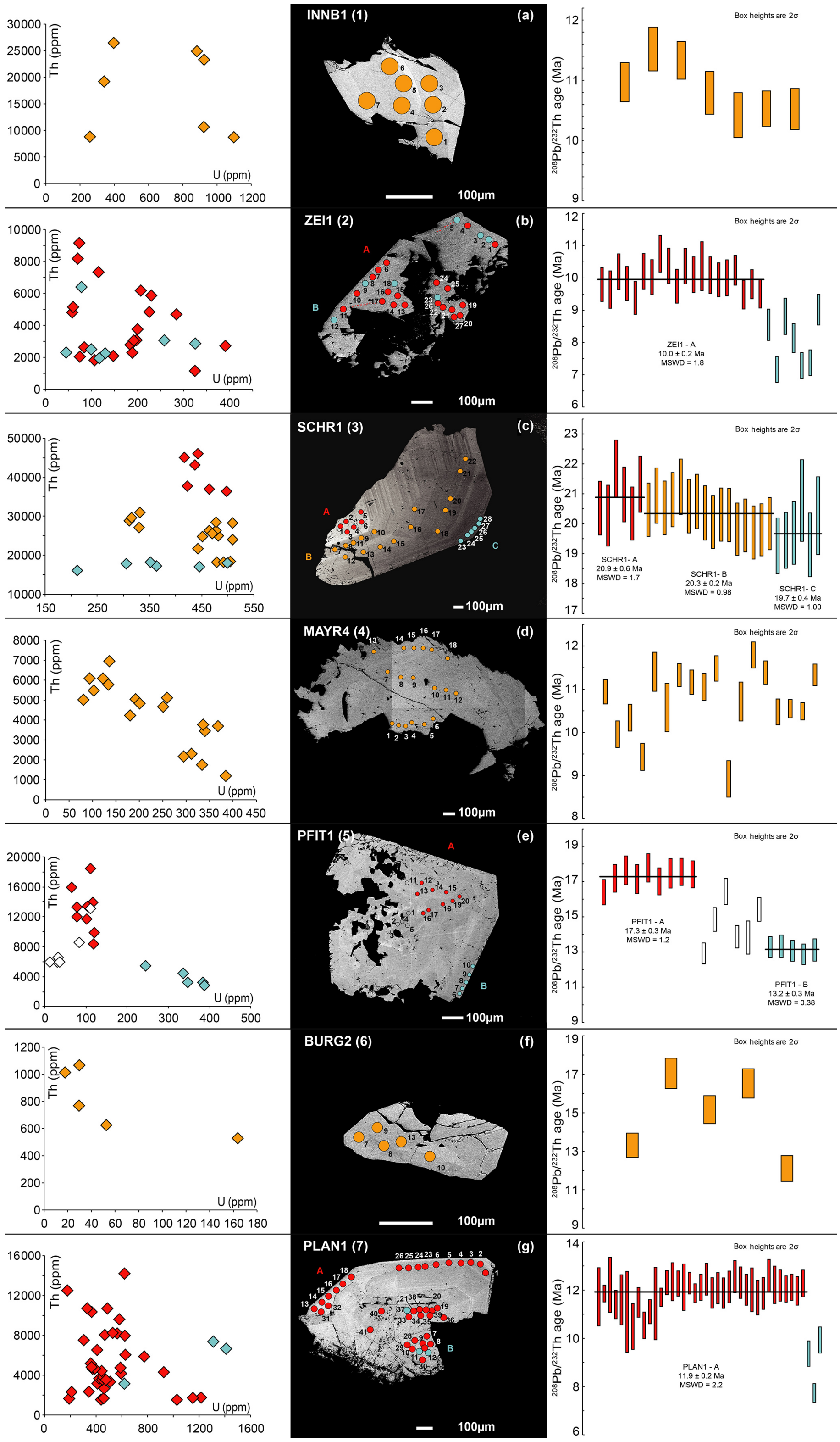

Figure 3. Chemical, textural and geochronological information of monazite grains from the western TW. On BSE images, colour-filled circles correspond to ion probe spot locations. Note that the square-shape shading in grain 4 is due to an artefact of composing BSE images with diverse contrast.

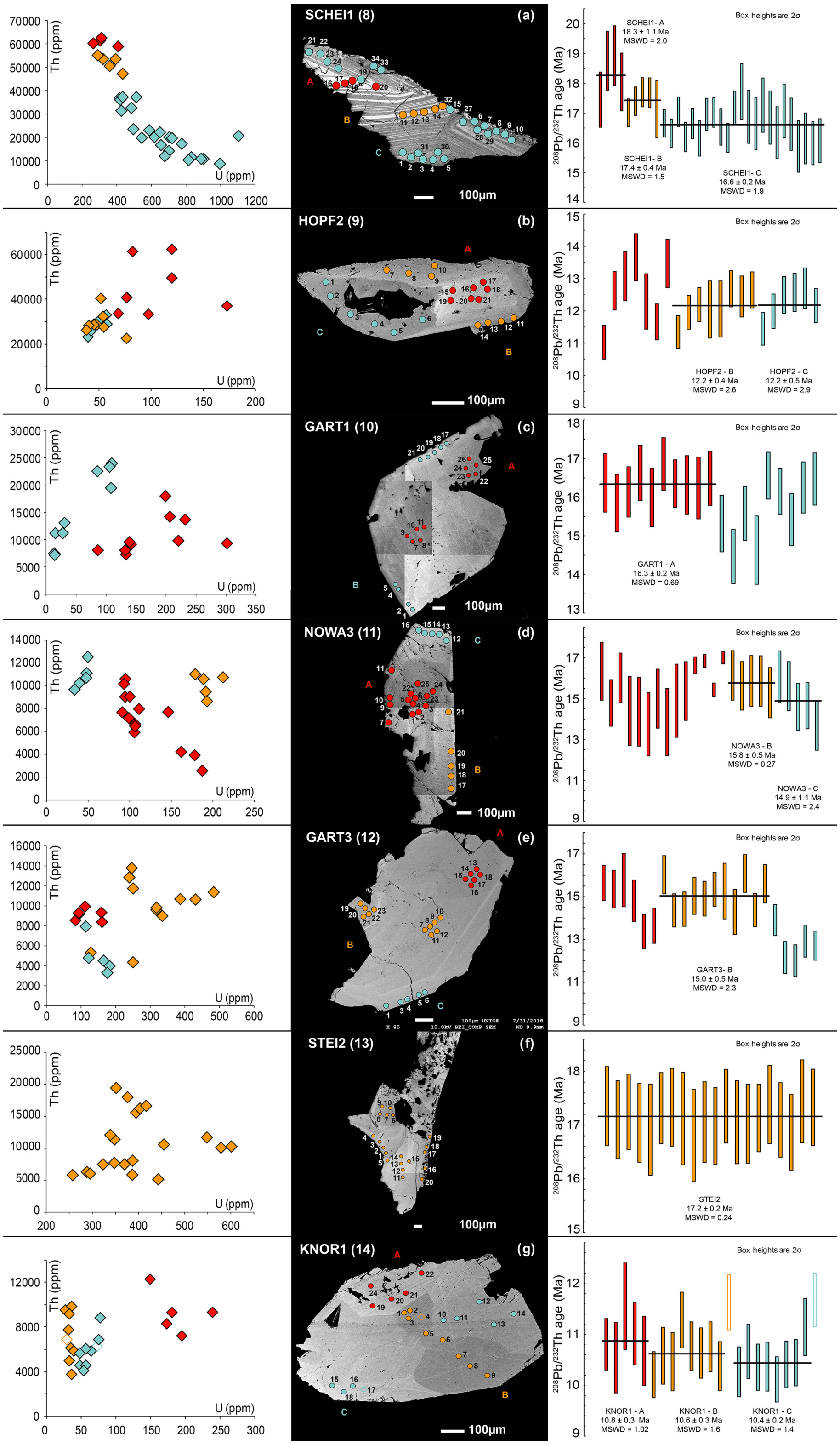

Figure 4. Chemical, textural and geochronological information of monazite grains from the central TW. On BSE images, colour-filled circles correspond to ion probe spot locations. Note that the square-shape shading in grains 10 and 11 is due to an artefact of composing BSE images with diverse contrast.

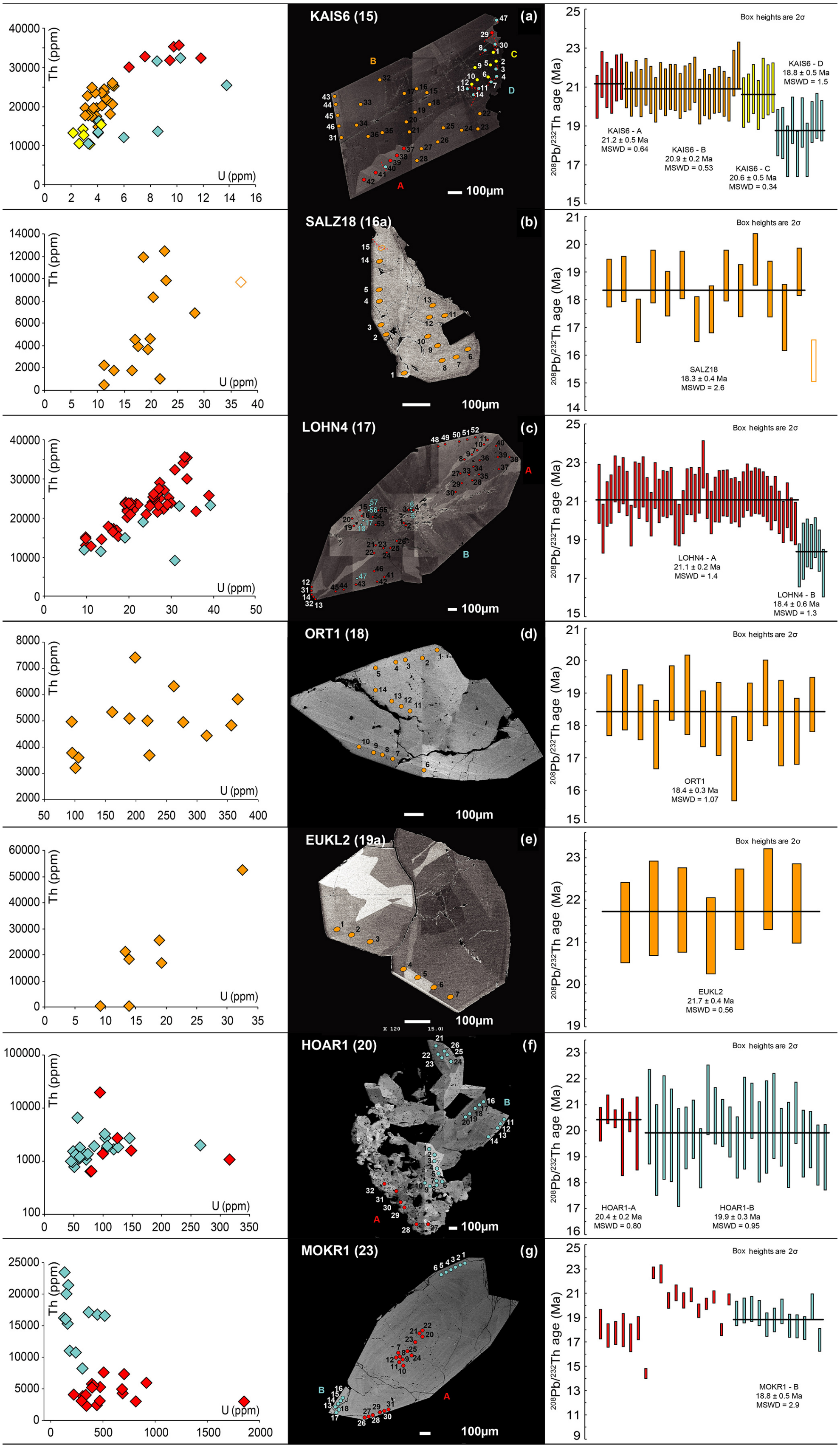
KAIS6 (15)
(a)
SALZ18 (16a)
(b)
LOHN4 (17)
(c)
ORT1 (18)
(d)
EUKL2 (19a)
(e)
HOAR1 (20)
(f)
MOKR1 (23)
(g)
Th (ppm)
U (ppm)
^{208}Pb/^{232}Th age (Ma)
Box heights are 2σ
100µm
KAIS6 - A 21.2 ± 0.5 Ma MSWD = 0.64
KAIS6 - B 20.9 ± 0.2 Ma MSWD = 0.53
KAIS6 - C 20.6 ± 0.5 Ma MSWD = 0.34
KAIS6 - D 18.8 ± 0.5 Ma MSWD = 1.5
SALZ18 18.3 ± 0.4 Ma MSWD = 2.6
LOHN4 - A 21.1 ± 0.2 Ma MSWD = 1.4
LOHN4 - B 18.4 ± 0.6 Ma MSWD = 1.3
ORT1 18.4 ± 0.3 Ma MSWD = 1.07
EUKL2 21.7 ± 0.4 Ma MSWD = 0.56
HOAR1-A 20.4 ± 0.2 Ma MSWD = 0.80
HOAR1-B 19.9 ± 0.3 Ma MSWD = 0.95
MOKR1 - B 18.8 ± 0.5 Ma MSWD = 2.9

Figure 5.

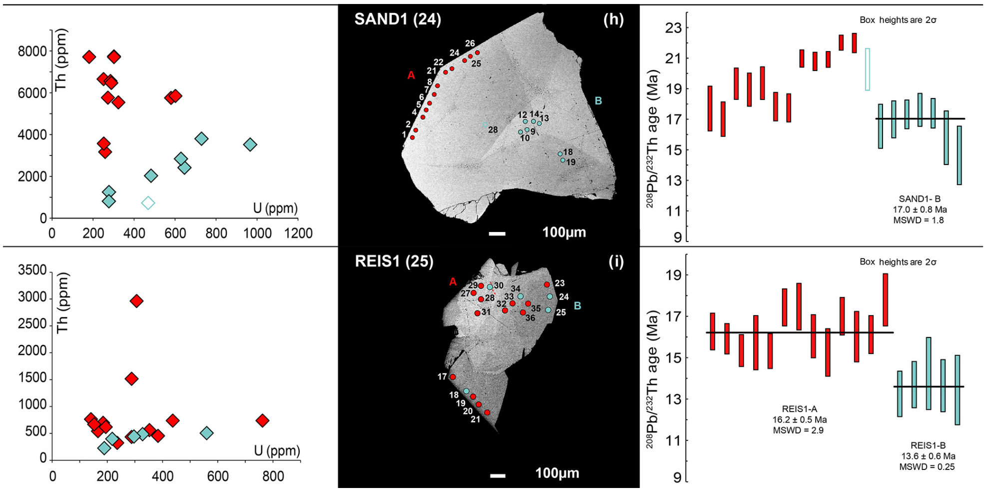

Figure 5. Chemical, textural and geochronological information of monazite grains from the eastern TW. On BSE images, colour-filled circles correspond to ion probe spot locations. Note that the square-shape shading in grains 15, 17, 18 and 20 is due to an artefact of composing BSE images with diverse contrast.

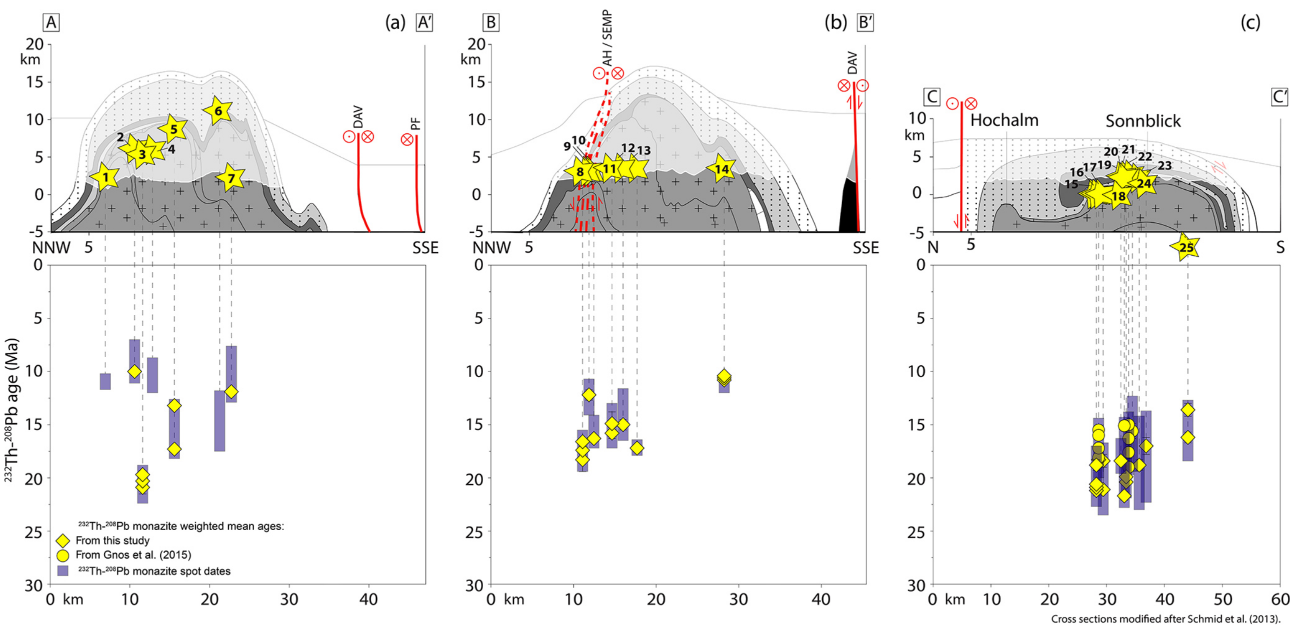

Figure 6. Cross sections of **(a)** the western part of the western subdome, **(b)** the central part of the western subdome and **(c)** the western end of the eastern subdome, modified after (Schmid et al., 2013). See Fig. 1 for locations and legend. Sample locations are indicated by yellow stars and identified by sample numbers listed in Table 1. Monazite crystallization ages are present in the lower part of the figure and are linked to each sample by light-grey dashed lines. Weighted mean ages from this study and from Gnos et al. (2015) are presented by yellow diamonds and yellow circles, respectively, and blue bars correspond to the range of single spot dates.

likely linked to the KNF and Mölltal fault (MöF) activity (samples 16, 21, 24 and 25; Fig. 7a and d; e.g. Favaro et al., 2017). In grains located in the western part of the eastern subdome, in the prolongation of the MöF (e.g. Kurz and Neubauer, 1996) (Fig. 1), numerous monazite growth domains yield ages between 15.6 ± 0.7 and 15.0 ± 0.5 Ma (bracketed by samples 22 and 21 from Gnos et al., 2015; Figs. 1, 6c, 7a and d; green circles in Fig. 7d; Table 4). These ages date the latest known activity of this shear zone to ~ 15 Ma. Whereas younger ages, associated with reactivation of fault zones are widespread in the central and western TW, tectonic movements seem to cease in the eastern TW after this time (Fig. 8c).

The youngest monazite growth domain ages, principally recorded in the western subdome, range from 13.2 ± 0.3 to 10.0 ± 0.2 Ma (samples 5 and 2; Table 4), indicating steps

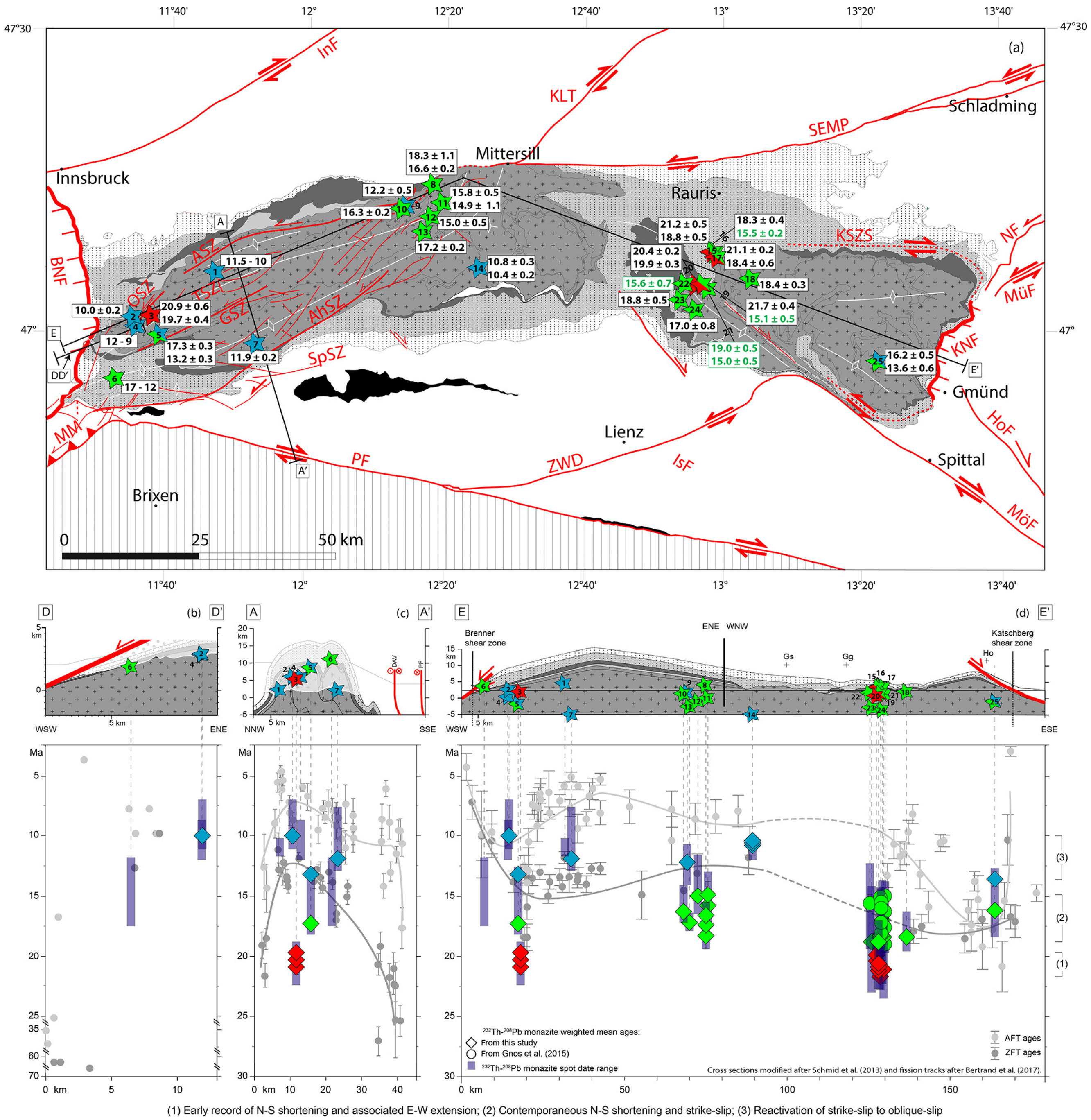

Figure 7. **(a)** Map of the TW from Fig. 1 with sample locations coloured as function of deformation episodes (coloured stars). See Fig. 1 for legend. **(b)** DD' NE–SW cross section across the BNF, **(c)** AA' NW–SE cross section perpendicular to the axial plane of the western subdome and **(d)** EE' longitudinal cross section parallel to the main axial plane of the TW metamorphic dome, modified after Bertrand et al. (2017). In the upper part, coloured and numbered stars correspond to sample locations and are linked to corresponding Th-Pb monazite ages by dashed vertical lines. Sample numbers refer to Table 1. In the lower part, monazite weighted mean ages from this study and from Gnos et al. (2015) are labelled by coloured diamond and circles, respectively, and the range of single spot dates is depicted by blue bars. The colour code used for diamonds and circles follows deformation episodes explained in the discussion. Note that most error bars are smaller than the size of the diamonds and circles. Zircon and apatite fission track ages are from the Bertrand et al. (2017) compilation; light- and dark-grey dots with error bars are displayed for comparison. Square brackets shown to the right delimit the main periods of monazite growth discussed in the text: (1) early record of N–S shortening and associated E–W extension, (2) contemporaneous N–S shortening and strike slip, (3) reactivation of strike slip to oblique slip.

of reactivation of the different sinistral strike-slip to oblique-slip movements along different faults (phase 3 and blue symbols in Fig. 7). Based on our monazite crystallization data, the oldest activities of this younger phase are recorded near the GSZ (sample 5) and in the prolongation of the AhSZ (samples 7 and 9). The youngest activities are recorded in association with the ASZ, OSZ and TSZ in Fig. 7a–c (samples 1, 2 and 4), and in the central TW in an area located south of the main fault systems (sample 14; Fig. 7a). In addition to faults activity at ∼ 12 Ma (Fig. 8), coeval strike-slip activity has also been documented in many areas of the central and western Alps (e.g. Bergemann et al., 2017, 2019; Berger et al., 2013; Gasquet et al., 2010; Grand'Homme et al., 2016a; Pleuger et al., 2012; Ricchi et al., 2019).

In summary, in the western TW, monazite ages (Fig. 1) constrain the activities of the ASZ (18–12 Ma, samples 8 and 9), AhSZ (17–12 Ma, samples 13 and 7), TSZ/OSZ (11.5–10 Ma, samples 1 and 2; older ages of sample 3 are probably related to extensional unroofing) and GSZ (17–13 Ma). In the eastern part, the MöF is active between 19 and 15 Ma.

5.2 Comparison with shear zone dating

A number of attempts to date shear zone activity in the TW using Ar-Ar, Rb-Sr and Sm-Nd techniques have been made in the past, which were, however, based on mineral separation techniques without a clear structural control on the dated grains (e.g. Blanckenburg et al., 1989; Glodny et al., 2008; Pollington and Baxter, 2010, 2011; Urbanek et al., 2002). An exception to this is the $^{40}Ar/^{39}Ar$ study of Schneider et al. (2013) on syn-kinematic phengite and K-feldspar which will be used in the following as a comparison (Table 2). Fissure monazite ages largely corroborate this work, similarly showing the longevity of different shear zones in the TW. The ages confirm that even though most of the dated monazite samples are only located in the damage zone in the vicinity of the core of the shear zones, fluid-filled fissures provide a sensitive system where tectonic activity triggers fluid-enhanced dissolution–precipitation reactions at lower greenschist to sub-greenschist facies conditions.

While Schneider et al. (2013) obtained crystallization age ranges of 33–15 Ma for the ASZ, 24–12 Ma for the TSZ and 20–7 Ma for the GSZ (Table 2), our data confirm fluid activity, and thus possible tectonic activity, at 18–12, 11.5–10 and 17–13 Ma, respectively (Fig. 7). However, the oldest dates from Schneider et al. (2013) might also be interpreted as older grains that have been aligned in the new foliation (Fig. 8). The data presented here indicate that all of the shear zones where potentially active at least until ∼ 13–12 Ma, and the Tuxer and/or Olperer shear zones even until ∼ 7 Ma, as suggested by younger dates observed in grain 2 (Figs. 3b, 6a and 7, Tables 3 and 4). However, the fissure monazite data do not date the initiation of the GSZ (Selverstone et al., 1991) nor the earliest activity of the TSZ (greenschist to amphibolite facies; Selverstone et al., 1984, 1991) or the ASZ

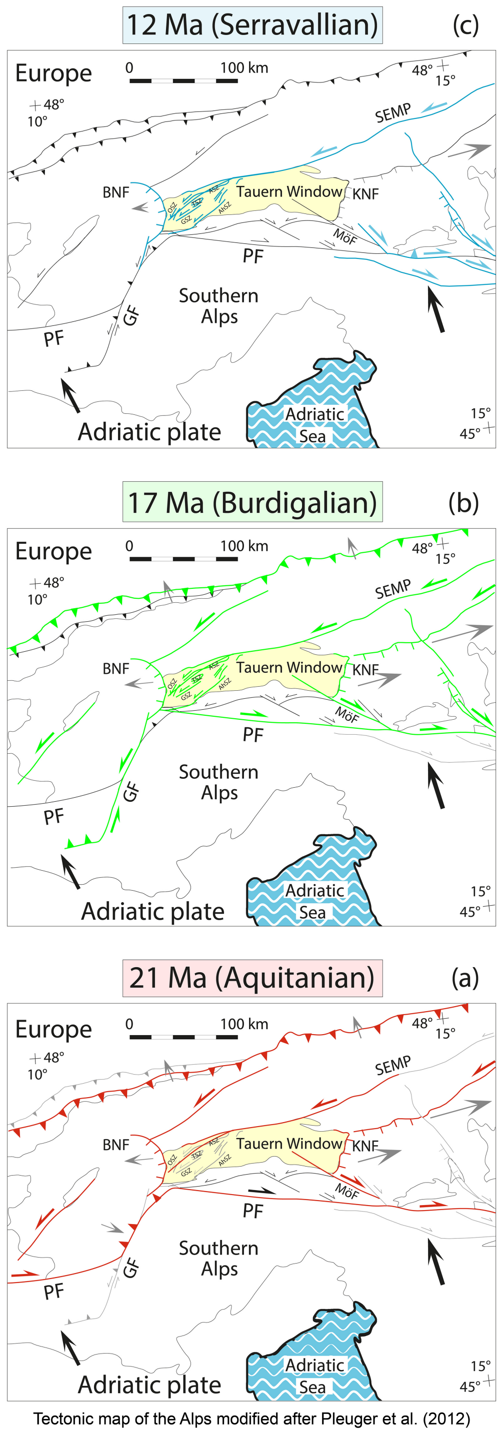

Figure 8. Tectonic map of the Alps based on Pleuger et al. (2012) showing active Cenozoic faults at ∼ 21 (in red), 17 (in green) and 12 Ma (in blue), respectively. Note that after 17 Ma the Giudicarie fault (GF) becomes active and hence the Periadriatic fault (PF) and the Mölltal fault (MöF, dextral fault at the southeastern corner of the TW) become inactive. Sinistral strike-slip faulting starts at ∼ 19 Ma and is affecting the western and central parts of the TW until at least 7 Ma. Future active faults are depicted in grey and inactive faults in black.

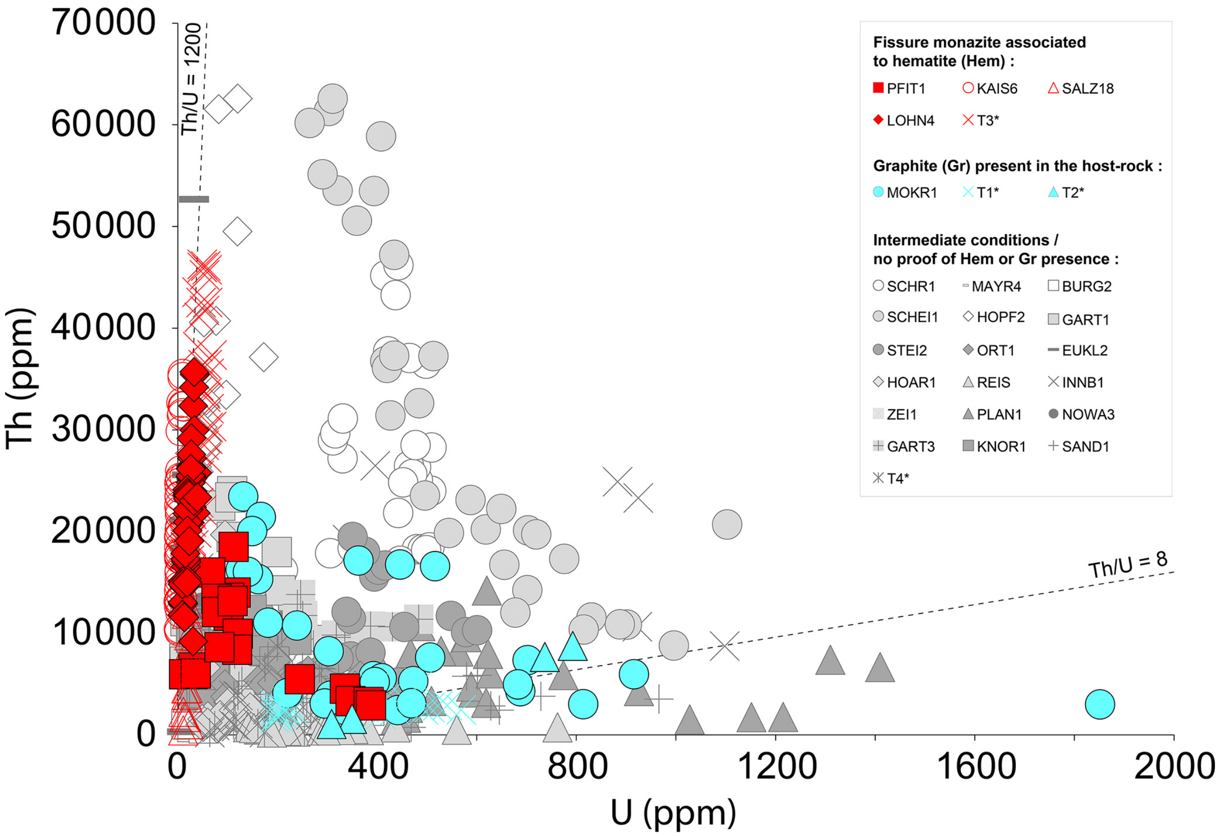

Figure 9. Th as function of U content obtained for all the monazite grains analysed in this study. Samples indicated by an asterisk are from Gnos et al. (2015). Fissure monazite grains associated with hematite (oxidizing conditions) are labelled in red, whereas grains hosted in graphite-bearing rocks (reducing conditions) are labelled in blue. Samples with intermediate composition and/or for which we have no information on the presence of hematite or graphite in the fissure environment are labelled in grey.

(greenschist facies; Cole et al., 2007), since their formation already started at amphibolite facies conditions. As Alpine fissures only form under greenschist facies conditions, the oldest monazite crystallization ages are younger than the data obtained by Schneider et al. (2013). This indicates that shear zone activity started earlier than the fissure monazite record. As the monazite age range of the younger fault activity is comparable to the data of Schneider et al. (2013) but is not the same for individual shear zones, it seems likely that all shear zones of the western TW were active as recently as 8–7 Ma.

5.3 Comparison with fission track data

There is a wealth of zircon fission track (ZFT) data that can assist in describing the exhumation and low-grade tectonic activity in the TW (Bertrand, 2014; Bertrand et al., 2017; Dunkl et al., 2003; Fügenschuh et al., 1997; Mancktelow et al., 2001; Most, 2003; Pomella et al., 2011; Steenken et al., 2002; Stöckhert et al., 1999; Viola et al., 2001; Wölfler et al., 2008) and apatite fission track (AFT) data (Bertrand, 2014; Bertrand et al., 2017; Coyle, 1994; Di Fiore, 2013; Foeken et al., 2007; Fügenschuh et al., 1997; Grundmann and Morteani, 1985; Hejl, 1997; Mancktelow et al., 2001; Most, 2003; Pomella et al., 2011; Staufenberg, 1987; Steenken et al., 2002; Viola et al., 2001; Wölfler et al., 2008, 2012).

Three cross sections, DD' (perpendicular to the BNF), AA' (perpendicular to the western limb of the western subdome) and EE' (parallel to the main axial plane of the TW), are presented in Fig. 7, redrawn after Bertrand et al. (2017) and Schmid et al. (2013). Zircon and apatite fission track data compiled by Bertrand et al. (2017) are displayed in the lower part of Fig. 7b–d and compared to fissure monazite ages. As described in Bertrand et al. (2017) (first model), fission track data along the AA' cross section (Fig. 7c) nicely display a dome-like shape, with younger ages recorded near the subdome axial plane, where cooling was slower. By contrast, along the EE' longitudinal cross section (Fig. 7d), ZFT and AFT are younger on the western and eastern borders of the TW where the two major extensional faults, the BNF and KNF, are respectively located. Perpendicular to the BNF (DD' cross section, Fig. 7b), the fission tracks record cooling ages younging from the footwall toward the plane of the normal fault (from 10 to 4 Ma for AFT; second model of Bertrand et al., 2017). Along the EE’ cross section, the youngest monazite ages (15–10 Ma) lie between zircon and apatite fission track data (grey and blue symbols), whereas the older ages (> 17 Ma) do not follow the cooling trend and are equal to or older than the ZFT data. This means that at least the fissure monazites recording older ages crystallized somewhere above ZFT closure temperatures of ∼ 240–280 °C (Bernet, 2009; Bernet and Garver, 2005; Reiners, 2005; Yamada et al., 1995) (Fig. 7d).

5.4 Monazite Th/U as monitor of oxidizing and reducing conditions

Extreme low and high Th/U ratios described in fissure monazite by Gnos et al. (2015) (T1, T2 and T3 samples in Fig. 9) are also observed in some grains from this study (red and blue labels in Fig. 9). Hydrothermal monazite from the TW associated with hematite in fissure typically displays very high Th/U ratios of around 1200 (Fig. 9, red labels; Table 1), whereas grains obtained from graphite-bearing host rocks show very low Th/U ratios around 8 (Fig. 9, blue labels; Table 1). This attests for oxidizing and reducing fluid conditions in the fissure environment, respectively.

The Th/U in monazite grains PFIT1 and MOKR1 would instead record a dynamic oxidation environment due to variable fluid conditions. In PFIT1 monazite, the Th/U decreases from core to rim, whereas within MOKR1 the opposite evolution is observed (Fig. 9). Thus, in the first case, the fissure environment evolves toward reducing conditions, whereas in the second case there is an evolution towards more oxidizing conditions. Many of the other grains indicate intermediate oxidizing conditions and they could not be assigned to one of the two categories defined above, as the presence of either hematite or graphite is uncertain (Fig. 9; grey labels).

6 Conclusions

Th-Pb ages of fissure monazite provide an extended record of exhumation of the TW during the Miocene. The investigated monazites crystallized at temperatures < 400 °C in the presence of hydrothermal fluids that circulated in open fissures formed through tectonic movements. The Th-Pb ages recorded by fissure monazites are in general agreement with previously published geochronological data and range between 21.7 ± 0.4 and 10.0 ± 0.2 Ma. Spot dates suggests that monazite crystallization in the metamorphic and structural TW dome occurred over a period of ∼ 16 Myr. The combination of structural and geochronological information allows relating monazite growth to tectonic movements that affected the TW. The three major growth episodes identified in this study, by dating monazite growth domains, are interpreted to be associated with N–S shortening associated with the E–W extension (22–20 Ma), contemporaneous N–S shortening and sinistral strike-slip movements (19–15 Ma) and reactivation of strike-slip/normal faulting (14–10 Ma). Overall, fissure monazite age recording indicates that in the TW Cenozoic faults show increased activity at ∼ 21, ∼ 17 and ∼ 12 Ma, probably due to reorganization of plate movements occurring at those times. Comparison of Th-Pb fissure monazite crystallization ages with existing crystallization and cooling ages (e.g. AFT, ZFT, white mica from fault zones) shows that the latest stages of monazite crystallization occurred at temperatures between apatite and zircon fission track “closure” temperatures. This enlarged dataset also supports previous observations on fissure monazite chemistry displaying extremely high Th/U ratios (∼ 1200) under oxidizing conditions in association with hematite.

Data availability. The data used in this study are available in Tables 3 and 4.

Supplement. The supplement related to this article is available online at: https://doi.org/10.5194/se-11-437-2020-supplement.

Author contributions. Fissure monazite samples were organized by EG and FW. Monazite samples for dating were selected by ER, CAB, EG and AB according to tectonic settings and fault activity of the study area. ER prepared the manuscript during her PhD project under the supervision of EG, with contributions from all coauthors. Sample preparation and BSE imaging were performed by ER and CAB. Data acquisition and reduction at the SwissSIMS and NordSIMS facility was, respectively, carried out by ER and CAB under the supervision of DR and MJW.

Competing interests. The authors declare that they have no conflict of interest.

Acknowledgements. We thank Sepp Brugger, Kurt Novak, Franz Gartner, Peter Hellweger, Adolf Meyer, Sebastian Planken-Steiner, Johann Rappold, Josef Rathgeb, Alexandre Salzmann, Maria Schaffhauser, Andreas Steiner, and Ermin Welzl for providing samples for this study. Urs Klötzli and Jan Pleuger are thanked for their helpful comments.

Financial support. This research has been supported by the Swiss National Science Foundation (grant no. 200020-165513). The NordSIMS facility received funding from the Swedish Research Council (infrastructure grant no. 2014-06375) and the Swedish Museum of Natural History; this is NordSIMS publication no. 636.

Review statement. This paper was edited by Bernhard Grasemann and reviewed by Jan Pleuger and Urs Klötzli.

References

Aleinikoff, J. N., Schenck, W. S., Plank, M. O., Srogi, L. A., Fanning, C. M., Kamo, S. L., and Bosbyshell, H.: Deciphering igneous and metamorphic events in high-grade rocks of the Wilmington complex, Delaware: Morphology, cathodoluminescence and backscattered electron zoning, and SHRIMP U-Pb geochronology of zircon and monazite, Bull. Geol. Soc. Am., 118, 39–64, https://doi.org/10.1130/B25659.1, 2006.

Ayers, J. C., Miller, C., Gorisch, B., and Milleman, J.: Textural development of monazite during high-grade metamorphism: Hydrothermal growth kinetics, with implications for U,Th-Pb geochronology, Am. Mineral., 84, 1766–1780, https://doi.org/10.2138/am-1999-11-1206, 1999.

Bergemann, C. A., Gnos, E., Berger, A., Whitehouse, M., Mullis, J., Wehrens, P., Pettke, T., and Janots, E.: Th-Pb ion probe dating of zoned hydrothermal monazite and its implications for repeated shear zone activity: An example from the Central Alps, Switzerland, Tectonics, 36, 671–689, https://doi.org/10.1002/2016TC004407, 2017.

Bergemann, C. A., Gnos, E., Berger, A., Whitehouse, M. J., Mullis, J., Walter, F., and Bojar, H. P.: Constraining long-term fault activity in the brittle domain through in situ dating of hydrothermal monazite, Terra Nov., 30, 440–446, https://doi.org/10.1111/ter.12360, 2018.

Bergemann, C. A., Gnos, E., and Whitehouse, M. J.: Insights into the tectonic history of the Western Alps through dating of fissure monazite in the Mont Blanc and Aiguilles Rouges Massifs, Tectonophysics, 750, 203–212, https://doi.org/10.1016/j.tecto.2018.11.013, 2019.

Bergemann, C. A., Gnos, E., Berger, A., Janots, E., and Whitehouse, M. J.: Dating tectonic activity in the Lepontine Dome and Rhone-Simplon Fault regions through hydrothermal monazite-(Ce), Solid Earth, 11, 199–222, https://doi.org/10.5194/se-11-199-2020, 2020.

Berger, A., Gnos, E., Janots, E., Whitehouse, M., Soom, M., Frei, R., and Waight, T. E.: Dating brittle tectonic movements with cleft monazite: Fluid-rock interaction and formation of REE minerals, Tectonics, 32, 1176–1189, https://doi.org/10.1002/tect.20071, 2013.

Bernet, M.: A field-based estimate of the zircon fission-track closure temperature, Chem. Geol., 259, 181–189, https://doi.org/10.1016/j.chemgeo.2008.10.043, 2009.

Bernet, M. and Garver, J. I.: Fission-track analysis of detrital zircon, Rev. Mineral. Geochem., 58, 205–237, 2005.

Bertrand, A.: Exhuming the core of collisional orogens, the Tauern Window (Eastern-Alps), A geochronological, modelling and structural study, PhD tesis, Freie Univ. Berlin, 2014.

Bertrand, A., Rosenberg, C., and Garcia, S.: Fault slip analysis and late exhumation of the Tauern Window, Eastern Alps, Tectonophysics, 649, 1–17, https://doi.org/10.1016/j.tecto.2015.01.002, 2015.

Bertrand, A., Rosenberg, C., Rabaute, A., Herman, F., and Fügenschuh, B.: Exhumation mechanisms of the Tauern Window (Eastern Alps) inferred from apatite and zircon fission track thermochronology, Tectonics, 36, 207–228, https://doi.org/10.1002/2016TC004133, 2017.

Blanckenburg, F. v., Villa, I. M., Baur, H., Morteani, G., and Steiger, R. H.: Time calibration of a PT-path from the Western Tauern Window, Eastern Alps: the problem of closure temperatures, Contrib. Mineral. Petrol., 101, 1–11, https://doi.org/10.1007/BF00387196, 1989.

Cherniak, D. J., Watson, E. B., Grove, M., and Harrison, T. M.: Pb diffusion in monazite: A combined RBS/SIMS study, Geochim. Cosmochim. Ac., 68, 829–840, https://doi.org/10.1016/j.gca.2003.07.012, 2004.

Cole, J., Hacker, B., Ratschbacher, L., Dolan, J., Seward, G., Frost, E., and Frank, W.: Localized ductile shear below the seismogenic zone: Structural analysis of an exhumed strike-slip fault, Austrian Alps, J. Geophys. Res.-Sol. Ea., 112, 1–15, https://doi.org/10.1029/2007JB004975, 2007.

Coyle, D. A.: The application of apatite fission-track analysis to problem in tectonics, PhD thesis, La Trobe Univ. Bundoora, Victoria, Australia, 1994.

Di Fiore, G.: Evoluzione Morfotettonica delle aree alpine "Sempione" e "Brennero" attraverso studi termocronologici di bassa temperatura, PhD thesis, Università di Bologna, 2013.

Dunkl, I., Frisch, W., and Grundmann, G.: Zircon fission-track thermochronology of the south-eastern part of the TW and the adjacent Austroalpine margin, Eastern Alps, Eclogae Geol. Helv., 96, 209–217, 2003.

Favaro, S., Handy, M. R., Scharf, A., and Schuster, R.: Changing patterns of exhumation and denudation in front of an advancing crustal indenter, Tauern Window (Eastern Alps), Tectonics, 36, 1053–1071, https://doi.org/10.1002/2016TC004448, 2017.

Fitz-Diaz, E., Cottle, J. M., Vidal-Reyes, M. I., and van der Pluijm, B.: In situ Th/Pb dating of monazite in fibrous veins: Direct dating of veins and deformation in the shallow upper crust of the Mexican Orogen, J. Struct. Geol., 124, 136–142, https://doi.org/10.1016/j.jsg.2019.04.004, 2019.

Foeken, J. P. T., Persano, C., Stuart, F. M., and ter Voorde, M.: Role of topography in isotherm perturbation: Apatite (U−Th)/He and fission track results from the Malta tunnel, Tauern Window, Austria, Tectonics, 26, https://doi.org/10.1029/2006TC002049, 2007.

Fügenschuh, B., Seward, D., and Mancktelow, N.: Exhumation in a convergent orogen: the western Tauern Window, Terra Nov., 9, 213–217, https://doi.org/10.1111/j.1365-3121.1997.tb00015.x, 1997.

Gardés, E., Jaoul, O., Montel, J. M., Seydoux-Guillaume, A. M., and Wirth, R.: Pb diffusion in monazite: An experimental study of $Pb^{2+} + Th^{4+} <=> 2Nd^{3+}$ interdiffusion, Geochim. Cosmochim. Ac., 70, 2325–2336, https://doi.org/10.1016/j.gca.2006.01.018, 2006.

Gardés, E., Montel, J. M., Seydoux-Guillaume, A. M., and Wirth, R.: Pb diffusion in monazite: New constraints from the experimental study of $Pb^{2+} <=> Ca^{2+}$ interdiffusion, Geochim. Cosmochim. Ac., 71, 4036–4043, https://doi.org/10.1016/j.gca.2007.06.036, 2007.

Gasquet, D., Bertrand, J. M., Paquette, J. L., Lehmann, J., Ratzov, G., Ascenção De Guedes, R. A., Tiepolo, M., Boullier, A. M., Scaillet, S., and Nomade, S.: Miocene to Messinian deformation and hydrothermal activity in a pre-Alpine basement massif of the French western Alps: New U-Th-Pb and argon ages from the Lauzière massif, Bull. Soc. Geol. Fr., 181, 227–241, https://doi.org/10.2113/gssgfbull.181.3.227, 2010.

Glodny, J., Ring, U., and Kühn, A.: Coeval high-pressure metamorphism, thrusting, strike-slip, and extensional shearing in the Tauern Window, Eastern Alps, Tectonics, 27, https://doi.org/10.1029/2007TC002193, 2008.

Gnos, E., Janots, E., Berger, A., Whitehouse, M., Walter, F., Pettke, T., and Bergemann, C. A.: Age of cleft monazites in the eastern Tauern Window: constraints on crystallization conditions of hydrothermal monazite, Swiss J. Geosci., 108, 55–74, https://doi.org/10.1007/s00015-015-0178-z, 2015.

Grand'Homme, A., Janots, E., Bosse, V., Seydoux-Guillaume, A. M., and Ascenção De Guedes, R. A.: Interpretation of U-Th-Pb in-situ ages of hydrothermal monazite-(Ce) and xenotime-(Y): evidence from a large-scale regional study in clefts from the western alps, Mineral. Petrol., 110, 787–807, https://doi.org/10.1007/s00710-016-0451-5, 2016a.

Grand'Homme, A., Janots, E., Seydoux-Guillaume, A. M., Guillaume, D., Bosse, V., and Magnin, V.: Partial resetting of the U-Th-Pb systems in experimentally altered monazite: Nanoscale evidence of incomplete replacement, Geology, 44, 431–434, https://doi.org/10.1130/G37770.1, 2016b.

Grand'Homme, A., Janots, E., Seydoux-Guillaume, A. M., Guillaume, D., Magnin, V., Hövelmann, J., Höschen, C., and Boiron, M. C.: Mass transport and fractionation during monazite alteration by anisotropic replacement, Chem. Geol., 484, 51–68, https://doi.org/10.1016/j.chemgeo.2017.10.008, 2018.

Grundmann, G. and Morteani, G.: The young uplift and thermal history of the central Eastern Alps (Austria/Italy), evidence from apatite fission track ages, Jahrb. Geol. Bundesanst, 128, 197–216, 1985.

Hejl, E.: "Cold spots" during the Cenozoic evolution of the Eastern Alps: Thermochronological interpretation of apatite fission-track data, Tectonophysics, 272, 159–173, https://doi.org/10.1016/S0040-1951(96)00256-9, 1997.

Janots, E., Berger, A., Gnos, E., Whitehouse, M., Lewin, E., and Pettke, T.: Constraints on fluid evolution during metamorphism from U–Th–Pb systematics in Alpine hydrothermal monazite, Chem. Geol., 326, 61–71, 2012.

Janots, E., Grand'Homme, A., Bernet, M., Guillaume, D., Gnos, E., Boiron, M.-C., Rossi, M., Seydoux-Guillaume, A.-M., and De Ascenção Guedes, R.: Geochronological and thermometric evidence of unusually hot fluids in an Alpine fissure of Lauzière granite (Belledonne, Western Alps), Solid Earth, 10, 211–223, https://doi.org/10.5194/se-10-211-2019, 2019.

Kurz, W. and Neubauer, F.: Deformation partitioning during updoming of the Sonnblick area in the Tauern Window (Eastern Alps, Austria), J. Struct. Geol., 18, 1327–1337, https://doi.org/10.1016/S0191-8141(96)00057-0, 1996.

Ludwig, K. R.: User's manual for a geochronological toolkit for Microsoft Excel (Isoplot/Ex version 3.0), Berkeley Geochronol. Cent. Spec. Publ., 4, 1–70, 2003.

Luth, S. W. and Willingshofer, E.: Mapping of the post-collisional cooling history of the Eastern Alps, Swiss J. Geosci., 101, 207–223, https://doi.org/10.1007/s00015-008-1294-9, 2008.

Mancktelow, N. S., Stöckli, D. F., Grollimund, B., Müller, W., Fügenschuh, B., Viola, G., Seward, D., and Villa, I. M.: The DAV and Pediatriatic fault systems in the Eastern Alps South of the Tauern window, Int. J. Earth Sci., 90, 593–622, https://doi.org/10.1007/s005310000190, 2001.

Most, P.: Late Alpine cooling histories of tectonic blocks along the central part of the Transalp-Traverse (Inntal-Gadertal): Constraints from geochronology, PhD thesis, University of Tübingen, p. 97, 2003.

Mullis, J.: P-T-t path of quartz formation in extensional veins of the Central Alps, Schweiz. Miner. Petrogr. Mitt, 76, 159–164, https://doi.org/10.5169/seals-57694, 1996.

Mullis, J., Dubessy, J., Poty, B., and O'Neil, J.: Fluid regimes during late stages of a continental collision: physical, chemical, and stable isotope measurements of fluid inclusions in fissure quartz from a geotraverse through the Central Alps, Switzerland, Geochim. Cosmochim. Ac., 58, 2239–2267, 1994.

Pleuger, J., Mancktelow, N., Zwingmann, H., and Manser, M.: K-Ar dating of synkinematic clay gouges from Neoalpine faults of the Central, Western and Eastern Alps, Tectonophysics, 550, 1–16, https://doi.org/10.1016/j.tecto.2012.05.001, 2012.

Pollington, A. D. and Baxter, E. F.: High resolution Sm-Nd garnet geochronology reveals the uneven pace of tectonometamorphic processes, Earth Planet. Sc. Lett., 293, 63–71, https://doi.org/10.1016/j.epsl.2010.02.019, 2010.

Pollington, A. D. and Baxter, E. F.: High precision microsampling and preparation of zoned garnet porphyroblasts for Sm-Nd geochronology, Chem. Geol., 281, 270–282, https://doi.org/10.1016/j.chemgeo.2010.12.014, 2011.

Pomella, H., Klötzli, U., Scholger, R., Stipp, M., and Fügenschuh, B.: The Northern Giudicarie and the Meran-Mauls fault (Alps, Northern Italy) in the light of new paleomagnetic and geochronological data from boudinaged Eo-/Oligocene tonalites, Int. J. Earth Sci., 100, 1827–1850, https://doi.org/10.1007/s00531-010-0612-4, 2011.

Putnis, A.: Mineral Replacement Reactions, Rev. Miner. Geochem., 70, 87–124, https://doi.org/10.2138/rmg.2009.70.3, 2009.

Reiners, P. W.: Zircon (U−Th)/He Thermochronometry, in: Reviews in Mineralogy and Geochemistry, vol. 58, 151–179, 2005.

Ricchi, E., Bergemann, C. A., Gnos, E., Berger, A., Rubatto, D., and Whitehouse, M. J.: Constraining deformation phases in the Aar Massif and the Gotthard Nappe (Switzerland) using Th-Pb crystallization ages of fissure monazite-(Ce), Lithos, 342/343, 223–238, https://doi.org/10.1016/j.lithos.2019.04.014, 2019.

Rosenberg, C. L. and Berger, A.: On the causes and modes of exhumation and lateral growth of the Alps, Tectonics, 28, https://doi.org/10.1029/2008TC002442, 2009.

Rosenberg, C. L. and Garcia, S.: Estimating displacement along the Brenner Fault and orogen-parallel extension in the Eastern Alps, Int. J. Earth Sci., 100, 1129–1145, https://doi.org/10.1007/s00531-011-0645-3, 2011.

Rosenberg, C. L. and Schneider, S.: The western termination of the SEMP Fault (eastern Alps) and its bearing on the exhumation of the Tauern Window, Geol. Soc. Lond. Spec. Publ., 298, 197–218, 2008.

Rosenberg, C. L., Schneider, S., Scharf, A., Bertrand, A., Hammerschmidt, K., Rabaute, A., and Brun, J. P.: Relating collisional kinematics to exhumation processes in the Eastern Alps, Earth-Sci. Rev., 176, 311–344, https://doi.org/10.1016/j.earscirev.2017.10.013, 2018.

Scharf, A., Handy, M. R., Favaro, S., Schmid, S. M., and Bertrand, A.: Modes of orogen-parallel stretching and extensional exhumation in response to microplate indentation and roll-back subduction (Tauern Window, Eastern Alps), Int. J. Earth Sci., 102, 1627–1654, https://doi.org/10.1007/s00531-013-0894-4, 2013.

Schmid, S. M., Fügenschuh, B., Kissling, E., and Schuster, R.: Tectonic map and overall architecture of the Alpine orogen, Eclogae Geol. Helv., 97, 93–117, https://doi.org/10.1007/s00015-004-1113-x, 2004.

Schmid, S. M., Scharf, A., Handy, M. R., and Rosenberg, C. L.: The Tauern Window (Eastern Alps, Austria): a new tectonic map, with cross-sections and a tectonometamorphic synthesis, Swiss J. Geosci., 106, 1–32, https://doi.org/10.1007/s00015-013-0123-y, 2013.

Schneider, S., Hammerschmidt, K., and Rosenberg, C. L.: Dating the longevity of ductile shear zones: Insight from $^{40}Ar/^{39}Ar$ in situ analyses, Earth Planet. Sc. Lett., 369–370, 43–58, https://doi.org/10.1016/j.epsl.2013.03.002, 2013.

Selverstone, J.: Evidence for east-west crustal extension in the Eastern Alps: Implications for the unroofing history of the Tauern Window, Tectonics, 7, 87–105, 1988.

Selverstone, J., Spear, F. S., Franz, G., and Morteani, G.: High-pressure metamorphism in the SW tauern window, Austria: P-T paths from hornblende-kyanite-staurolite schists, J. Petrol., 25, 501–531, https://doi.org/10.1093/petrology/25.2.501, 1984.

Selverstone, J., Morteani, G., and Staude J.-M: Fluid channelling during ductile shearing: transformation of granodiorite into aluminous schist in the Tauern Window, Eastern Alps, J. Metamorph. Geol., 9, 419–431, 1991.

Seydoux-Guillaume, A. M., Montel, J. M., Bingen, B., Bosse, V., de Parseval, P., Paquette, J. L., Janots, E., and Wirth, R.: Low-temperature alteration of monazite: Fluid mediated coupled dissolution-precipitation, irradiation damage, and disturbance of the U-Pb and Th-Pb chronometers, Chem. Geol., 330/331, 140–158, https://doi.org/10.1016/j.chemgeo.2012.07.031, 2012.

Sharp, Z. D., Masson, H., and Lucchini, R.: Stable isotope geochemistry and formation mechanisms of quartz veins; extreme paleoaltitudes of the Central Alps in the Neogene, Am. J. Sci., 305, 187–219, 2005.

Spencer, C. J., Kirkland, C. L., and Taylor, R. J. M.: Geoscience Frontiers Strategies towards statistically robust interpretations of in situ U e Pb zircon geochronology, Geosci. Front., 7, 581–589, https://doi.org/10.1016/j.gsf.2015.11.006, 2016.

Stacey, J. S. and Kramers, J. D.: Approximation of terrestrial lead isotope evolution by a two-staged model, Earth Planet. Sc. Lett., 26, 207–221, 1975.

Staufenberg, H.: Apatite fission-track evidence for postmetamorphic uplift and cooling history of the Eastern Tauern Window and the surrounding Austroalpine (Central Eastern Alps, Austria), Jahrb. Geol. Bundesanst, 130, 571–586, 1987.

Steenken, A., Siegesmund, S., Heinrichs, T., and Fügenschuh, B.: Cooling and exhumation of the Rieserferner Pluton (Eastern Alps, Italy/Austria), Int. J. Earth Sci., 91, 799–817, https://doi.org/10.1007/s00531-002-0260-4, 2002.

Stöckhert, B., Brix, M. R., Kleinschrodt, R., Hurford, A. J., and Wirth, R.: Thermochronometry and microstructures of quartz-a comparison with experimental flow laws and predictions on the temperature of the brittle-plastic transition, J. Struct. Geol., 21, 351–369, https://doi.org/10.1016/S0191-8141(98)00114-X, 1999.

Urbanek, C., Frank, W., Grasemann, B., and Decker, K.: Eoalpine versus Tertiary deformation: dating of heterogeneously partitioned strain (Tauern Window, Austria), in Abstract volume, edited by: PanGeo Austria, 183–184, 2002.

Viola, G., Mancktelow, N. S., and Seward, D.: Late oligocene-neogene evolution of Europe-Adria collision: New structural and geochronological evidence from the Giudicarie fault system (Italian Eastern Alps), Tectonics, 20, 999–1020, https://doi.org/10.1029/2001TC900021, 2001.

Wölfler, A., Dekant, C., Danišík, M., Kurz, W., Dunkl, I., Putiš, M., and Frisch, W.: Late stage differential exhumation of crustal blocks in the central Eastern Alps: Evidence from fission track and (U-Th)/He thermochronology, Terra Nov., 20, 378–384, https://doi.org/10.1111/j.1365-3121.2008.00831.x, 2008.

Wölfler, A., Stüwe, K., Danišík, M., and Evans, N. J.: Low temperature thermochronology in the Eastern Alps: Implications for structural and topographic evolution, Tectonophysics, 541, 1–18, https://doi.org/10.1016/j.tecto.2012.03.016, 2012.

Yamada, R., Tagami, T., Nishimura, S., and Ito, H.: Annealing kinetics of fission tracks in zircon?: an experimental study, Chem. Geol., 122, 249–258, 1995.